

**GUIDELINES FOR ANALYZING THE CAPACITY OF D-REGIONS  
WITH PREMATURE CONCRETE DETERIORATION OF ASR/DEF**

John B. Mander  
Zachry Professor of Design and Construction Integration  
Zachry Department of Civil Engineering

Madhu M. Karthik  
Graduate Assistant Researcher  
Zachry Department of Civil Engineering

and

Stefan Hurlebaus  
Peter C. Foster Career Development Professor  
Zachry Department of Civil Engineering

Report 0-5997-P2  
Project 0-5997  
Project Title: Structural Assessment of "D" Region Affected by Premature  
Concrete Deterioration

Performed in cooperation with the  
Texas Department of Transportation  
and the  
Federal Highway Administration

Published: March 2015

TEXAS A&M TRANSPORTATION INSTITUTE  
College Station, Texas 77843-3135



## **DISCLAIMER**

This research was performed in cooperation with the Texas Department of Transportation (TxDOT) and the Federal Highway Administration (FHWA). The contents of this report reflect the views of the authors, who are responsible for the facts and the accuracy of the data presented herein. The contents do not necessarily reflect the official view or policies of the FHWA or TxDOT. This report does not constitute a standard, specification, or regulation.

The United States Government and the State of Texas do not endorse products or manufacturers. Trade or manufacturers' names appear herein solely because they are considered essential to the object of this report.

## **ACKNOWLEDGMENTS**

Funding for this project was provided via a contract with the Texas Department of Transportation (TxDOT) (Project 0-5997) with Mr. Wade Odell serving as Project Director. The guidance of Mr. Odell and the project control group is gratefully acknowledged.



# TABLE OF CONTENTS

List of Figures .....	ix
List of Tables .....	xi
Preface to Second Edition .....	xiii
1. Forward .....	1
2. Analysis Schema .....	3
2.1 Scope .....	3
2.2 Stage 1: Analysis Using Beam Theory .....	3
2.3 Stage 2: Strut-and-Tie Analysis .....	11
2.4 Stage 3: Analysis Using Compatibility Strut-and-Tie Methods .....	15
2.4.1 Stage 3.1: C-STM Based on Undamaged Material Properties .....	15
2.4.2 Stage 3.2: C-STM Allowing for ASR/DEF Damage and Its Effects .....	16
2.5 Stage 4: Establish Acceptability of Structure .....	17
3. Compatibility Strut-and-Tie Formulation .....	19
3.1 Modeling Truss Action .....	19
3.2 Modeling Arch Action .....	24
3.3 Modeling the Combined Truss and Arch Action .....	24
3.4 Stress and Strain Transformation for Flexural Equivalence .....	27
3.5 C-STM Geometry and Axial Rigidity Assignments .....	31
3.5.1 Truss Geometry .....	31
3.5.2 Axial Rigidity .....	32
3.6 Element Constitutive Material Relations .....	33
3.6.1 Reinforcing Steel .....	34
3.6.2 Diagonal Concrete Struts .....	34

3.6.3	Concrete Tensile Strength.....	35
3.6.4	Concrete Compression Chord Members.....	38
3.6.5	Modified Material Properties to Account for ASR/DEF .....	38
3.7	Ultimate Strength and Softening of Constitutive Relations .....	45
3.7.1	Strut-and-Tie Strength Checks.....	45
3.8	Computational Implementation.....	45
4.	Modeling ASR/DEF Expansion in Reinforced Concrete Structures .....	53
4.1.	Introduction.....	53
4.2.	Modeling ASR/DEF Expansion in Saturated Prisms.....	54
4.3.	Modifications to Account for Temperature and Moisture Variations .....	65
4.4.	Closure and Key Findings.....	69
5.	Worked Example: Determining Expansion Strains Caused by ASR/DEF.....	71
5.1.	Introduction.....	71
5.2.	Parameters for Modeling Expansion in C-Beam Specimen .....	71
5.3.	Modeling ASR/DEF Expansion in C-Beam Specimen .....	85
5.4.	Discussion.....	89
5.5.	Closure and Key Findings.....	90
6.	Worked Example: Analysis Schema for C-Beam Specimens .....	93
6.1	Scope .....	93
6.2	The Structure .....	93
6.3	Stage 1: Strength Analysis Using Beam Theory .....	95
6.4	Stage 2: Strength Analysis Using Strut-and-Tie Modeling.....	98
6.5	Stage 3: Strength and Deformation Capacity Using Compatibility Strut-and-Tie Computational Modeling .....	103

6.6 C-STM Results and Discussion.....	114
6.7 Concluding Remarks on Worked Example.....	120
7. Closure.....	123
References .....	125
Appendix A: Stage 1–3 Analysis–C-Beam Specimens .....	131



## LIST OF FIGURES

Figure 2–1: Flowchart for Analysis Procedure of Bridge Piers.....	4
Figure 2–2: Bridge Pier and Equivalent Beam Model for Flexure Analysis.....	5
Figure 2–3: Joint Arch Mechanism in Beam-Column Joint. ....	10
Figure 2–4: Strut-and-Tie Model of (a) Cantilever Bent (b) Straddle Bent. ....	13
Figure 3–1: Truss Model Idealization for a Fixed-Fixed Beam-Kim and Mander (1999). ....	21
Figure 3–2: Results of Convergence Study for Different Numerical Integration Schemes for C-STM Analysis. ....	22
Figure 3–3: Composition of Classic Arch and Truss Action That Leads to the Overall Compatibility Strut-and-Tie Model. ....	25
Figure 3–4: Constitutive Stress-Strain Relationship for Compression Chord Elements. ....	29
Figure 3–5: Diagonal Concrete Elements.....	37
Figure 3–6: Concrete Tension Stiffening Ties.....	37
Figure 3–7: Deteriorated Specimen Appearance, and the Modeled Transverse Strains in the C-Beam Out-of-Plane Direction.....	40
Figure 3–8: Assumed Arching Mechanism Between Hoops for Rectangular Sections (Mander, 1983). ....	43
Figure 3–9: Confined Strength Determination from Lateral Confining Stresses for Rectangular Sections (Mander, 1983). ....	43
Figure 3–10: Modified Stress-Strain Model for Steel to Account for Prestressing Effects Due to ASR/DEF.....	46
Figure 3–11: SAP2000 Screenshot: Steel Truss (Top); Concrete Truss (Bottom).....	48
Figure 3–12: Nonlinear Constitutive Material Properties.....	49
Figure 4–1: Expansion Model for ASR/DEF Induced Expansion in Concrete. ....	55
Figure 4–2: Stress-Strain Models for Components of Reinforced Concrete. ....	57

Figure 4–3: Effects of Compressive and Tensile Loads on ASR/DEF Induced Expansion. ....	60
Figure 4–4: Stress-Strain Models for Various Components. ....	61
Figure 4–5: Variation of Characteristic Time with Relative Weight Increase. ....	68
Figure 5–1: Reinforcement Layout of C-Beam Specimen .....	72
Figure 5–2: Information Pertinent to Model Expansion Strains in C-Beam Specimen.....	74
Figure 5–3: Computation of Average Tensile Loads from C-STM in the C-Beam Specimen due to Post-Tension Load .....	76
Figure 5–4: Observed and Computed Expansion Strain–Specimen 3. ....	87
Figure 6–1: Elevation and Cross-Section of the C-Beam Specimens.....	94
Figure 6–2: Shear Force and Bending Moment Diagram of the Equivalent Beam Model of C-Beam Specimen 1 (Specimen 4) and [Specimen 3].....	99
Figure 6–3: Strut-and-Tie Model for C-Beam Specimen 1. ....	100
Figure 6–4: Failure Pattern Observed at the Beam-Column Joint of C-Beam Specimen 1. ....	102
Figure 6–5: Modeling the C-Beam Specimens without and with ASR/DEF Damage .....	104
Figure 6–6: Cracked Reinforced Concrete Material Properties.....	105
Figure 6–7: Actual and Modified Stress-Strain Models for Reinforcing Steel to Account for Prestressing Effects in C-Beam Specimen 4. ....	116
Figure 6–8: Force-Deformation Results for Specimens 1, 4, and 3.....	117
Figure 6–9: Computed Sequence of Non-Linear Behavior Events. ....	119

## LIST OF TABLES

Table 3–1: Convergence Study of Higher Order Truss Models for a Cantilever Beam.....	21
Table 3–2: Elastic Truss Member Axial Rigidities.....	33
Table 5–1: Properties for C-Beam Specimen 3 .....	76
Table 5–2: Computation of Reinforcement Ratio and Maximum Expansion Strain for C-Beam Specimen 3 .....	86
Table 6–1: Material Properties and Test Results.....	95
Table 6–2: Results of Stage 1 Flexure Analysis (Without Deterioration).....	96
Table 6–3: Results of Stage 1 Shear Analysis.....	97
Table 6–4: Results for Stage 2 SAT Analysis.....	103
Table 6–5: Prestrains in C-STM Members for C-Beam Specimens.....	115
Table 6–6: Result for C-Beam Specimens 1, 4, and 3.....	120





## **PREFACE TO SECOND EDITION**

The second edition to the 'Guidelines for Determining the Capacity of D-Regions with Premature Concrete Deterioration of ASR/DEF' in essence is an update of the first edition 0-5997-P1 (Mander et al., 2012a), with findings and improved analysis techniques developed since 2012. The two major additions to this edition are Chapters 4 and 5.

Chapter 4 describes the development of a new minimalistic expansion model that is developed for ASR/DEF related expansion in reinforced concrete structures. The proposed model provides a method to predict the transient variation of expansion strains that are caused by ASR/DEF related expansion in reinforced concrete. Chapter 5 shows the application of the expansion model to the C-Beam specimen in detail. Based on the modeled expansion strains, the prestrains that need to be applied on the C-STM of a structure to simulate the effects of ASR/DEF can be obtained directly. This is markedly different from the recommended values of the prestress that were made in the first edition of the guidelines, which still can be used as a simplified first-order analysis, or when sufficient information to develop the expansion model is not available.

Worked example 1 in the first edition of the guidelines, which was the application of the C-STM technique to column bent cap, is not included in this revised edition. That example can be seen in Chapter 4 of Technical Report 0-5997-1 (Mander et al., 2012b).

Any revisions/additional information from the first edition is marked with a vertical side-bar in the left margin. Note that since Chapters 4 and 5 are entirely new, they are indicated by the side-bar next to the chapter heading.



# 1. FORWARD

When a bridge engineer encounters a design or analysis problem concerning a bridge substructure, that structure will commonly have a mixture of member types, some slender, and some squat. Slender members are generally governed by flexure, and normal beam theory should suffice for analysis and design. Squat members can often be handled by beam theory too, although nowadays designers have a choice and may opt to use strut-and-tie (SAT) models.

When the structure possesses a mixture of beam (B-) regions and deep or disturbed (D-) regions the dilemma facing the structural engineer is: What method should one use for structural analysis and design?

The issue becomes even more murky when a structure already exists, but shows signs of damage and deterioration from the effects of Alkali Silica Reaction (ASR), Delayed Ettringite Formation (DEF), or other deterioration mechanisms. The engineer is faced with a second dilemma: How do deteriorated material properties get incorporated into the analysis?

It is well-known that the behavior of deep beams or disturbed (or “D”) regions in a structural system cannot be accurately described according to conventional beam theory alone. This is due to the high irregularity of internal stress and strain distributions, accompanied by the interaction of flexure and shear. As a result, the coupled flexure and shear analysis of structural concrete members, especially deep beams, have been a contentious issue to both researchers and structural engineers for decades.

Conventional U.S. design standards for D-regions have historically been based on empirically derived expressions. The concept of strut-and-tie modeling (SAT) was first introduced as a method of strength design in the AASHTO LRFD Bridge Design Specification (2010) in 1994, and the ACI 318 Building Code Requirements for Structural Concrete (2011) in 2002. However, as a SAT model only satisfies force equilibrium and is intentionally formulated as a lower bound (plastic) solution, the critical mode of failure (i.e., element or nodal failure) is often illusive to the designer. Thus the ultimate failure mechanism might lead to an undesirable brittle collapse when imposed to overload scenarios.

Current nonlinear shear analysis models for structural concrete deep beams are generally complicated to use and have limited applicability or appeal to practicing engineers. Clearly, it is desirable to have a model that is derived from rational mechanics and validated with experimental evidence that can be implemented into commercially available structural analysis software. Therefore, a *Compatibility Strut-and-Tie Model* (C-STM) that is intended for the nonlinear analysis of shear critical reinforced concrete structures is presented.

These guidelines seek to demystify the above mentioned dilemmas. More specifically, guidelines are presented for determining the capacity of D-regions without and with premature concrete deterioration, in particular ASR and DEF effects.

In many cases either beam theory, or SAT methods should suffice in assessing the strength and safety of bridge substructures with or without ASR/DEF effects. However, as a supplementary analysis tool the C-STM approach can be used to augment the design process by accurately assessing the force-deformation response and nonlinear failure modes of deep beams with small span to depth ratios or D-regions.

## 2. ANALYSIS SCHEMA

### 2.1 SCOPE

This section presents the analysis methodology to be followed for the analysis of the structural capacity of bridge piers. The flowchart shown in Figure 2–1 depicts the procedure and the branching decision points that either terminate the analysis or trigger additional analyses to provide additional insights into expected behavior of bridge piers.

### 2.2 STAGE 1: ANALYSIS USING BEAM THEORY

As a first step in the analysis of a bridge pier as shown in Figure 2–2, it is assumed that flexural plastic hinge forms first, and the analysis is conducted based on flexural bending theory. The steps in this analysis technique can be summarized as described in the following steps:

**Step 1:** Determine first yield flexural capacity,  $M_y^b$ .

Calculate the beam yield moment ( $M_y^b$ ) at first yield of longitudinal steel given by:

$$M_y^b = C_s(d - d') + C_c(d - kd / 3) \quad (2-1)$$

in which  $d$  = depth to the centroid of tensile reinforcement from the extreme compression fiber;  $d'$  = depth to the centroid of compression steel from the extreme compression fiber;  $C_s = A'_s f_s$  when  $f_s \leq f_y$  and  $C_c = 0.85 f'_c ab$  where  $A'_s$  = the area of compression reinforcement;  $f_s$  = stress in steel corresponding to strain  $\epsilon_s$ ;  $f_y$  = yield stress of reinforcing steel;  $f'_c$  = concrete compressive strength;  $b$  = breadth of the section; and  $k$  is the elastic compression zone coefficient as given by Park and Paulay (1975):

$$k = \sqrt{(\rho_L + \rho'_L)^2 n^2 + 2(\rho_L + \rho'_L d'/d)n + (\rho_L + \rho'_L)n} \quad (2-2)$$

in which  $\rho_L$  = the ratio of tension reinforcement;  $\rho'_L$  = the ratio of compression reinforcement; and  $n$  = the modular ratio of steel to concrete.

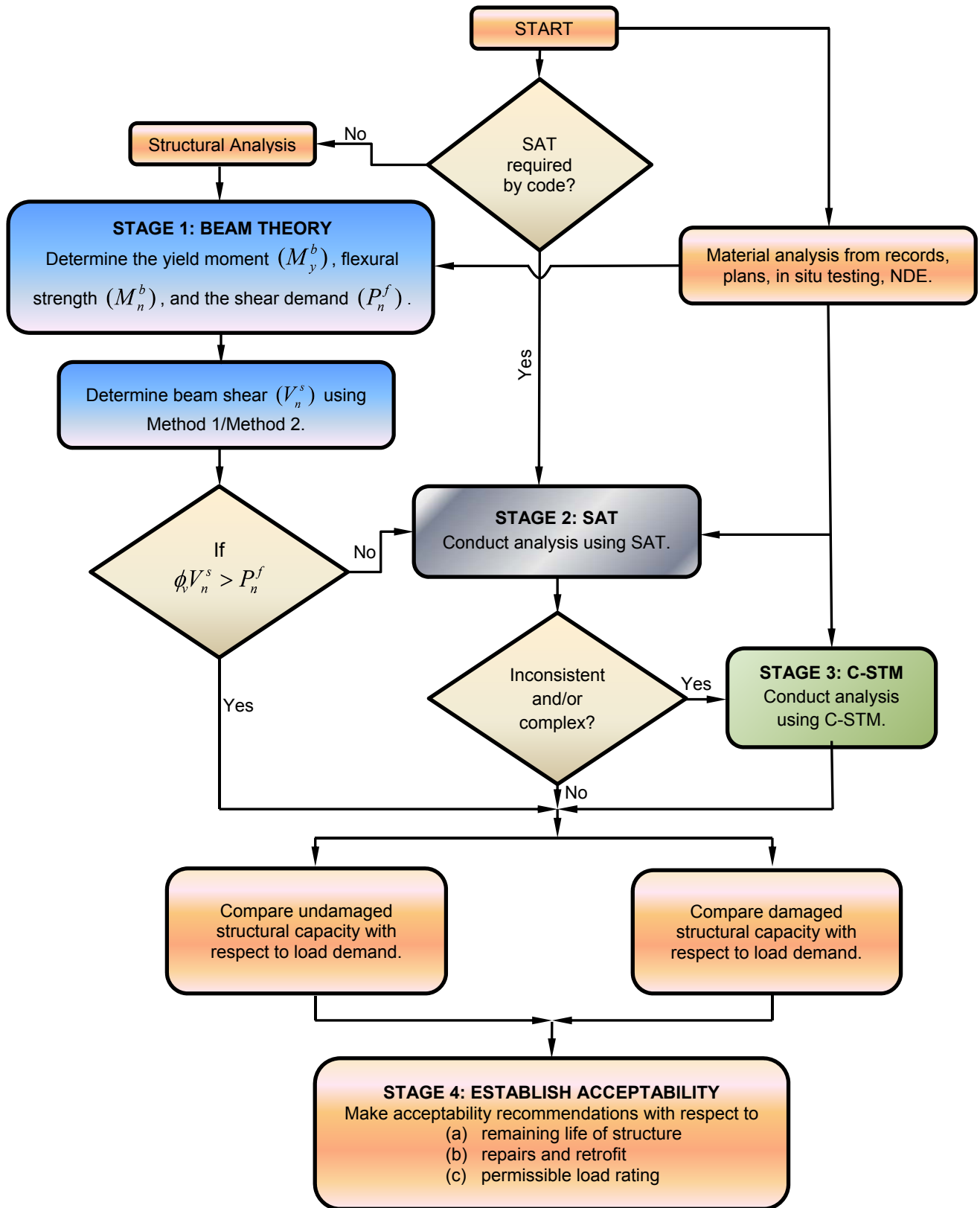
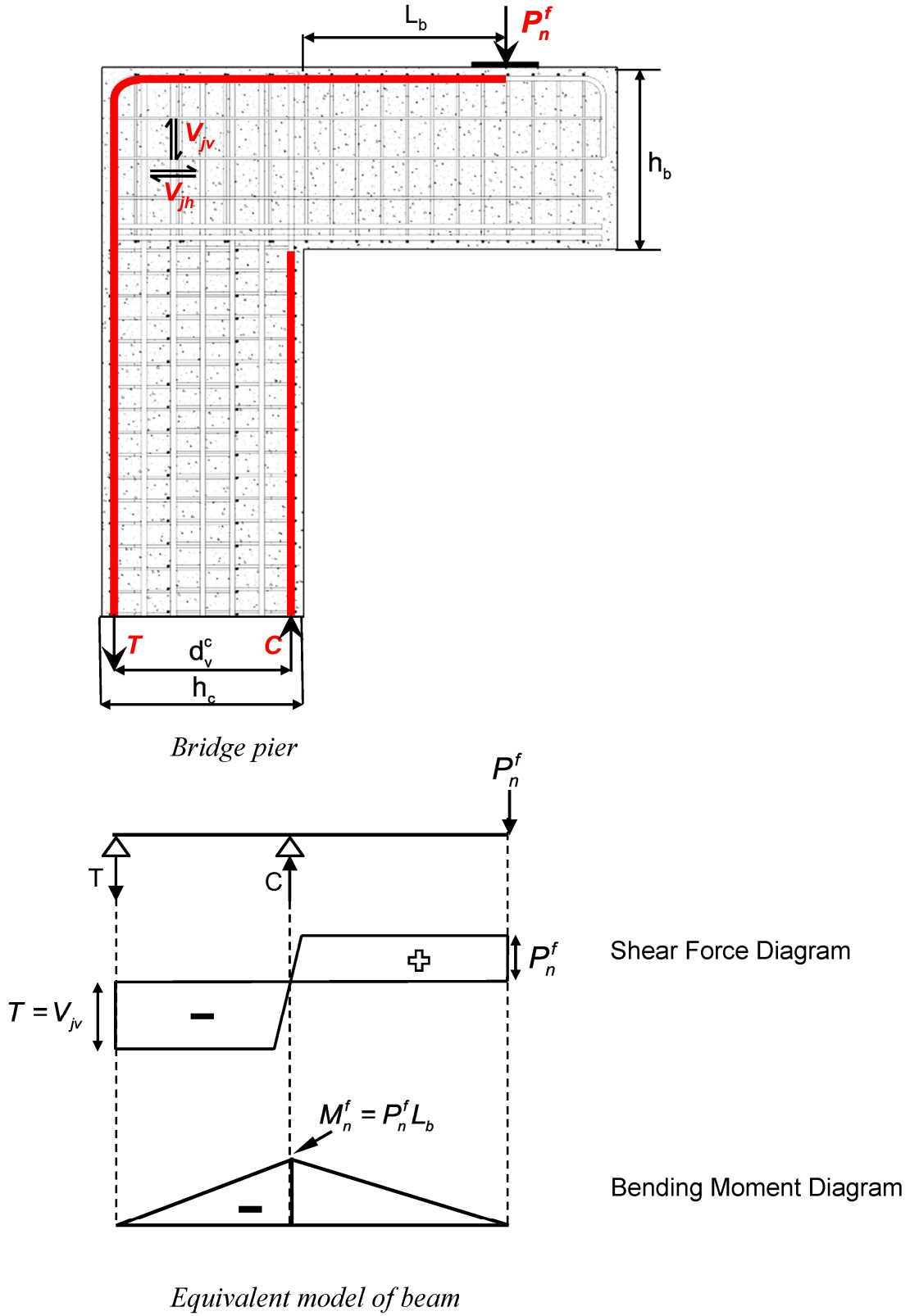


Figure 2–1: Flowchart for Analysis Procedure of Bridge Piers.



**Figure 2-2: Bridge Pier and Equivalent Beam Model for Flexure Analysis.**

The externally applied load that causes first yield is given by:

$$P_y^b = M_y^b / L_b \quad (2-3)$$

where  $L_b$  = distance from the point of application of the load to the face of the column.

**Step 2:** Determine nominal flexural moment,  $M_n^f$ .

The flexural moment ( $M_n^f$ ) of the beam is calculated as:

$$M_n^f = C_s(d - d') + C_c(d - a / 2) \quad (2-4)$$

in which  $a = \beta_1 c$  is the depth of the equivalent rectangular stress-block for which  $c$  is the neutral axis depth and  $\beta_1$  = the equivalent rectangular stress-block parameter given as:

$$0.65 \leq \beta_1 = 0.85 - 0.05(f'_c \text{ (ksi)} - 4) \leq 0.85 \quad (2-5)$$

**Step 3:** Determine externally applied load based on flexure,  $P_n^f$ .

Based on the flexural capacity ( $M_n^f$ ), the externally applied load ( $P_n^f$ ) is determined:

$$P_n^f = M_n^f / L_b \quad (2-6)$$

**Step 4:** Determine beam shear capacity,  $V_n^s$ .

The shear capacity ( $V_n^s$ ) of the beam is computed as:

$$V_n^s = V_c + V_s + V_p \quad (2-7)$$

in which  $V_p$  = component of shear carried by prestressing tendons, if any;  $V_s$  = shear carried by steel; and  $V_c$  = shear carried by concrete given by:

$$V_c = 0.0316 \beta \sqrt{f'_c} b_v d_v \quad (2-8)$$

where  $f'_c$  = concrete strength in ksi units;  $b_v$  = section web width across shear plane;  $d_v$  = effective shear depth taken as  $d_v = jd$  or not less than the greater of  $0.9d$  (where  $d$  = effective depth), or  $0.72h$  (where  $h$  = overall depth).

For sections with steel transverse to the longitudinal axis of the member ( $\alpha = 90^\circ$ ), the shear carried by the hoops and /or cross ties is given by:



$$V_s = A_v f_y \frac{d_v}{s} \cot \theta \quad (2-9)$$

where  $A_v$  = cross-sectional area of hoopset;  $s$  = hoopset spacing; and  $\theta$  = shear crack angle inclined from the longitudinal axis.

AASHTO LRFD (2010) specifications permit  $\beta$  and  $\theta$  in Eq. (2-8) and (2-9) to be calculated by one of the following two methods:

Method 1: Simplified Procedure

For reinforced (non-prestressed) concrete members, values of  $\beta = 2.0$  and  $\theta = 45^\circ$  can be used. Thus, the shear carried by concrete is the same as the well-known historic ACI-318 (2011) method.

Method 2: General Sectional Procedure

This method is based on the simplified version of the Modified Compression Field Theory (MCFT) (Bentz et al., 2006). In this method the parameters  $\beta$  and  $\theta$  can be determined as described below.

For sections containing the minimum amount of transverse reinforcement as specified in AASHTO LRFD (2010),  $\beta$  is determined as:

$$\beta = \frac{4.8}{1 + 750\varepsilon_s} \quad (2-10)$$

where  $\varepsilon_s$  = net longitudinal tensile strain in the section at the centroid of the tensile reinforcement determined as explained later.

For sections that do not contain the minimum amount of shear reinforcement as specified in AASHTO LRFD (2010),  $\beta$  is determined as:

$$\beta = \frac{4.8}{(1 + 750\varepsilon_s)} \frac{51}{(39 + s_{xe})} \quad (2-11)$$

where  $s_{xe}$  = the crack spacing parameter is given by:

$$12.0(in.) \leq s_{xe} = s_x \frac{1.38}{a_g + 0.63} \leq 80.0(in.) \quad (2-12)$$

where  $a_g$  = maximum aggregate size in inches;  $s_x$  = the lesser of either  $d_v$  (effective shear depth) or the maximum distance between layers of longitudinal crack control reinforcement, where the area of the reinforcement in each layer is not less than  $0.003b_v s_x$ .

The crack angle  $\theta$  for any of the above cases is given by:

$$\theta = 29 + 3500\varepsilon_s \quad (2-13)$$

In Eqs.(2-10), (2-11), and (2-13),  $\varepsilon_s$  can be determined from the following expression:

$$\varepsilon_s = \frac{\left( \frac{|M_u|}{d_v} + 0.5N_u + |V_u - V_p| - A_{ps}f_{po} \right)}{E_s A_s + E_p A_{ps}} \quad (2-14)$$

where  $|M_u|$  = factored moment, not to be taken less than  $|V_u - V_p| d_v$ ;  $V_u$  = factored shear force;  $V_p$  = component of shear carried by prestressing tendon;  $N_u$  = factored axial force taken as positive if tensile and negative if compressive;  $A_s$  = area of non-prestressing tensile steel;  $A_{ps}$  = area of prestressing steel on the flexural tension side of the member;  $f_{po}$  (pre-tensioned members) = stress in strands when concrete is cast around them, and  $f_{po}$  (post-tensioned members) = average stress in the tendons when the post-tensioning is completed, or for usual levels of prestressing  $f_{po} = 0.7f_{pu}$  for both pre and post-tensioning;  $f_{pu}$  = ultimate stress in the prestressing tendon;  $E_s$  and  $E_p$  = modulus of elasticity of reinforcing steel and prestressing steel respectively; and  $A_s$  = area of reinforcing steel.

**Step 5:** Check strength hierarchy.

Once the externally applied load based on flexure ( $P_n^f$ ) and the shear capacity ( $V_n^s$ ) are calculated, the strength hierarchy can be determined based on:

IF  $\phi V_n^s > P_n^f$

THEN shear has a measure of reserve capacity and the beam should fail in flexure.

IF  $\phi V_n^s < \phi_f P_n^f$

THEN the factored shear capacity may be insufficient leading to a shear failure of the bridge pier.

In the above  $\phi = 0.90$  and  $\phi_f = 0.90$  are the strength reduction factors for shear and flexure, respectively, as per AASHTO LRFD *Bridge Design Specifications* (2010).

**Step 6:** Determine the shear capacity of the beam-column joint regions.

For the beam-column joint regions in bent caps the joint shear capacity needs to be determined in the direction in which the shear steel (hoopsets) is oriented. Thus, the vertical joint shear ( $V_{jv}$ ) determined from the shear force diagram (Figure 2–2) of the bridge bent cap can be transformed (if necessary) as follows:

$$V_{jh} = \frac{h_c}{h_b} V_{jv} \quad (2-15)$$

in which  $h_b$  and  $h_c$  are the overall depth of the beam and column, respectively.

The joint capacity can be assessed as:

$$V_n^j = V_{arch} + V_{truss} \quad (2-16)$$

where  $V_{arch}$  = shear carried by the corner-to-corner diagonal concrete arch (defined later); and  $V_{truss} = \sum A_{sv} f_y$  = the shear carried by the hoops and/or cross ties, in which  $\sum A_{sv}$  = the total area of steel given by all hoops/ties within the joint region.

There is a parabolic distribution of stress in the corner-to-corner arch in the beam-column zone which can further be simplified as shown in Figure 2–3a and b. From Figure 2–3c,  $V = P \sin \alpha$ . The total tensile force across the arch equals  $P/2 = (jd / \sin \alpha) b_w f_t'$ , which implies the shear contribution from the corner-to-corner joint arch is given by:

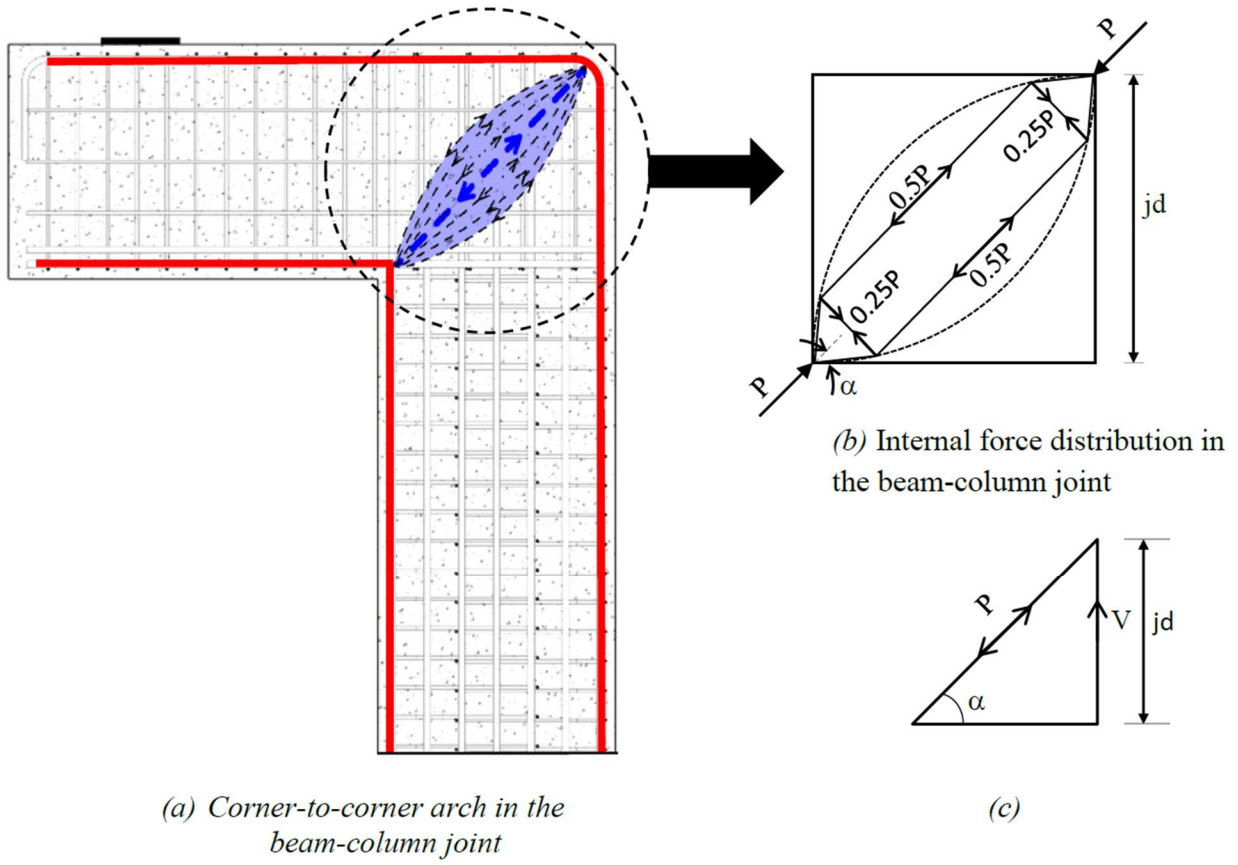


**Figure 2–3: Joint Arch Mechanism in Beam-Column Joint.**

$$V_{arch} = 0.253\sqrt{f'_c \text{ (ksi)}}b_vjd = 8\sqrt{f'_c \text{ (psi)}}b_vjd \quad (2-17)$$

taking  $f'_t = 0.126\sqrt{f'_c \text{ (ksi)}} = 4\sqrt{f'_c \text{ (psi)}}$ .

For the beam-column joint to be safe in shear the following should be satisfied:

$$\phi V_n^j > V_{jv} \quad (2-18)$$

From the above analysis, if it is determined that the beam has a measure of reserve capacity then the analysis can essentially be stopped at this point. However, if either the beam or the beam-column joint is a shear critical section, then further investigation is warranted. In such a case, or when required by the code, the strut-and-tie technique of analysis can be used for further analysis, which is discussed in the next section.

### 2.3 STAGE 2: STRUT-AND-TIE ANALYSIS

The strut-and-tie modeling technique is a lower bound plastic truss model that is particularly useful for design. It can also be adopted for strength analysis, and may be particularly useful for structures that possess stocky members and a significant number of D (disturbed) regions. Using an SAT approach, a structure with D-regions is modeled as a truss, which consists of three types of elements: struts, ties, and nodes. Struts represent concrete that carries compressive loads while tensile loads are carried by ties representing steel reinforcements. Struts and ties intersect at nodes. Nodes are labeled by the element forces intersecting at the nodes; “C” represents compression while “T” stands for tension. Based on the type of member forces at the node, the nodes can be classified as CCC, CCT, CTT, and so on.

The truss geometry of the strut-and-tie model is based on the direction of stress flow in the D-region. The ties are aligned along the reinforcement layout, whereas the struts are oriented based on the compressive stress flow trajectories. It is also reasonable to determine the truss geometry based on the cracks that can be seen on a structural member as illustrated in Figure 2–4b.

Once the truss geometry is determined, the nodal geometries must be established in order to calculate the stresses on each of the nodal faces. These calculated stresses must not exceed the allowable stresses for each nodal face. The nodes can be proportioned either as a hydrostatic node

or as a non-hydrostatic node. In a hydrostatic node the principal stresses are equal on all sides of the node; hence the ratio of each nodal face is directly proportional to the force being applied to the nodal face. However, often the nodal dimensions are inconsistent with the beam details such as the location of the reinforcement and depth of the flexural compression zone. In the case of non-hydrostatic nodes the stresses applied to each nodal face is different as the node is sized based on the beam details. As a result of this the nodal geometry is synchronized with the beam details. Additionally, higher values of shear span-to-depth ratio can also lead to unrealistically large struts in the case of hydrostatic nodes.

Based on the above concepts, a strut-and-tie model for a cantilever bent and a straddle bent are shown in Figure 2–4. The forces in the truss elements can be determined by a simple truss analysis. The stresses in each of the truss elements and nodes are then checked against the allowable stresses.

The allowable concrete compressive stresses on the nodal face depend on the type of node. The allowable stresses in the nodal regions are defined as follows:

For	CCC nodes	$f_{cu} = 0.85f'_c$	
	CCT nodes	$f_{cu} = 0.75f'_c$	(2-19)
	CTT nodes	$f_{cu} = 0.65f'_c$	

The limiting compressive stress within a strut ( $f_{cu}$ ) is given by:

$$f_{cu} = \frac{f'_c}{0.8 + 170\varepsilon_1} \leq 0.85f'_c \quad (2-20)$$

in which  $\varepsilon_1$  = principal tension strain given by:

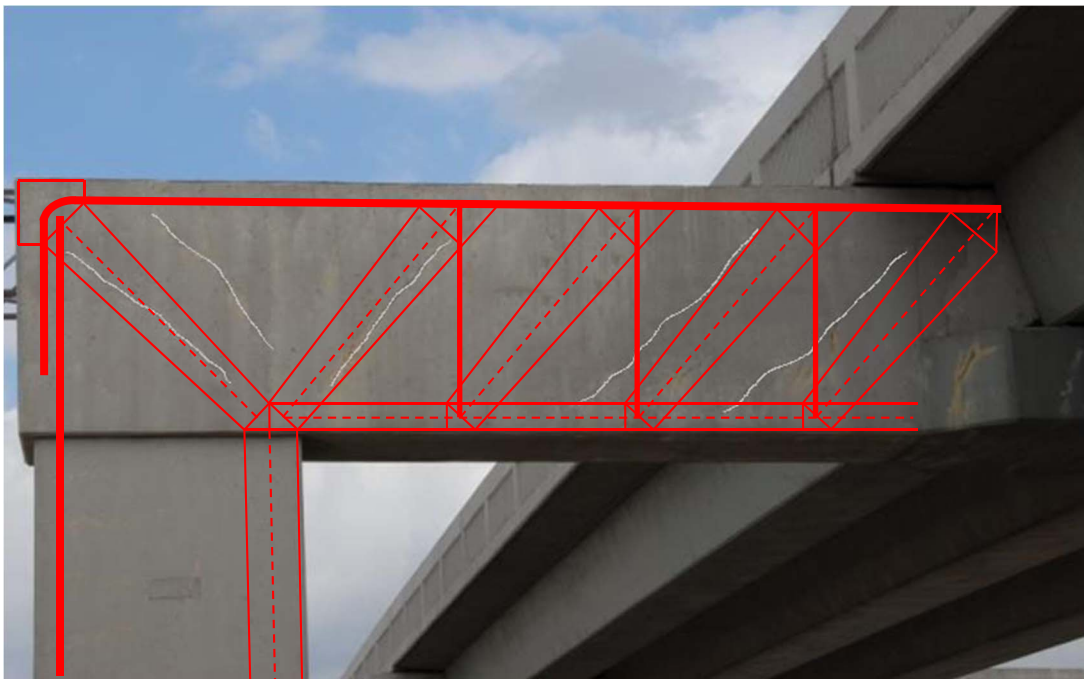
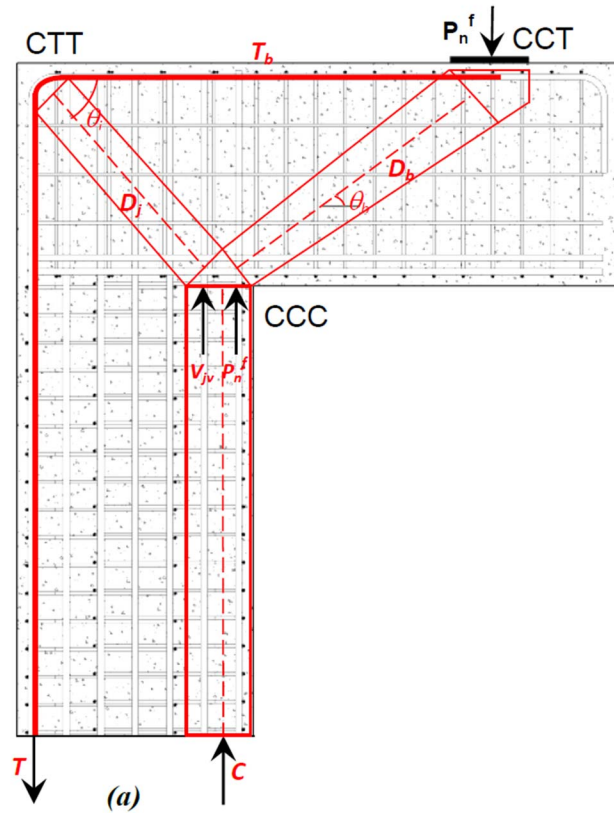
$$\varepsilon_1 = \varepsilon_s + (\varepsilon_s + 0.002) \cot^2 \alpha_s \quad (2-21)$$

where  $\varepsilon_s$  = tensile strain in the direction of the tension tie; and  $\alpha_s$  = the smallest angle between the compressive strut and adjoining tension tie.

The nominal resistance of a strut/node is given as:

$$P_n = f_{cu} A_{cs} \quad (2-22)$$

where  $A_{cs}$  = effective cross-sectional area of the strut/node.



(b)

Figure 2-4: Strut-and-Tie Model of (a) Cantilever Bent (b) Straddle Bent.

The nominal resistance of a tension tie is given by:

$$P_n = f_y A_{st} + A_{ps} [f_{pe} + f_y] \quad (2-23)$$

where  $f_y$  = yield strength of reinforcing steel;  $A_{st}$  = area of reinforcing steel in the tension tie;  $A_{ps}$  = area of prestressing steel;  $f_{pe}$  = stress in prestressing steel after losses.

A generalized stepwise procedure on how to build a strut-and-tie model for a bridge pier as illustrated in Figure 2–4 is as follows.

**Step 1:** Determine the truss and node geometry.

The first step in doing a strut-and-tie analysis is to determine the geometry of the truss and the nodes. The width of the compression chords in the column and the beam can be determined based on the depth of the triangular stress-block or the equivalent rectangular stress-block. The base of the CCC node can be proportioned based on the externally applied load that causes beam flexure ( $P_n^f$ ) and the vertical component of shear in the beam-column joint ( $V_{jv}$ ). The width of the CCT node is taken to be equal to the width of the bearing pad, and the CTT node is dimensioned based on the bending radius of longitudinal reinforcement. The struts can be drawn based on the dimension of the nodes. This will also provide the inclination angle of the diagonal struts.

**Step 2:** Solve the determinate truss.

It is assumed that the beam tension steel yields, that is,  $T_b = A_s f_y$ . Considering equilibrium of forces at the nodes, the forces in all the members of the truss can be determined.

**Step 3:** Determine critical node.

The critical node can be determined based on the nodal strength of each of the nodes. Based on the nodal dimensions and the allowable stress (Eq. 2-19), the nodal capacity can be determined. Based on this information the critical node is identified.



**Step 4:** Determine shear demand.

The shear demand on the bridge pier can be determined based on the most critical strut/tie or nodal zone.

Though the strut-and-tie modeling technique is an efficient method of analysis for shear critical members, it is observed that there could be inconsistencies or added complexity due to the nature of the structure that is being analyzed. Additionally, further difficulties in reaching a conclusion are likely, if the factored shear capacity based on SAT analysis is lower than the factored capacity from Stage 1 of the analysis even though the nominal capacity from SAT analysis is higher. Also, the results of the SAT analysis are based on reasonable assumptions, which could lead to varying results depending on the assumptions made.

This calls for a more advanced analysis technique that adopts the concepts of the strut-and-tie method and gives an idea about the overall behavior of the structure. One such technique, the compatibility strut-and-tie modeling, is developed in the next chapter.

## **2.4 STAGE 3: ANALYSIS USING COMPATIBILITY STRUT-AND-TIE METHODS**

As mentioned above, strut-and-tie analysis methods are strictly lower bound solutions. Such solutions adhere to the principles of equilibrium, but are both silent on and unable to predict deformations of the structure.

### **2.4.1 Stage 3.1: C-STM Based on Undamaged Material Properties**

To obtain a more holistic view of structural behavior that provides a complete force vs. deformation pathway to failure, compatibility of member deformations must be incorporated into the analysis. This approach is referred to as the *Compatibility Strut-and-Tie Model* (C-STM).

As this approach is relatively new, a complete background and theoretical formulation is presented in the next chapter. As the bookkeeping for this class of nonlinear analysis would be time consuming, it is suggested that nonlinear structural analysis software (e.g., SAP2000) be used for the analysis. In this stage of analysis the undamaged material properties are used in evaluating the behavior of the structure.

### 2.4.2 Stage 3.2: C-STM Allowing for ASR/DEF Damage and Its Effects

It is well-known that ASR/DEF can cause the concrete to deteriorate. The effects of ASR/DEF on the structure can be explained as follows:

- ASR/DEF effects cause the concrete to swell.
- This in turn may cause the cover concrete to badly crack and in some cases cause spalling.
- Meanwhile swelling of the core concrete occurs, but this is constrained in part by the presence of longitudinal and transverse reinforcement.
- Tensile strains that are induced put the reinforcing steel to be in a state of prestress.
- In turn, this prestress effect, which is similar to adding an axial force, increases the stiffness and can slightly enhance the strength of the members most affected by ASR/DEF.

The effects of ASR/DEF on the structure can be modeled in C-STM by introducing the effects of deteriorated cover concrete, concrete core confinement, prestressing forces, and modifying the stress-strain relation of steel accordingly.

Based on an assessment of the extent of damage due to ASR/DEF effects observed in the structure, the damage can be categorized into three classes: '*slight*', '*moderate*', and '*heavy*' damage. Based on the degree of confinement of core concrete and the extent of weakened cover concrete, and their respective contributions to the total area of the compression chord, a weighted average concrete compressive strength is determined. In lieu of a more precise analysis to determine the extent of expansion and the corresponding amount of prestressing force to be applied on the longitudinal and transverse reinforcement, recommended factors can be used for determining the prestressing forces based on the extent of damage. A C-STM analysis with the modified properties gives the behavior of the structure with ASR/DEF damage.

Based on the results from the three stages of analysis presented above, the structural capacity of the damaged/undamaged structure can be compared to the load demand on the structure. Based on these comparisons, acceptability criterion can be set for a structure; this constitutes stage 4 of the analysis schema.

## 2.5 STAGE 4: ESTABLISH ACCEPTABILITY OF STRUCTURE

Based on the analysis conducted on the structure in the previous three stages, a structural engineer must be able to make recommendations and establish the acceptability of an existing structure that may or may not be subjected to any form of deterioration/damage. The engineer must be able to make acceptability recommendations with respect to:

- (a) The remaining life of the structure: This would essentially give ample time to the state DOTs to plan ahead in time on how to deal with the existing structure and/or plan alternate strategies.
- (b) Repairs or retrofit: Such remediation can be done in order to strengthen the existing structure and give it added service life to enable it to perform as designed.
- (c) Permissible load rating: By limiting the permissible loads on the structure, the service life of the structure can be extended.

The first two stages of analysis, using beam theory and SAT analysis, would give the structural engineer just an idea about the maximum load that the structure can withstand before it starts to show signs of distress or even fails. However, stage 3 of the analysis (where the C-STM technique is adopted) gives the overall force-deformation of the structure, which helps to better predict its behavior and make a more definitive engineering judgment on the structure's acceptability condition. The C-STM analysis technique will aid the structural engineer to make a more accurate educated prediction about the behavior of the structure.

The different stages of analysis for the C-Beam specimens including the C-STM technique is presented in Chapter 6.



### 3. COMPATIBILITY STRUT-AND-TIE FORMULATION

It is well-known that the shear resistance in structural concrete elements is resisted by a combination of truss and arch action (Park and Paulay, 1975). Truss action is associated with the shear resistance provided by the transverse reinforcement (Ritter, 1899; Mörsch, 1909; Dilger, 1966; Paulay, 1971; Kim and Mander, 1999, 2000, and 2007). Arch action becomes prevalent in squat reinforced concrete members, particularly those with wide webs where a direct compression load path (arch) exists between the applied load and the supports. These two primary mechanisms are further considered in what follows.

#### 3.1 MODELING TRUSS ACTION

Figure 3–1a illustrates a variable angle crack pattern that typically forms in the disturbed regions of a fixed-fixed reinforced concrete deep beam. After the development of first cracking, diagonal concrete compression struts are tied together by the longitudinal and transverse reinforcing steel, thus resembling a truss. Starting with a differential portion of this truss, Kim and Mander (1999, 2007) integrated this over the beam length to develop a “continuum truss” model where cracking was implicitly smeared in order to obtain the shear stiffness in a numerical form.

Alternative numerical integration schemes were then considered by Kim and Mander (1999, 2007) to model the discrete crack patterns typically observed in reinforced concrete beams and are explored further herein. For a fixed-fixed beam, the simplest of these numerical integration schemes uses a two-point Gaussian quadrature solution leading to a so-called two-point Gauss Truss shown in Figure 3–1b. Note the solid lines represent tension ties (reinforcing steel), and the dashed lines represent diagonal compression struts (concrete). Through experimental and analytical validation, Kim and Mander (1999, 2007) found the two-point Gauss Truss to be a suitably accurate numerical integration scheme for capturing both shear and flexure deformations of disturbed regions with fixed-fixed end conditions. Higher order numerical schemes were also considered; however the two-point Gauss Truss model has the appeal of being statically determinate (due to anti-symmetry).

By taking only one-half of an anti-symmetric fixed-fixed beam that is represented by the two-point Gauss Truss, a statically determinant cantilever remains, which can be represented by a so-called *Single-Point Gauss Truss*. In order to confirm the numerical accuracy of the proposed

single-point Gauss Truss, a convergence study of higher order numerical integration schemes was conducted. Based on recommendations of Kim and Mander (1999, 2000), the axial rigidities assigned to each truss member at the  $i^{th}$  integration point are given by:

$$(EA)_{Ti} = \omega_i E_s A_{sh} \frac{L}{s} \quad (3-1)$$

$$(EA)_{di} = \frac{0.5\omega_i}{\sqrt{x_i + \tan^2 \theta_i}} E_c A_v \quad (3-2)$$

$$(EA)_L = A_L E_s \quad (3-3)$$

in which  $(EA)_{Ti}$  = axial rigidity of the transverse reinforcement ties (where  $\omega_i$  = numerical weight factor for transverse reinforcement defined in Table 3–1,  $E_s$  = Young's Modulus for steel,  $A_{sh}$  = area of one set of stirrups,  $L$  = member length, and  $s$  = stirrup spacing);  $(EA)_{di}$  = axial rigidity of the diagonal concrete struts (where  $x_i$  = normalized coordinate of the  $i^{th}$  integration point,  $\theta_i$  = strut angle relative to longitudinal steel,  $E_c$  = Young's Modulus for concrete,  $A_v = b_w d$  is the shear area of concrete,  $b_w$  = beam width, and  $d$  = the effective depth of the beam from the extreme concrete compression fiber to the centroid of the tension steel); and  $(EA)_L$  = axial rigidity of the longitudinal reinforcement ties (where  $A_L$  = is the sectional area of steel assigned to the longitudinal tension tie).

Table 3–1 presents four different numerical integration schemes that were considered in this convergence study: single, two, and three-point Gauss quadrature, and Boole's rule. A 3 ft. by 2 ft. (900 x 600 mm) cantilevered beam was used as an illustrative example with a span to depth ratio of 1, and longitudinal and transverse reinforcing ratios of 0.010 and 0.003, respectively, where each integration scheme is depicted at the top of Figure 3–2. The right column of Table 3–1 presents the relative elastic shear stiffness ( $K$ ) of each truss normalized with respect to the two-point Gauss Truss. Although some variability between schemes exists, it can be concluded that any reasonable integration scheme may be used to provide a satisfactory representation of shear stiffness. However, a more in-depth study should be considered to compare the flexure-shear interaction between truss models.

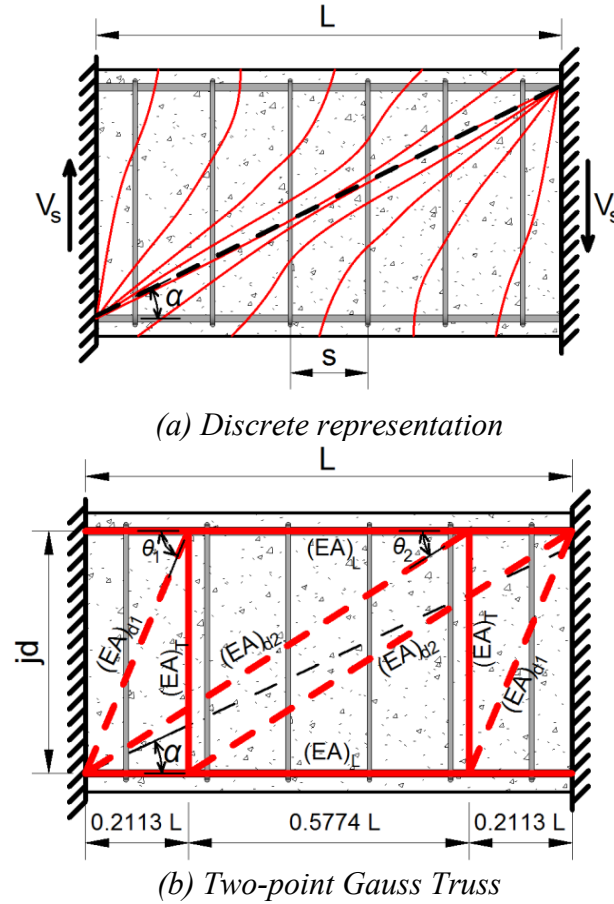
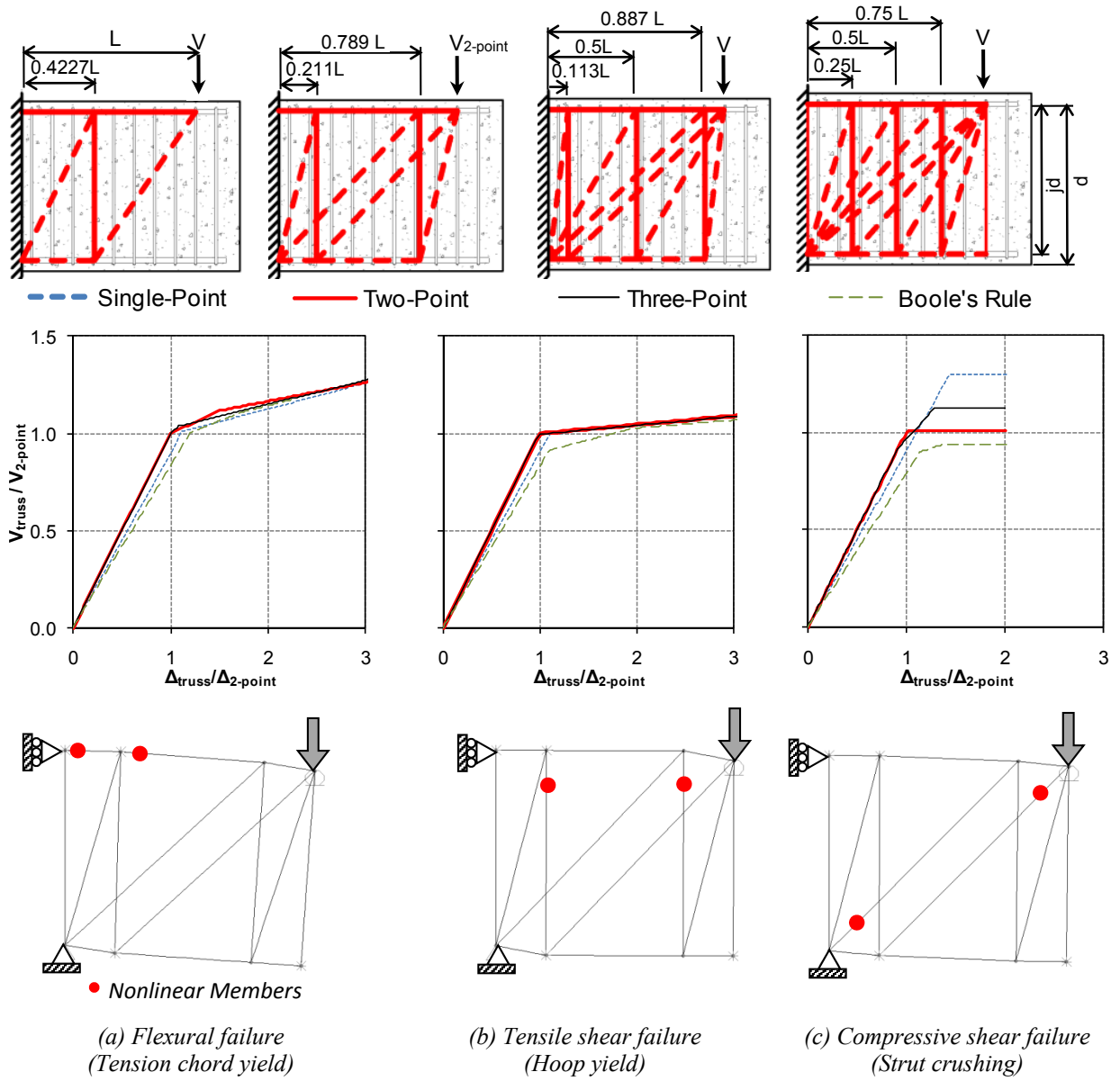


Figure 3–1: Truss Model Idealization for a Fixed-Fixed Beam-Kim and Mander (1999).

Table 3–1: Convergence Study of Higher Order Truss Models for a Cantilever Beam.

Numerical Scheme	$i$	$x_i$	$\omega_i$	$\frac{K_{Truss}}{K_{2-point}}$
Single-Point Gauss	1	0.42265	1	1.0429
	2	0.57735	1	
Two-Point Gauss	1	0.21132	0.5	<b>1.0000</b>
	2	0.78868	0.5	
Three-Point Gauss	1	0.11270	5/18	1.0007
	2	0.50000	8/18	
	3	0.88730	5/18	
Boole's Rule	1	0.00	7/90	0.9371
	2	0.25	32/90	
	3	0.50	12/90	
	4	0.75	32/90	
	5	1.00	7/90	



**Figure 3-2: Results of Convergence Study for Different Numerical Integration Schemes for C-STM Analysis.**



Figure 3–2 shows the force-deformation response of each truss model normalized with respect to the two-point Gauss Truss solution considering the following nonlinear mechanisms: (a) flexural steel yielding; (b) transverse steel yielding; and (c) concrete strut crushing. Each truss is modeled using well-known commercial structural analysis software SAP2000™ (1995), and considers a bilinear stress-strain relationship with 3 percent strain hardening stiffness for steel, and an elasto-plastic response with a maximum compression stress of  $0.85f'_c$  for the concrete struts.

When nonlinear behavior is governed by longitudinal tensile steel yielding (Figure 3–2a), the post-yield force-deformation response is ductile. Despite similar yield strengths, the single-point Gauss Truss model resulted in a slightly more flexible elastic stiffness than the higher order Gauss quadrature truss models. The Boole's truss was the most flexible of the truss models and provided slightly lower initial yield strength, but had a similar post yield response.

When nonlinear behavior is governed by transverse steel yielding (Figure 3–2b), similar stiffness results were obtained. However, the post yield stiffness was less than that with longitudinal steel yielding. This shows that yielding of the transverse reinforcement can lead to large shear deformations with small increases in applied load.

When nonlinear behavior is governed by strut crushing (Figure 3–2c), the ultimate strength had a variation up to 30 percent with the single-point truss giving the largest difference. An elasto-plastic response of concrete was used for illustrative purposes only and does not accurately model concrete crushing; hence the response of each was stopped at a ductility of two.

In summary, for cantilever modeling, the single-point Gauss Truss is evidently a sufficiently accurate model for considering the nonlinear flexure-shear interaction relative to the higher order truss models when the failure mechanism is controlled by longitudinal and transverse steel yielding. However, for mechanisms controlled by strut crushing, a convergence study is recommended to ensure the single-point Gauss Truss does not over-estimate the failure mechanism.

### 3.2 MODELING ARCH ACTION

Arch action consists of a compressive stress field forming a diagonal corner-to-corner concrete strut that is tied back by the longitudinal reinforcement as shown in Figure 3–3a. The strut is assumed to have a parabolic stress distribution with a strut width that is proportional to the depth and length of the beam as given below (Holden et al., 2003):

$$W_A = 0.375 jd / \cos \alpha \quad (3-4)$$

This approach is similar to that proposed for coupling beams by Paulay (1971).

### 3.3 MODELING THE COMBINED TRUSS AND ARCH ACTION

Figure 3–3 presents the combined C-STM that is comprised of: (a) arch action acting through the center of the beam cross-section; and (b) truss action acting along the outside stirrup legs. Figure 3–3c shows the amalgamated response of arch and truss action, where displacement compatibility is inherently accounted for such that the two mechanisms work in parallel to one another. A method of apportioning the relative contributions of arch and truss action is described as follows.

Different methods of allocating the shear resisting mechanisms have previously been proposed based on the following parameters: (i) strength (Paulay, 1971; Kim and Mander, 1999); (ii) stiffness (Zhu et al., 2003); (iii) geometry (Hwang et al., 2000); and (iv) the shear span-to-internal lever arm ratio (FIP-Commission 3, 1996). An investigation into the merits of each of these strategies was conducted, and the following conclusion was drawn: varying the proportions of arch and truss action resulted in minimal differences of the elastic force-deformation response. However, significant differences in the nonlinear response of the flexure and shear failure mechanisms were observed. Hence to accurately model the flexure-shear interaction, it is considered necessary to apportion the arch and truss mechanisms according to the longitudinal and transverse reinforcement ratios in order to account for strength and  $L / jd$  in order to account for geometry.

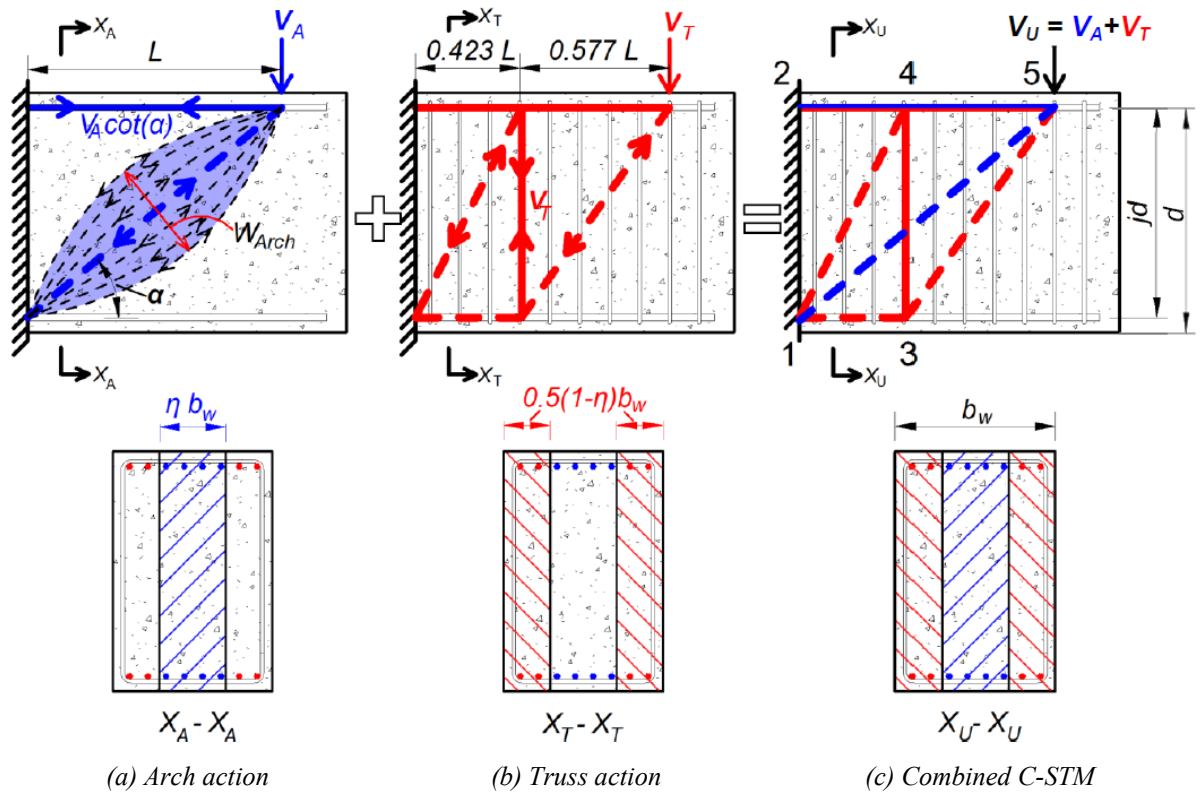


**Figure 3-3: Composition of Classic Arch and Truss Action That Leads to the Overall Compatibility Strut-and-Tie Model.**

An arch breadth scalar  $\eta$  is proposed to apportion the section breadth (shown in the cross-sections of Figure 3–3) and is defined by the following ratio:

$$\eta = \frac{V_{Arch}}{V_{Arch} + V_{Truss}} = \frac{\rho_L f_y}{\rho_L f_y + \rho_T f_{yh} j \cot^2 \alpha} \quad (3-5)$$

in which  $V_{Arch}$  = maximum shear force resisted by arch action that is proportional to the longitudinal reinforcement given below; and  $V_{Truss}$  = maximum shear force resisted by truss action that is proportional to the transverse reinforced given as:

$$V_{Arch} = f_y A_L \tan \alpha = \rho_L f_y b_w d \tan \alpha \quad (3-6a)$$

$$V_{Truss} = f_{yh} A_{sh} L / s = \rho_T f_{yh} b_w j d \cot \alpha \quad (3-6b)$$

where  $\alpha$  = the corner-to-corner diagonal angle;  $\rho_L = A_L / b_w d$  is the volumetric ratio of longitudinal steel to concrete;  $A_L$  = is the area of longitudinal reinforcement contributing to the tension tie;  $\rho_T = A_{sh} / b_w s$  is the volumetric ratio of transverse steel to concrete over one hoop spacing;  $f_y$  = yield strength of the longitudinal steel;  $f_{yh}$  = yield strength of the transverse steel; and  $j = (1 - d' / d)$  the internal lever arm coefficient.

The total shear resistance of the combined C-STM  $V_U$ , as shown in Figure 3–3c, can now be defined as:

$$V_U = V_A + V_T \quad (3-7)$$

where  $V_A$  = is the shear resistance from arch action; and  $V_T$  = is the shear resistance from truss action.

In order to maintain deformation compatibility and equilibrium between the arch and truss mechanisms, it is assumed that the section breadth  $b_w$  is proportioned according to the component strength as follows:

$$\frac{V_A}{V_U} = \frac{\eta b_w}{b_w} \quad ; \quad \frac{V_T}{V_U} = \frac{(1-\eta)b_w}{b_w} \quad (3-8)$$

where  $\eta b_w$  = the arch breadth, and  $(1-\eta)b_w$  = the truss breadth as shown in the cross-sections of Figure 3–3a and b, respectively.

Figure 3–3d and e illustrates the results of the arch breadth scalar  $\eta$  (Eq. 3-5) when plotted against  $L/jd$  with varying ratios of transverse to longitudinal reinforcement. As one might intuitively expect, this relationship shows that arch action is more prominent in beams with smaller  $L/jd$  and  $\rho_T/\rho_L$  ratios, while truss action has more of an effect in beams with larger  $L/jd$  and  $\rho_T/\rho_L$  ratios. Others have made similar conclusions (Hsu, 1996).

### 3.4 STRESS AND STRAIN TRANSFORMATION FOR FLEXURAL EQUIVALENCE

A primary difficulty associated with truss modeling approaches is the limitation of selecting a single truss model geometry that captures the full elastic and inelastic force-deformation response. For doubly reinforced sections, it is proposed that the longitudinal C-STM flexural chords (members 1-3 (compression), and 2-4-5 (tension) in Figure 3–3c) be aligned with the respective compression steel centroids so that the internal lever arm is represented as  $jd = d - d'$ , where  $d$  and  $d'$  are the respective centroids of the tension and compression steel and  $j = (1 - d'/d)$  is the internal lever arm coefficient. A similar approach was used and validated by Kim and Mander (1999, 2000) in order to incorporate cyclic behavior. However, because the centroids of the steel compression force ( $C_s$ ) and the concrete compression force ( $C_c$ ) may not coincide, it is necessary to transform the concrete constitutive material properties accordingly so that the transposition of the concrete element force ( $C_c$ ) will provide a similar moment in order to satisfy the sectional moment capacity throughout the analysis.

Historically the truss geometry for strut-and-tie models has been mostly based on an elastic stress field analysis and typically ignores the presence of compression steel (Hwang et al., 2000; Drucker, 1961; Thürlimann et al., 1983). Other researchers contend that the use of elastic stress analysis is inappropriate when assessing the ultimate limit state of a structure due to highly nonlinear development of strains associated with D-regions (MacGregor, 1992; Salem and Maekawa, 2006; Yun, 2000; Sritharan and Ingham, 2003). The proposed transformation theory (described below) provides a method that accounts for both compression steel and the nonlinear behavior of concrete compression chord element in accordance with standard stress-block analysis

that is incorporated over the entire range of loading. Figure 3–4a illustrates a standard flexural stress block analysis performed on a doubly reinforced concrete section, assuming plane sections remain plane purely for the purposes of defining the concrete compression force, where the concrete tensile strength is assumed as zero. The neutral axis depth  $c$  can be defined such that  $c = kd$ , where  $k$  is the elastic compression zone coefficient given by Park and Paulay (1975) as:

$$k = \sqrt{(\rho_L + \rho'_L)^2 n^2 + 2(\rho_L + \rho'_L d'/d)n + (\rho_L + \rho'_L)n} \quad (3-9a)$$

For column members an additional modification is made to allow for the axial force given by Eq. (3–9 b) (Arnold, 2004).

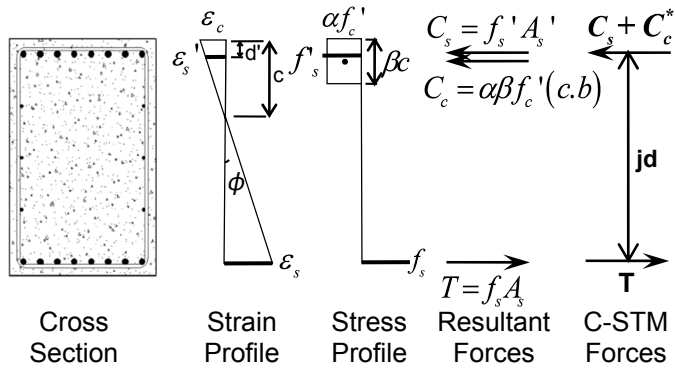
$$k = \sqrt{\left(\rho_L + \rho'_L + \left(\frac{P}{f'_c b d}\right)\left(\frac{f'_c}{f_s}\right)\right)^2 n^2 + 2\left(\rho_L + \rho'_L\left(\frac{d'}{d}\right) + \left(\frac{P}{f'_c b d}\right)\left(\frac{f'_c}{f_s}\right)\right)n - \left(\rho_L + \rho'_L + \left(\frac{P}{f'_c b d}\right)\left(\frac{f'_c}{f_s}\right)\right)n} \quad (3-9b)$$

where  $d$  = the effective depth of the beam from the extreme concrete compression fiber to the centroid of the tension steel;  $d'$  = the depth from the extreme compression fiber to the centroid of the compression reinforcement;  $\rho$  = the ratio of tension reinforcement;  $\rho'$  = the ratio of compression reinforcement;  $n$  = the modular ratio of steel to concrete;  $b$  = the section breadth;  $f'_c$  = concrete compression strength; and  $P$  = axial force plus prestressing force (if any).

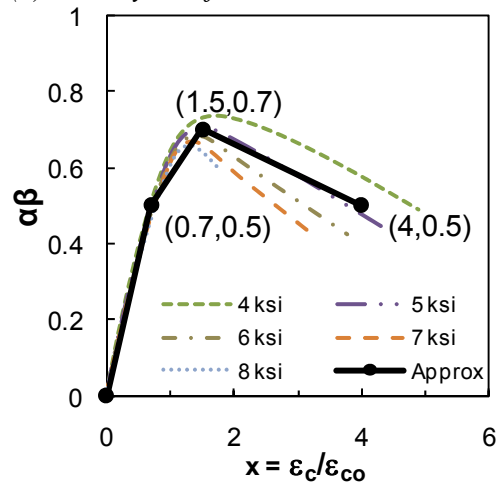
Because the C-STM compression chord member is located at the steel centroid, a transformation of the concrete stress block force  $C_c$  is required to convert it to an equivalent C-STM force that coincides with C-STM compression chord member. Section equilibrium requires:

$$P = (C_s + C_c^*) - T \quad (3-10)$$

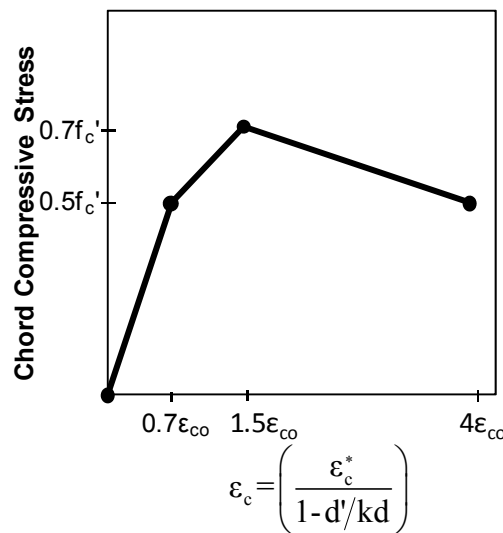
in which  $P$  = the applied axial load ( $P = 0$  for beams);  $T = A_s E_s \varepsilon_s$  (where  $A_s$  = representative area of longitudinal tension steel, and  $\varepsilon_s$  = tensile steel strain);  $C_s = A'_s E_s \varepsilon'_s$  (where  $A'_s$  = representative area of longitudinal compression steel, and  $\varepsilon'_s$  = compression steel strain); and  $C_c^*$  = transformed concrete force discussed below.



(a) Doubly reinforced stress block analysis



(b) Stress block parameters (Karthik and Mander, 2011)



(c) Key stress-strain parameters

Figure 3–4: Constitutive Stress-Strain Relationship for Compression Chord Elements.

The effective concrete strain  $\varepsilon_c^*$  measured by the C-STM chord member can be defined in terms of the extreme compressive concrete strain using the strain compatibility relationships:

$$\varepsilon_c^* = \varepsilon_s' = \varepsilon_c \left( 1 - \frac{d'}{kd} \right) \quad (3-11)$$

Hence, the concrete compression force can be expressed in terms of equivalent concrete stress block and related to  $\varepsilon_s' = \varepsilon_c^*$  as follows:

$$C_c = \alpha\beta f_c'(kd.b) = \varepsilon_c^* \psi E_c A_c \quad (3-12)$$

in which  $\alpha\beta$  = the stress block parameters used to define the equivalent stress block, where  $\alpha$  = effective average concrete stress ratio, and  $\beta$  = effective stress block depth factor;  $f_c'$  = concrete strength;  $\varepsilon_c^*$  = C-STM concrete compression chord strain;  $\psi$  = a compatibility correction scalar; and  $A_c = kd b$  is the area assigned to the concrete chord element.

Rearranging Eq. (3-12) and substituting Eq. (3-11), the compatibility correction scalar can be expressed as:

$$\psi = \frac{\alpha\beta f_c'}{\varepsilon_c^* E_c} = \frac{\alpha\beta}{(1 - d'/kd) xn} \quad (3-13)$$

in which  $x = \varepsilon_c / \varepsilon_{co}$  is the normalized concrete compression strain at the extreme compression fiber;  $\varepsilon_{co} = 0.002$  for unconfined concrete; and  $n = E_c \varepsilon_{co} / f_c'$  (where  $E_c = 60000 \sqrt{f_c'(psi)}$  =  $5000 \sqrt{f_c'(MPa)}$  is the initial tangent modulus) (Mander et al., 1988).

The only remaining unknown variables in Eq. (3-13) are  $\alpha\beta$  and the nonlinear strain,  $x$ . The nonlinear relationship between these two stress block variables is shown in Figure 3–4b (Karthik and Mander, 2011), where a tri-linear relationship is used to approximate the stress block parameters. The key stress-strain parameters for obtaining the concrete chord members constitutive relationship can be obtained through a direct axis transformation as shown in Figure 3–4c: where stress is a function of  $\alpha\beta f_c'$ , and the strain is a function of  $x \varepsilon_{co}$ , as derived from Eq. (3-13). The transformed constitutive relation used for concrete chord members is then



derived by substituting appropriate values of  $f'_c$  and  $(1 - d'/kd)$  into Figure 3–4c. An application of this is presented later.

A similar analysis for singly reinforced beams may be applied where the location of the compression chord member can be defined as follows. For members that do not exceed the elastic limit in the concrete compression stress block, the internal lever arm may be defined such that  $jd = d - kd/3$  (where  $k$  = the elastic compression zone coefficient defined in Eq. 3-9). For members that do exceed the elastic stresses, a more appropriate representation of the internal lever arm may be defined using an ultimate limit state analysis such that  $jd = d - \beta_1 c/2$  (where  $\beta_1$  is the standard code-based stress block factor, and  $c$  is the neutral axis depth calculated by satisfying section equilibrium).

### **3.5 C-STM GEOMETRY AND AXIAL RIGIDITY ASSIGNMENTS**

The C-STM shown in Figure 3–3c can be adapted for any deep beam or disturbed region and modeled using structural analysis software. Each member in the C-STM is comprised of two elements that model the individual behavior of steel and concrete in that member. The two elements are constrained together in order to give the combined steel-concrete response. The C-STM requires the following parameters to be defined in order to model the constitutive behavior of truss members: (i) truss geometry to define the member force; and (ii) axial rigidities of the steel and concrete elements to define elastic deformations.

#### **3.5.1 Truss Geometry**

As previously discussed, the primary difficulty associated with accurate truss modeling is the limitation of selecting a single truss model geometry that captures the force-deformation over a range of both elastic and inelastic response. The truss geometry is defined by first locating the node coordinates for the compression and tension chord members. This is done in accordance with the foregoing section, where the location of the compression chord member varies for doubly and singly reinforced sections.

The horizontal coordinates of the boundary nodes are either defined by: (i) an applied load/bearing support (i.e., Node 5 in Figure 3–3c is defined by the centroid of the applied load);

or (ii) at the intersecting lines of thrust from the beam and column members (i.e., Node 1 in Figure 3–3c is defined at the intersection of the compression steel in the beam and supporting column represented as a fixed boundary). The transverse tension ties in the truss mechanism are then located according to the selected numerical truss as defined in Figure 3–2 (i.e., Nodes 3 and 4 in Figure 3–3c are defined by single-point Gauss quadrature).

### 3.5.2 Axial Rigidity

For each C-STM member, the expected composite steel-concrete response is modeled using separate elements for steel and concrete, respectively. Each element is assigned elastic axial rigidities as specified in Table 3–2, where the member numbers refer to Figure 3–3c. Some comments on Table 3–2 follow.

For tension chord members (row 1 of Table 3–2), the presence of longitudinal distribution steel along the web may be accounted for by using an effective steel area:

$$A_s^* = \frac{\bar{A}_s \bar{d}}{d} \quad (3-14)$$

where  $\bar{A}_s$  = the total area of longitudinal plus distribution reinforcement acting in tension;  $\bar{d}$  = the effective depth to the centroid of  $\bar{A}_s$ ; and  $d$  = section depth to the longitudinal tension reinforcement.

For tension and compression chord members (row 1 and 2 of Table 3–2), the concrete area is assumed to be the same so that cyclic effects can to be accounted for, if necessary.

For transverse truss members (row 3 of Table 3–2), the total area of transverse reinforcement is evaluated as the number of hoops actively participating in the truss mechanism  $N_h$ , where  $N_h = \text{int}[L/s - 1]$  is the number of hoopsets. Also, the effective tension area of concrete for the transverse tie is taken as twice the cover depth ( $c_c$ ) plus the stirrup hoop diameter ( $d_h$ ), multiplied over the length of actively participating hoops ( $N_h s$ ), thus defining the area of concrete surrounding the stirrup legs.

**Table 3–2: Elastic Truss Member Axial Rigidities.**

Member	Steel		Concrete		Comments
	$E$	$A$	$E$	$A$	
2 – 4 4 – 5	$E_s$	$A_s$	$E_c$	$b.kd$	Tension Chord
1 – 3	$E_s$	$A'_s$	$\psi_E E_c$	$b.kd$	*Compression Chord
3 – 4	$E_s$	$N_h A_{sh}$	$E_c$	$(4c + 2d_h) N_h s$	† Active Hoop steel including tension stiffening effect
1 – 5	–	–	$E_c$	$\frac{0.375 \eta b_w jd}{\cos \alpha}$	Concrete Strut in Arch Mechanism
1 – 4	–	–	$E_c$	$\frac{0.5(1-\eta)b_w jd}{\sqrt{0.423 + \tan^2 \alpha}}$	Concrete Strut in Truss Mechanism
3 – 5	–	–	$E_c$	$\frac{0.5(1-\eta)b_w jd}{\sqrt{0.577 + \tan^2 \alpha}}$	Concrete Strut in Truss Mechanism

$$*\psi_E = \text{strain compatibility coefficient} = \frac{\sqrt{f'_c(\text{psi})}}{168(1-d'/kd)} = \frac{\sqrt{f'_c(\text{MPa})}}{14(1-d'/kd)}$$

In lieu of a more precise analysis it is recommended that  $\psi_E = 0.6$

†  $N_h = \text{int}[L/s - 1]$  is the integer part of active hoops in truss mechanism

For the concrete arch member (row 4 of Table 3–2), the strut width is given by Eq. (3-4) and is multiplied by the apportioned arch strut width  $\eta b_w$  to obtain the strut area.

For the concrete strut members in the truss mechanism (row 5 and 6 of Table 3–2), the strut width is defined using Eq. (3-2) (Kim and Mander, 1999, 2000), where the normalized coordinate of the  $i^{\text{th}}$  integration point  $x_i$  is taken as 0.423 and 0.577 (in accordance with Table 3–1) for the concrete elements 1-4 and 3-5, respectively. These are multiplied by the apportioned truss strut width  $(1-\eta)b_w$  to obtain the respective strut areas.

### 3.6 ELEMENT CONSTITUTIVE MATERIAL RELATIONS

The elastic parameters of the C-STM model are defined by the truss geometry and axial rigidities. In order to define the strength of each element, nonlinear constitutive material relationships for cracked reinforced concrete are applied as follows.

### 3.6.1 Reinforcing Steel

For simplicity, the reinforcing steel is approximated using a bi-linear stress-strain relationship with 3 percent strain hardening beyond yielding. Where necessary, a more accurate material model may be applied in order to allow for bond slip or where a bilinear slope does not provide suitable accuracy.

### 3.6.2 Diagonal Concrete Struts

From the works of Vecchio and Collins (1986), Mau and Hsu (1987), and Hsu and Zhang (1997) it is well-known that the compression strength of diagonal concrete struts in reinforced concrete beams and panel elements is reduced as a result of the tensile strain acting orthogonal to the compression strain. This concrete softening phenomenon was investigated by Collins and his research group; one rendition of their work is modeled by the following relationship (Vecchio and Collins, 1986):

$$\zeta = \frac{f_{2,\max}}{f'_c} = \frac{1}{0.8 + 0.34 \left| \frac{\varepsilon_1}{\varepsilon_{co}} \right|} \leq 1.0 \quad (3-15)$$

where  $\zeta$  = the softening coefficient;  $f_{2,\max}$  = the 'softened' concrete strength;  $\varepsilon_{co}$  = the principal compression strain typically taken as 0.002; and  $\varepsilon_1$  = the principal tensile strain acting perpendicular to compression strut.

This relationship is typically incorporated in each step of a hand analysis, or directly embedded into a nonlinear Finite Element Modeling (FEM) formulation where the softening coefficient is continuously updated to satisfy equilibrium (Rots et al., 1985). However, when applying this in commercial structural analysis software (such as SAP2000<sup>TM</sup>, 1995), the user is restricted to the initial input parameters and hence a more direct approximation is required. Accordingly, Eq. (3-15) can be conveniently recast as:

$$\zeta = \frac{1}{1 + \left\langle \frac{\varepsilon_1 - 0.0012}{3 \varepsilon_{co}} \right\rangle} \quad (3-16)$$

where  $\langle \bullet \rangle$  are Macaulay brackets, and the value 0.0012 can be thought of as a fracture strain such that only when  $\varepsilon_1 > 0.0012$  the concrete softens. The strain  $\varepsilon_1$  can be assessed from dummy strain elements (with  $EA=1$ ) perpendicular to the diagonal concrete struts as described later.

Vecchio and Collins (1993) and Belarbi and Hsu (1995) conducted extensive experimental studies to investigate the behavior of softened concrete. Based on the compression softening data obtained from panel test results (Vecchio, 2000) presented in Figure 3–5a the softening coefficient can be represented by:

$$\zeta = \frac{1}{1 - 0.25(\varepsilon_1/\varepsilon_2)} \quad (3-17)$$

where  $\varepsilon_2$  = the compression strain (negative) in the diagonal member. The strains  $\varepsilon_1$  and  $\varepsilon_2$  can be obtained from the C-STM analysis.

In comparing the experimental force-deformation results of C-Beam Specimen 3 with 4 (Mander et al., 2015), it was evident that there needs to be a simple method to discriminate between softened confined and unconfined concrete. Unconfined softened concrete occurs where there is an absence of completely enclosed or hooked hoops around a badly damaged concrete section which results in large transverse strains. It is proposed to distinguish between confined and unconfined softened concrete by the two different softened concrete models shown in Figure 3–5b.

The softened constitutive relations for the diagonal concrete struts can now be defined by modifying the Mander et al. (1988) model to reduce the concrete stress and strain given by:

$$f_c = \frac{\zeta f'_c x^r}{r - 1 + x^r} \quad (3-18)$$

in which  $\zeta f'_c$  = softened concrete stress;  $x = \varepsilon_c / (\zeta \varepsilon_{co})$  is the softened concrete strain coefficient (where  $\varepsilon_{co} = 0.002$ ); and  $r = E_c / (E_c - E_{sec})$  (where  $E_{sec} = f'_c / \varepsilon_{co}$ ). The softened concrete stress-strain relationship can be approximated as a linear response as shown in Figure 3–5b.

### 3.6.3 Concrete Tensile Strength

The contribution provided by the concrete tensile strength, commonly referred to as “tension stiffening” (Vecchio and Collins, 1986), is typically ignored in many force-based strut-and-tie

models (MacGregor, 1992; Collins and Mitchell, 1991; Collins, 1978; Hwang et al., 2000). By assuming strain compatibility between concrete and steel, the overall member tensile force is simply the summation of the steel and concrete forces for a given strain (Collins and Mitchell, 1991; Vecchio and Collins, 1986). Thus the combined steel and concrete elements that make up the tension members 2-4-5, and 3-4 in Figure 3–3c, intrinsically provide the overall tension stiffened response.

Tension stiffening models vary for different situations and structures; hence the following three approaches are recommended for the C-STM:

- For longitudinal and transverse reinforcing steel bars, tension stiffening is modeled by considering a fracture energy method (Petersson, 1980) as shown in Figure 3–6. The fracture energy  $G_f$  is defined as the energy required to create one unit area of cracking in which  $G_f = hg_f$ , where  $h = 3d_a$  is the crack band width taken as three aggregate diameters; and  $g_f$  = the area under the stress-strain softening diagram. The stress-strain relationship is defined using a tri-linear stress-strain relationship given by:

$$f_t = E_c \varepsilon_t \quad \text{for} \quad \varepsilon_t \leq \varepsilon_t' \quad (3-19a)$$

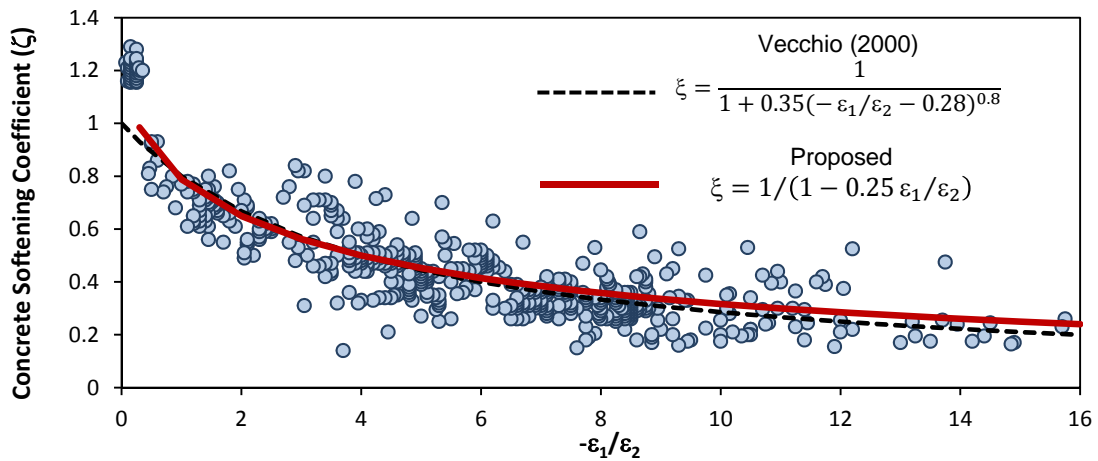
$$f_t = \frac{f_t'}{3} \quad \text{for} \quad \varepsilon_t = \frac{2}{3} \varepsilon_u \quad (3-19b)$$

$$f_t = 0 \quad \text{for} \quad \varepsilon_t = \varepsilon_u \quad (3-19c)$$

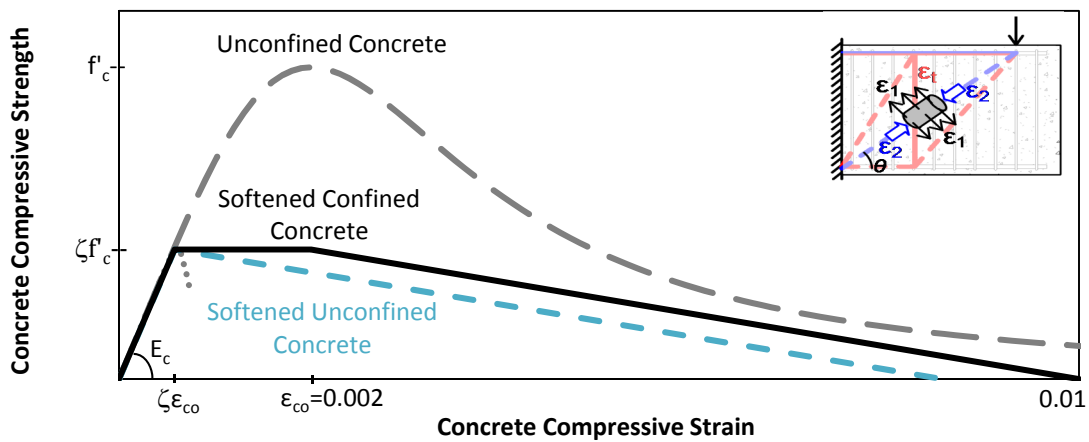
in which  $f_t$  = average concrete tensile stress;  $\varepsilon_t$  = average concrete tensile strain;  $\varepsilon_t'$  = strain at peak tensile stress;  $f_t' = 4\sqrt{f_c'}$  (psi) is typically used to define the concrete tensile strength (Collins and Mitchell, 1991); and  $\varepsilon_u$  = ultimate tensile strain where stress can no longer be transferred and is defined by Eq. (3-20).

$$\varepsilon_u = \frac{18 G_f}{5 f_t' h} \quad (3-20)$$

Based on experimental results, Petersson (1980) noted that the fracture energy  $G_f$  for normal-



(a) Compression Softening Data Obtained from Panel Tests (Vecchio, 2000)



(b) Compression Softened Concrete Model

**Figure 3-5: Diagonal Concrete Elements**

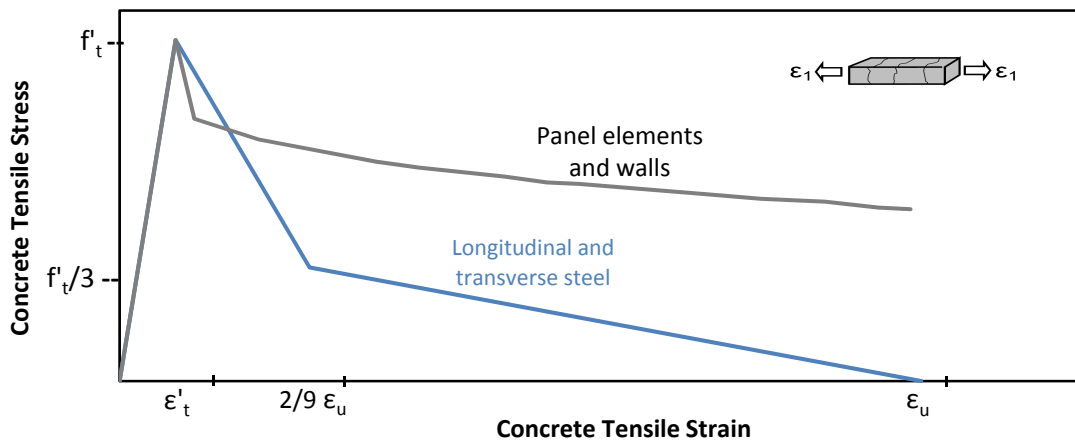


**Figure 3-6: Concrete Tension Stiffening Ties.**

weight concrete typically ranges from  $0.343 - 0.571(\text{lbs/in}) \equiv 60 - 100(\text{N/m})$ . Alternatively, for simplicity,  $\varepsilon_u$  is assumed as the steel yield strain in this work.

- In the case of panel and wall structures with a dense network or reinforcing steel, the descending branch model proposed by Vecchio and Collins (1986) may be more appropriate as shown in Figure 3–6. That is:

$$f_t = \frac{\alpha_1 \alpha_2 f'_t}{1 + \sqrt{500 \varepsilon_t}} \quad \text{for} \quad \varepsilon_t > \varepsilon'_t \quad (3-21)$$

where  $\alpha_1$  and  $\alpha_2$  = factors to account for bond characteristics of reinforcement.

- For structures with experimental results, parameterized models can be applied to model the stress-strain relations used for concrete tension stiffening.

### 3.6.4 Concrete Compression Chord Members

As previously discussed, the transformed constitutive relation used for concrete chord members is derived by substituting appropriate values of  $f'_c$  and  $(1 - d'/kd)$  into Figure 3–4c to obtain the stress-strain relationship of the concrete compression chord member.

### 3.6.5 Modified Material Properties to Account for ASR/DEF

The effects of ASR/DEF on the structure can be taken into account in the C-STM analysis technique by modifying the material properties based on expansion strain modeling, observations, and experimental data. The extent of damage on the structure can be categorized into three classes: 'slight', 'moderate', and 'heavy' damage. Based on this assessment the following material properties should be adopted in the analysis.

#### 1. Assess deteriorated cover concrete properties

The assigned concrete strength within each concrete truss member needs to be appropriately factored to account for the damage caused by ASR/DEF expansion in cover concrete. The modified concrete strength is defined as:

$$f'_{cASR} = \lambda f'_c \quad (3-22)$$



where  $\lambda$  = the strength reduction factor, which is based on the extent of damage observed. The right column of Figure 3–7 shows the average of the modeled transverse tensile expansion strains ( $\varepsilon_1$ ) in the beam and column of the deteriorated C-Beam specimens. The horizontal bands indicate the range of transverse strains for undamaged ( $0 < \varepsilon_1 < 0.0012$ ), '*slight*' ( $0.0012 < \varepsilon_1 < 0.006$ ), '*moderate*' ( $0.006 < \varepsilon_1 < 0.016$ ), and '*heavy*' ( $\varepsilon_1 > 0.016$ ) damage. Substituting the range of  $\varepsilon_1$  values into Eq. (3-16) results in the following range of strength reduction factors; default values of  $\lambda$  are also recommended if precise values of  $\varepsilon_1$  are unknown but the visually observed degree of damage is as indicated by Figure 3–7.

- For '*slight*' damage                       $1 > \lambda > 0.55$                       Default  $\lambda = 0.75$
- For '*moderate*' damage                       $0.55 > \lambda > 0.30$                       Default  $\lambda = 0.40$
- For '*heavy*' damage                       $\lambda < 0.30$                       Default  $\lambda = 0.30$

The out-of-plane photographs and the crack pattern observations presented in Figure 3–7 shows the physical state of the C-Beam specimens that fall into the category of undamaged, '*slight*', '*moderate*', and '*heavy*' damage. Note that the crack pattern on '*moderately*' damaged Specimen 4 looks similar to the crack pattern on the '*heavily*' damaged Specimen 3. However, the cracks in the out-of-plane direction of Specimen 3 were wider compared to Specimen 4. It was also observed that the crack width strains (sum of crack widths/overall width) in the beam and column out-of-plane region were about half that of the surface strains that were measured from the DEMEC points from the same region. Thus, it is possible to relate the crack width strains with the actual expansion strains and thus determine the extent of damage caused by ASR/DEF expansion on the structure from Figure 3–7.

## 2. Assess concrete core confinement properties

ASR/DEF effect causes the concrete to swell. The swelling of core concrete is constrained by longitudinal and transverse reinforcement, which effectively confines the core concrete. To account for this effect the confinement ratio ( $K_{cc} = f'_{cc} / f'_{co}$  where  $f'_{co}$  = in situ concrete strength) has to be determined to obtain the confined concrete stress ( $f'_{cc}$ ). The procedure to evaluate the confinement ratio is described below (Mander et al., 1988).

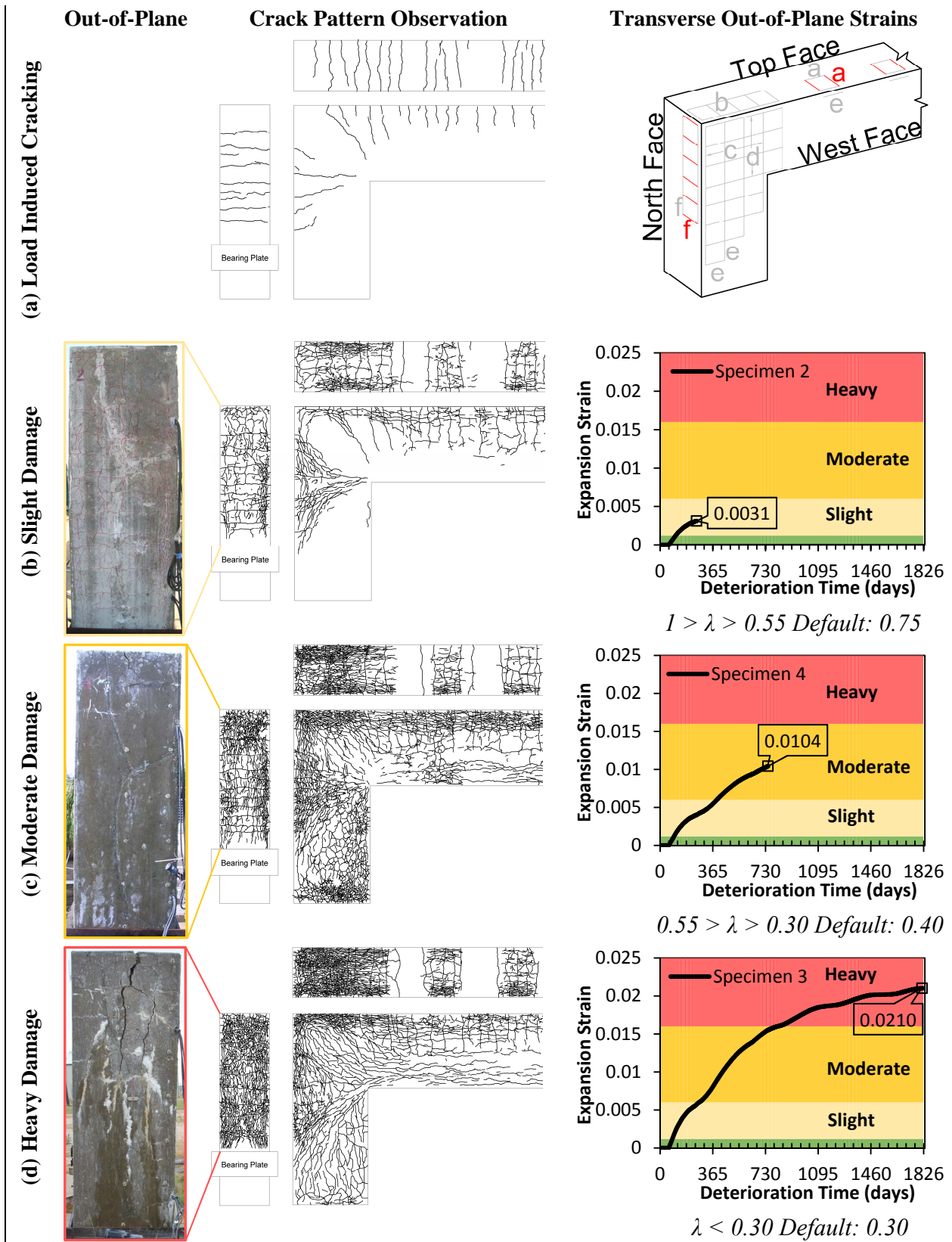


**Figure 3–7: Deteriorated Specimen Appearance, and the Modeled Transverse Strains in the C-Beam Out-of-Plane Direction.**

The effective confining stress in the x and y direction  $f'_{lx}$  and  $f'_{ly}$  are given as:

$$\begin{aligned} f'_{lx} &= k_e \rho_x f_y \\ f'_{ly} &= k_e \rho_y f_y \end{aligned} \quad (3-23)$$

where  $k_e$  = confinement effectiveness coefficient (defined below);  $f_y$  = yield stress of reinforcing steel;  $\rho_x$  and  $\rho_y$  are the volumetric ratio of lateral confining steel parallel to the x and y axis, respectively, given as:

$$\begin{aligned} \rho_x &= \frac{A_{sx}}{sd_c} \\ \rho_y &= \frac{A_{sy}}{sb_c} \end{aligned} \quad (3-24)$$

in which  $A_{sx}$  and  $A_{sy}$  = total area of lateral reinforcement parallel to the x and y axes, respectively;  $s$  = spacing of hoop sets;  $d_c$  = core dimension in y direction; and  $b_c$  = core dimension in the x direction. The confinement effectiveness coefficient ( $k_e$ ) is the ratio of area of effectively confined core concrete ( $A_e$ ) to the concrete core area of the section ( $A_{cc}$ ).

$$k_e = \frac{A_e}{A_{cc}} \quad (3-25)$$

In rectangular sections the transverse steel bows outward between the longitudinal bars, hence arching action will occur between the longitudinal bars that are fully supported in position by an angle bend in the transverse steel as shown in Figure 3–8. The arching action is assumed to take the form of a second degree parabola with an initial tangent slope of 45°. The area of one such parabola is given by  $(w'_i)^2 / 6$ , where  $w'_i$  is the  $i^{th}$  clear transverse spacing between longitudinal bars in which arching action of concrete develops. In the case of a lightly confined rectangular section, the parameter  $w'$  along the y axis is taken as the depth of the neutral axis ( $kd$ ) minus the distance from the extreme compression fiber to the longitudinal bar. The net area of ineffectively confined concrete for the  $n$  longitudinal bars supported in the corners of the bent transverse hoops is given by:

$$\sum_{i=1}^n (w'_i)^2 / 6 \quad (3-26)$$

The total effectively confined core concrete area is defined as:

$$A_e = \left[ b_c d_c - \sum_{i=1}^n (w'_i)^2 / 6 \right] \left( 1 - 0.5 \frac{s'}{b_c} \right) \left( 1 - 0.5 \frac{s'}{d_c} \right) \quad (3-27)$$

in which  $s'$  = clear longitudinal spacing between hoop bars in which arching action of concrete develops.

The concrete core area of the rectangular section is given by:

$$A_{cc} = b_c d_c (1 - \rho_{cc}) \quad (3-28)$$

where  $\rho_{cc}$  = volumetric ratio of longitudinal steel in the confined core. Note that the term  $(1 - \rho_{cc})$  in the above equation effectively removes the presence of longitudinal bars from the confined concrete area. From these the confinement effectiveness coefficient ( $k_e$ ) can be determined from Eq. (3-25).

The ratios  $f'_{lx} / f'_{co}$  and  $f'_{ly} / f'_{co}$  are determined, the smaller of these ratios is taken as  $f'_{l1} / f'_{co}$ , and the larger is taken as  $f'_{l2} / f'_{co}$ . The confinement ratio ( $K_{cc} = f'_{cc} / f'_{co}$ ) is determined from the chart shown in Figure 3-9. Thus, the confined concrete stress is then determined as  $f'_{cc} = K_{cc} f'_{co}$ , where  $f'_{co}$  in situ concrete strength.

The strain ( $\varepsilon_{cc}$ ) corresponding to the maximum confined concrete stress ( $f'_{cc}$ ) is defined as:

$$\varepsilon_{cc} = \varepsilon_{co} (1 + 5(K_{cc} - 1)) \quad (3-29)$$

in which  $\varepsilon_{co}$  = the strain corresponding to the unconfined concrete strength (usually  $\varepsilon_{co} = 0.002$ ).

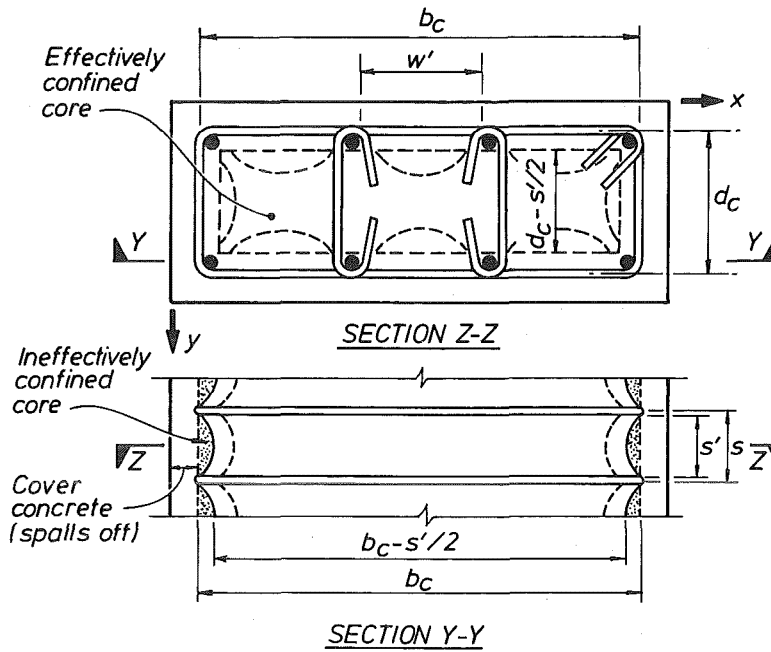


Figure 3-8: Assumed Arching Mechanism Between Hoops for Rectangular Sections (Mander, 1983).

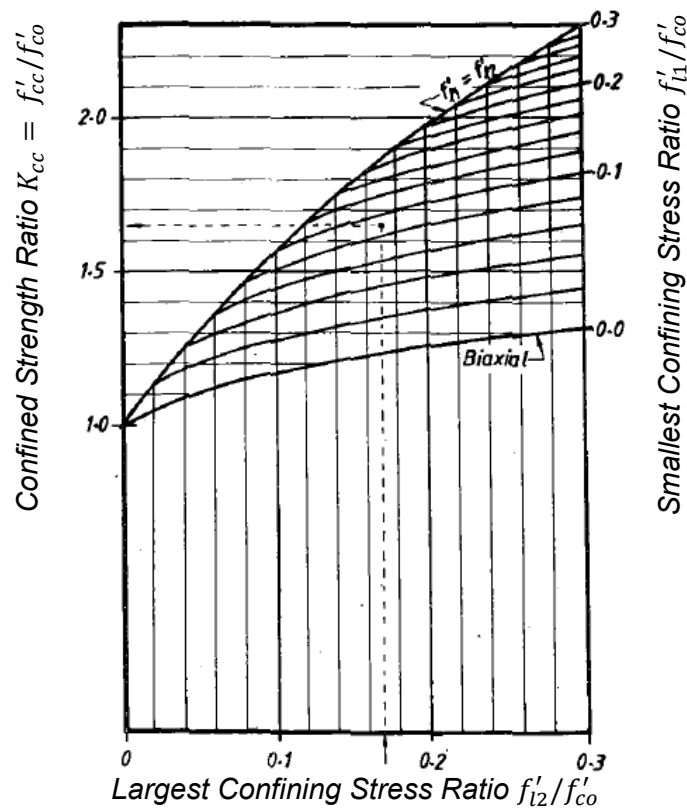


Figure 3-9: Confined Strength Determination from Lateral Confining Stresses for Rectangular Sections (Mander, 1983).

### 3. Compute effective concrete strength

Both the cover and core concrete areas contribute to the area of the struts in the C-STM model. Therefore to account for the reduction in concrete strength in the cover concrete and the effects of confinement in the core concrete, a weighted average concrete strength is computed based on the area contribution of the cover concrete and the core concrete to the overall area of the strut elements.

### 4. Prestress effects in longitudinal bars and hoops

The constraint offered by longitudinal reinforcement and transverse hoops to the swelling of core concrete puts tensile strains on the reinforcing steel, which puts the concrete in a state of prestress. The prestressing forces can be evaluated based on the expansion strains in the specimen, at the end of its exposure period. For this, the expansion model that is formulated and applied to the C-Beam specimens (presented in the following chapters) can be used to determine the expansion strains and hence compute the corresponding prestressing force. In lieu of the above exhaustive expansion strain analysis, the following recommended values can be used.

Depending on the extent of damage ('slight', 'moderate', or 'heavy') due to ASR/DEF effects the following recommendations are made for prestressing stresses ( $f_{ps}$ ) in longitudinal reinforcement:

- slight damage  $f_{ps} = 0.3f_y$
- moderate damage  $f_{ps} = 0.5f_y$
- heavy damage  $f_{ps} = 1.1f_y$

in which  $f_y$  = yield stress of longitudinal reinforcement.

Similarly the recommendation for prestressing stresses in hoops are:

- slight damage  $f_{ps} = 0.5f_{yh}$
- moderate damage  $f_{ps} = 1.0f_{yh}$
- heavy damage  $f_{ps} = 1.25f_{yh}$

in which  $f_{yh}$  = yield stress of transverse hoops.

Appropriate modifications to the stress-strain behavior of the reinforcing steel have to be made to account for the prestressing effects. The modified stress-strain relation of steel is shown in Figure 3–10 in which  $\varepsilon_{ps}$  = prestrain corresponding to prestressing stress ( $f_{ps}$ ).

### **3.7 ULTIMATE STRENGTH AND SOFTENING OF CONSTITUTIVE RELATIONS**

The exact failure mechanism for deep beams or disturbed regions is difficult to define due to unknown (a priori) hierarchy of failure mechanisms, particularly given the fact that shear failure alone can be of four types: diagonal tension, web crushing, nodal failure, or sliding shear. In reality the type of failure is heavily dependent on the member geometry and reinforcement detailing, and is often a combination of events that lead to the formation of the final collapse mechanism. In the C-STM, steel yielding, concrete crushing, and concrete softening are intrinsically accounted for through the material constitutive relationships previously described. However, a more thorough post analysis assessment may be required in order to assess other possible critical failure mechanisms.

#### **3.7.1 Strut-and-Tie Strength Checks**

Strut-and-tie modeling predisposes itself to defining failure as either: yielding of reinforcing ties, crushing of a strut, anchorage failure of reinforcing ties, or nodal failure. The member forces in the C-STM can be used to check that the force does not exceed the strength defined using conventional SAT design procedures for anchorage and nodal failures.

### **3.8 COMPUTATIONAL IMPLEMENTATION**

The computational analysis of the C-STM described in the above sections can be implemented using structural analysis software and carried out in six steps as discussed in what follows.

**Step 1:** Assign node coordinates

For doubly reinforced sections the longitudinal chord members (members 2-4-5 tension, and 1-3 compression of Figure 3–3c) are defined at the respective longitudinal steel centroids. The horizontal coordinates of the boundary nodes are either defined by: (i) an applied load/bearing support (i.e., Node 5 in Figure 3–3c is defined by the centroid of the applied load); or (ii) at the intersecting lines of thrust from the beam and column members (i.e., Node 1 in Figure 3–3c is

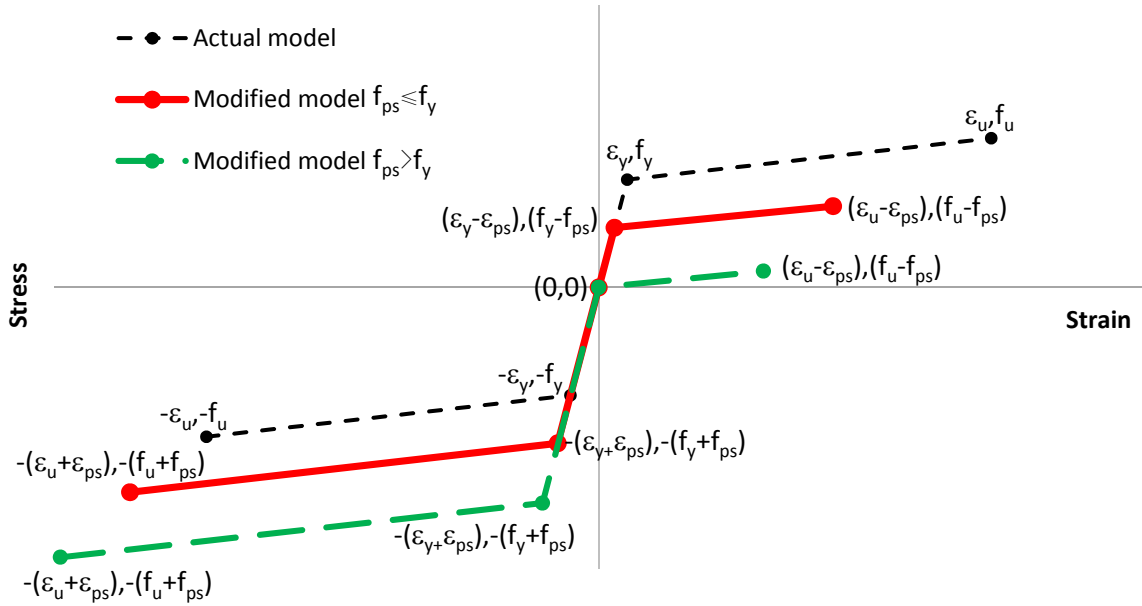


**Figure 3–10: Modified Stress-Strain Model for Steel to Account for Prestressing Effects Due to ASR/DEF.**



defined at the intersection of the compression steel in the beam and supporting column represented as a fixed boundary). The transverse tension ties in the truss mechanism are then located according to the selected numerical truss scheme (i.e., Nodes 3 and 4 in Figure 3–3c are defined by single-point Gauss quadrature).

**Step 2:** Assign steel and concrete elements

The steel and concrete elements of the C-STM can be modeled using separate trusses with nodes constrained together to give the combined steel-concrete member response. This is most easily simulated by duplicating the assigned nodes in the out-of-plane axis to form two separate trusses, and constraining the degrees of freedom for each of the duplicate nodes. Steel and concrete elements are then drawn with pinned-end connections between the appropriate node points as shown in Figure 3–11.

The expressions presented in Table 3–2 are used to define the stiffness and axial area assignments for each steel and concrete element of the C-STM model. The arch breadth scalar  $\eta$  is used to apportion the contribution of arch and truss action defined as a function of the longitudinal and transverse reinforcement and members' span-to-depth ratio given by Eq. (3-5).

Alternatively, the arch breadth scalar can be obtained graphically using Figure 3–3e, where the span to depth ratio is used to determine the arch breadth scalar according to the ratio of transverse to longitudinal reinforcement. Once defined, element areas are assigned as axial cross-sectional areas with an associated material property that defines the elastic stiffness, thus defining the element's axial rigidity.

**Step 3:** Assign nonlinear constitutive material relationships

At this stage, the elastic response of the C-STM is defined by steps 1 and 2; hence nonlinear constitutive material relations for cracked reinforced concrete are now used to define the element's nonlinear behavior. Figure 3–12 shows the theoretical stress-strain relationships used to define the concrete constitutive relations for: (a) diagonal concrete struts; (b) concrete chord members; and (c) concrete tension behavior used in conjunction with all truss elements that also possess steel. To account for the ASR/DEF effects, the modified material properties as discussed in section 3.6.5 have to be considered.

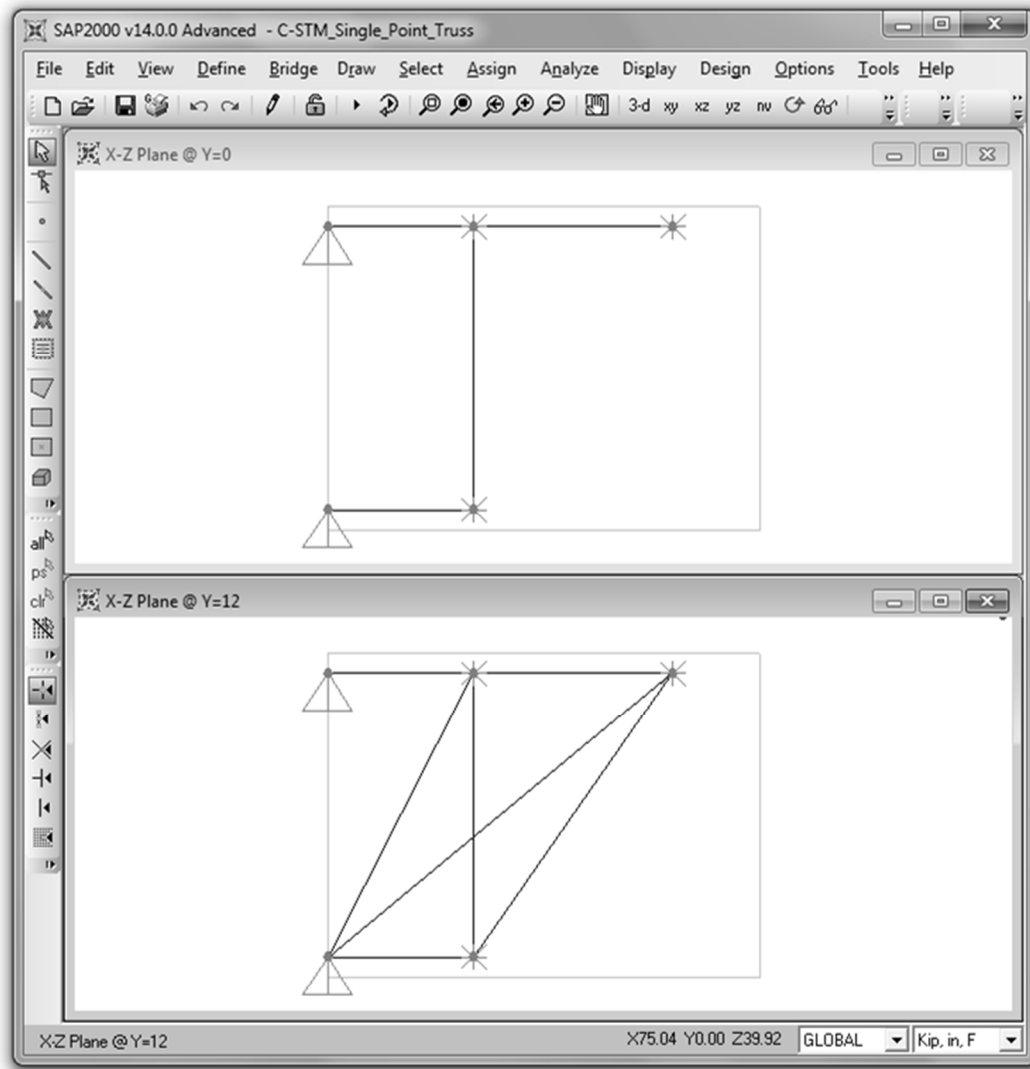
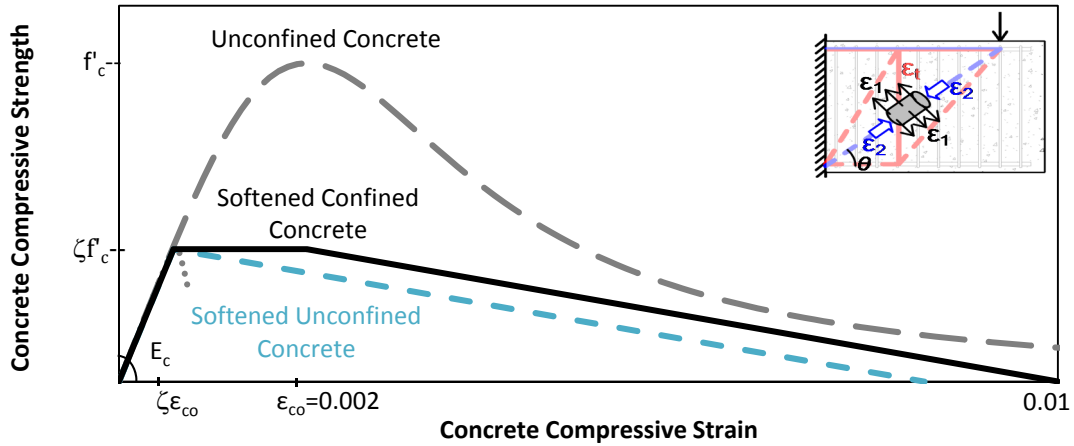
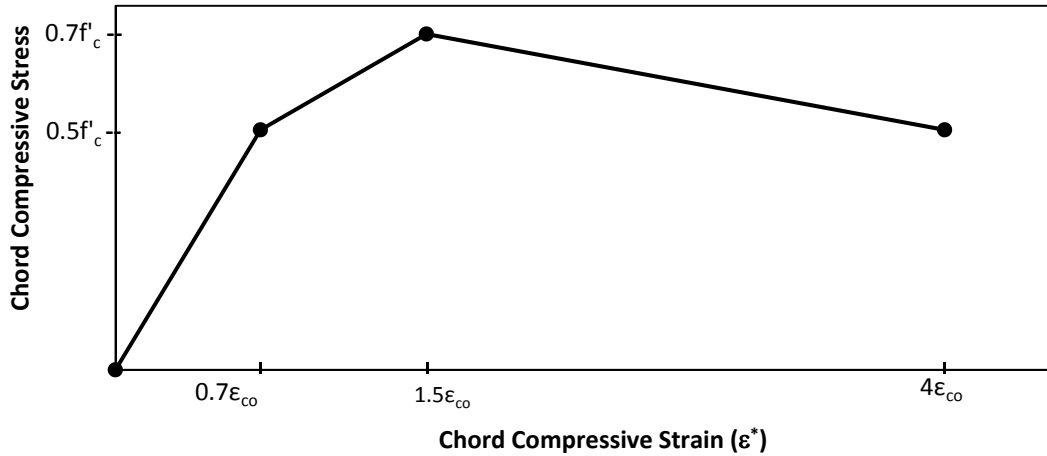


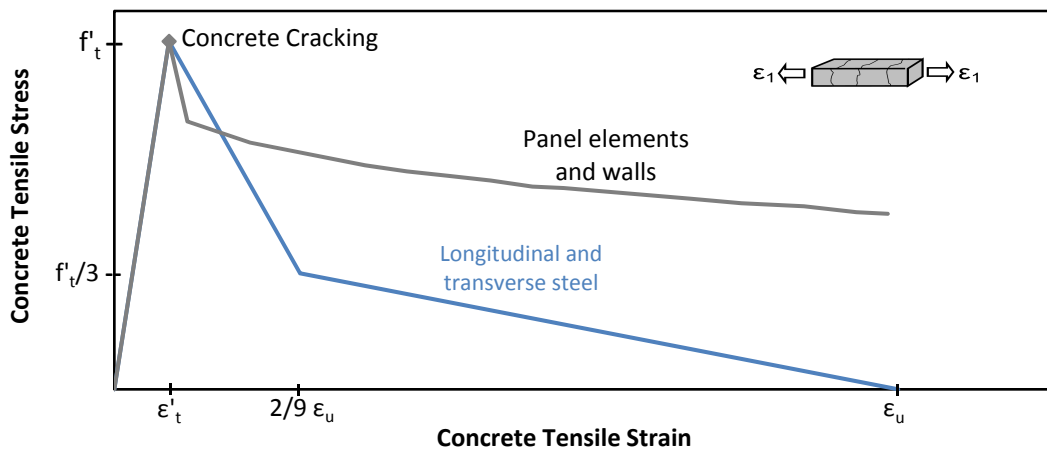
**Figure 3–11: SAP2000 Screenshot: Steel Truss (Top); Concrete Truss (Bottom).**



(a) Diagonal Web Members



(b) Compression Chord Elements



(c) Tension Stiffened Elements

Figure 3–12: Nonlinear Constitutive Material Properties.

**Step 4:** Assign load cases

Load patterns are assigned at node locations as either forces or displacements in order to replicate the structure's loading pattern. Other parameter inputs include: loading control either specified as load or displacement control; incremental step size; results saved at final load or incremental load steps; and other nonlinear parameters. However in SAP2000<sup>TM</sup> (1995), in order to perform an analysis in displacement control, additional joints have to be introduced without altering the structural behavior of the system. Joint displacements are provided at these joints, and the corresponding forces are calculated to obtain the overall force-deformation behavior of the system.

**Step 5:** Run analysis

The analysis can now be run for the desired load cases as input by the user. Once complete, the user can progressively step through the deformed shape to review the formation of nonlinear behavior.

**Step 6:** Post analysis investigation

Axial forces, displacements, and other output parameters can then be exported to a spreadsheet so that a post analysis investigation can be conducted. The axial force in each member can be individually assessed in order to ensure that the force does not exceed any other strength failure criteria (i.e., anchorage failure, nodal crushing, concrete softening, etc.). Because element strains are not given as an explicit output in SAP2000<sup>TM</sup> (1995), an alternative means of defining the strain is required. This can be done using one of the following techniques:

- (a) The element strain can be defined in terms of the element force divided by the axial rigidity as shown below:

$$\varepsilon = \frac{F}{EA} \quad (3-30)$$

where  $EA$  is constant in the elastic range, hence this can only be applied prior to nonlinear behavior.

- (b) For members that reach nonlinear deformations, the strain can be obtained from the link deformations. The link deformations can be divided by their actual member length to obtain the strain in that member.

(c) Alternatively to the above methods, a third truss called a ‘strain-meter truss,’ can be defined in the out-of-plane axis similar to the steel and concrete trusses such that each node is constrained accordingly. Truss elements with a unit axial rigidity (i.e.,  $EA = 1$ ) can be drawn between the desired nodes as *Strain Members* so that the (small) force resisted is equal to the strain as shown in Eq. (3-30). This will provide the composite steel-concrete axial strain associated between the selected two node points. Note: this method was verified in this research using the previously mentioned methods providing identical comparisons for vertical and horizontal members. However, some minor numerical discrepancies were observed in the diagonal concrete members where the results from step (b) would deviate with highly nonlinear behavior.

Application of the C-STM modeling technique is presented in Chapter 6.



## **4. MODELING ASR/DEF EXPANSION IN REINFORCED CONCRETE STRUCTURES**

### **4.1. INTRODUCTION**

Alkali-Silica Reaction (ASR) can be described as a chemical reaction between the alkalis in the cement and the reactive silica in the aggregates, which react to form alkali-silica gel. This gel absorbs moisture and expands causing the concrete to crack. Delayed Ettringite Formation (DEF) is the formation of ettringite in hardened concrete when the concrete is subjected to high temperatures, generally greater than 160°F, during curing and is exposed to moisture later in its life. This, like ASR, causes the hardened concrete to expand and thereby induces tensile cracking.

The effects of ASR and DEF on long-term concrete behavior have been studied extensively over the past few years. Studies have shown that several factors affect ASR expansion in concrete, such as alkali content of the cement, reactivity of aggregates, temperature and humidity among others. The majority of previous studies, however, have concentrated on the effects of ASR on plain concrete; only a few are related to reinforced concrete. It has been established that external restraint (compressive) stresses and passive restraint stresses induced by reinforcement (confinement) can significantly influence the expansion caused by ASR on reinforced concrete (Hobbs, 1988; Jones and Clark, 1996; Multon et al., 2006). The effect of DEF induced expansion on reinforced concrete also has gained significant attention in recent times. Again, there is sufficient evidence to show that externally applied stresses and/or internal restraint stresses induced by confining or longitudinal reinforcement can significantly reduce the expansion caused by DEF in reinforced concrete (Bouzabata et al., 2012).

Although extensive research has been conducted to model the expansion caused by ASR in concrete, a review of past investigations show that a majority of the work has been limited to plain concrete. The effects of compressive stresses on ASR expansion have not been solved by predictive models using the concepts of chemoelasticity (Multon et al., 2006). Additionally, most of the research combines the finite element method with the chemical mechanism to come up with a model for expansion in concrete due to ASR (Ulm et al., 2000; Li and Coussy, 2002; Capra and

Sellier, 2003; to name a few). These methods are complex and difficult to effectively implement in a regular design office engineering practice.

A minimalist semi-empirical strain-based model for the analysis of swelling strains in reinforced concrete members due to ASR/DEF expansion is presented. The validation of the proposed model with experimental observations made on specimens cast and cured in saturated conditions in a laboratory test setting is presented in Mander et al. (2015). Later, modifications are proposed to the model to account for realistic field temperature and moisture content (partial saturation) variations. The validation of the modified model is presented in Mander et al. (2015), where the expansion strains from the model are compared with the observed expansion strains in field-cured large scale specimens showing signs of ASR and DEF.

#### 4.2. MODELING ASR/DEF EXPANSION IN SATURATED PRISMS

Based on an examination of experimental results, expansion over time follows the general form presented in Figure 4–1 for plain and reinforced concrete. Therefore, a semi-empirical model to estimate the expansion strains in reinforced concrete caused due to ASR/DEF expansion over time is developed herein. A hyperbolic tangent function is proposed for the backbone equation which has the general form

$$\varepsilon(t) = \varepsilon_{\rho}^{\max} \tanh \left\langle \frac{t - t_o}{t_r} \right\rangle \quad (4-1)$$

in which  $\varepsilon(t)$  = the expansion strain in reinforced concrete due to the combined effects of ASR and DEF expansion at time  $t$ ;  $\varepsilon_{\rho}^{\max}$  = the maximum expansion in concrete which is a function of reinforcement ratio  $\rho$ ;  $t_o$  = the initiation time when expansion due to ASR/DEF commences;  $t_r$  = the 'rise time' of the hyperbolic tangent line which is the time from the beginning of ASR/DEF induced expansion to when the maximum expansion is reached along the tangent line; and  $\langle \bullet \rangle$  are the Macaulay brackets which represent a common engineering notation used to describe if  $t - t_o < 0$ , then  $(t - t_o) = 0$ . The parameters  $t_o$  and  $t_r$  are empirically determined from the experimental expansion observations.



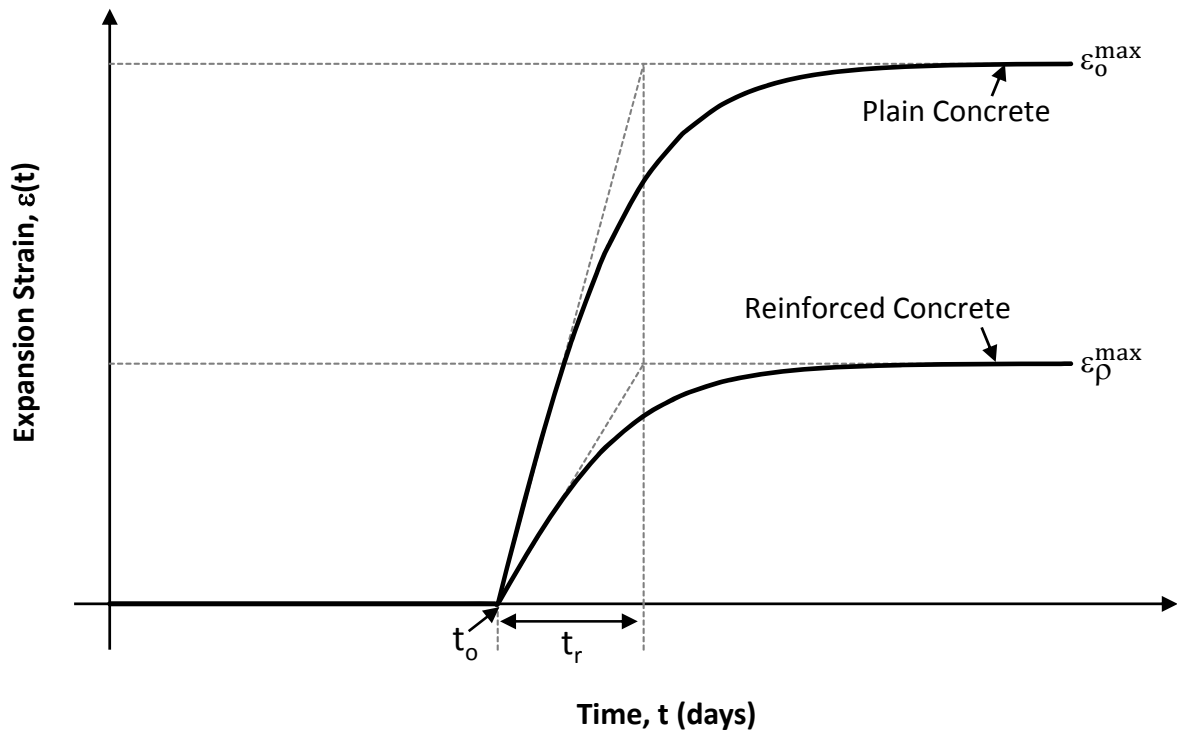


**Figure 4–1: Expansion Model for ASR/DEF Induced Expansion in Concrete.**

The other unknown parameter in (4-1), the maximum expansion in concrete  $\varepsilon_{\rho}^{\max}$ , is determined based on a strain energy approach. The strain energy density ( $u$ ) of the concrete prism of area  $A$ , length  $L$  as shown in Figure 4–2a and subjected to an axial stress,  $\sigma$ , is given by:

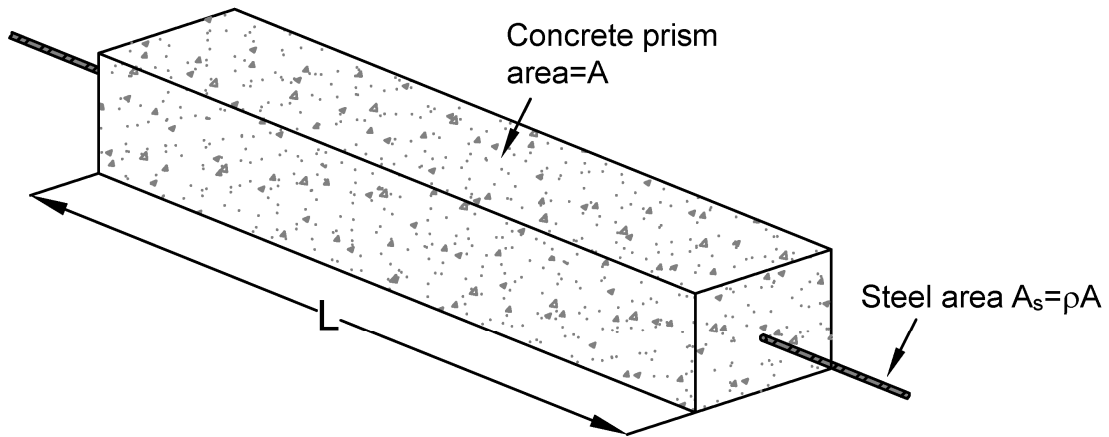
$$u = \int_0^{\varepsilon} \sigma d\varepsilon \quad (4-2)$$

where  $\varepsilon$  and  $\sigma$ , respectively, are the strain and stress. In the simple case, to compute the strain energy in reinforced concrete, the strain energy in concrete ( $U_c$ ) and steel ( $U_s$ ) needs to be calculated.

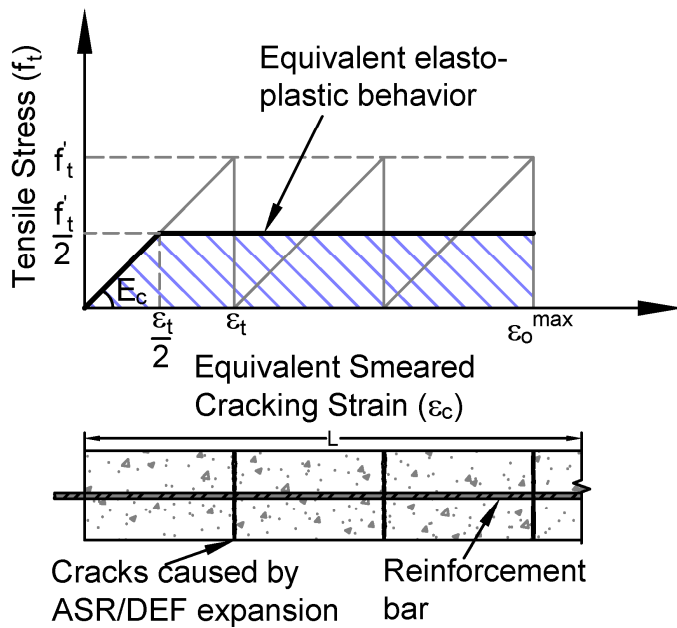
Figure 4–2b shows an equivalent elasto-plastic stress-strain relation of concrete in tension that is adopted for this study. This can be explained as follows. Consider the rectangular concrete specimen in Figure 4–2a with a single reinforcing bar running through the center of the specimen. The longitudinal free expansion of the concrete specimen is restrained by the reinforcing bar. As the ASR/DEF induced expansion within the concrete proceeds over time, the concrete reaches its maximum tensile strength, and a crack forms about the mid-length of the specimen. This results in the concrete tensile strength at the crack to be zero. As further expansion occurs, the maximum concrete tensile strength is reached mid-way on either side of the cracked specimen, resulting in cracks at every quarter–point of the specimen. The next set of cracks are formed at the 1/8<sup>th</sup> points of the concrete specimen. This phenomena may be considered as a 'divide and conquer mechanism'; accordingly the process continues until the cracks are spaced about the maximum aggregate size. At its final cracked state, as shown in Figure 4–2b, the tensile strength of concrete at the cracks will be zero, but the concrete will possess some tensile strength between the cracks. The effective saw tooth model of the tensile stress-strain relation averaged over the length of the prism of concrete can be represented by the equivalent elasto-plastic model shown in Figure 4–2b. The concrete strain energy density which is the shaded area beneath the stress-strain curve shown in Figure 4–2b is given as:

$$u_c = \frac{E_c}{2} \left[ \varepsilon_c^2 - \left\langle \varepsilon_c - \frac{\varepsilon_t}{2} \right\rangle^2 \right] \quad (4-3)$$

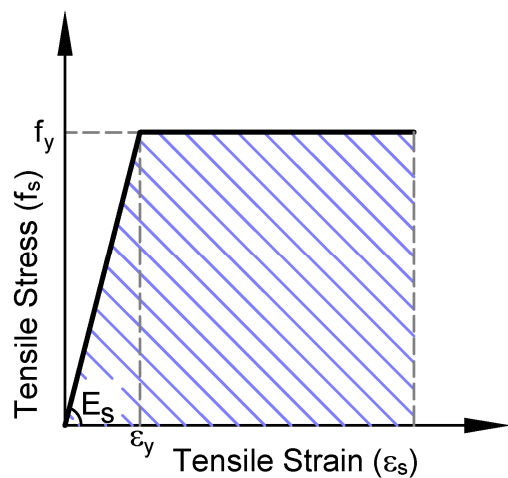
in which  $E_c$  = Young's modulus of concrete;  $\varepsilon_c$  = tensile strain in concrete;  $\varepsilon_t$  = strain



(a) Idealized Reinforced Concrete Prism Subjected to the Expansion Effects of ASR/DEF



(b) Elasto-Plastic Model of Concrete in Tension



(c) Elasto-Plastic Model of Reinforcing Steel

**Figure 4-2: Stress-Strain Models for Components of Reinforced Concrete.**

corresponding to tensile strength of concrete ( $f'_t$ ); and  $\langle \bullet \rangle$  are the Macaulay brackets.

Figure 4–2c shows the elasto-plastic stress-strain relation of reinforcing steel. Depending on the reinforcement ratio of the reinforced concrete structure, two cases require consideration. First, when the expansion strains caused by the combined ASR/DEF expansion are greater than the yield strain of the reinforcing steel and second when the strains are below the yield strain. The strain energy density of steel which is the area under the curve in Figure 4–2c is given by:

$$u_s = \frac{E_s}{2} \left[ \varepsilon_s^2 - \langle \varepsilon_s - \varepsilon_y \rangle^2 \right] \quad (4-4)$$

in which  $E_s$  = Young's modulus of steel;  $\varepsilon_s$  = tensile strain in steel;  $\varepsilon_y$  = yield strain of reinforcing steel. When the strain is below the yield strain, the term in the Macaulay brackets  $\langle \bullet \rangle$  in Eq. (4-4) is set to zero.

Multiplying Eqs. (4-3) and (4-4) with their respective concrete and steel volume gives the total strain energy of concrete ( $U_c$ ) and steel ( $U_s$ ), respectively. Using the principle of conservation of energy, the work done by ASR/DEF related expansion in plain concrete ( $U_{PC}$ ) is equal to the work done by ASR/DEF related expansion in reinforced concrete ( $U_{RC}$ ), that is,

$$U_{PC} = U_{RC} = U_c + U_s \quad (4-5)$$

The maximum strain in plain concrete is represented by  $\varepsilon_o^{\max}$  as shown in Figure 4–2b. Assuming strain compatibility in reinforced concrete results in the same strain in concrete and steel ( $\varepsilon_c = \varepsilon_s$ ). Making necessary substitutions in Eq. (4-5) and rearranging the terms gives the following conditional quadratic equation:

$$\frac{1}{2} \rho n \varepsilon_s^2 \left( 1 - \left\langle 1 - \frac{\varepsilon_y}{\varepsilon_s} \right\rangle^2 \right) + \frac{\varepsilon_t}{2} \varepsilon_s - \frac{\varepsilon_t}{2} \varepsilon_o^{\max} = 0 \quad (4-6)$$

Solving Eq. (4-6) for the two cases, Case I when the expansion strains are beyond the yield strain of the reinforcement and Case II where the expansion strains are lesser than the yield strain, respectively, gives rise to the following two equations:

For  $\varepsilon_s > \varepsilon_y$

$$\varepsilon_\rho^{\max} = \frac{\varepsilon_o^{\max} \left[ 1 + \left( \rho n \frac{\varepsilon_y}{\varepsilon_t} \right) \left( \frac{\varepsilon_y}{\varepsilon_o^{\max}} \right) \right]}{1 + \left( 2\rho n \frac{\varepsilon_y}{\varepsilon_t} \right)} \quad (4-7a)$$

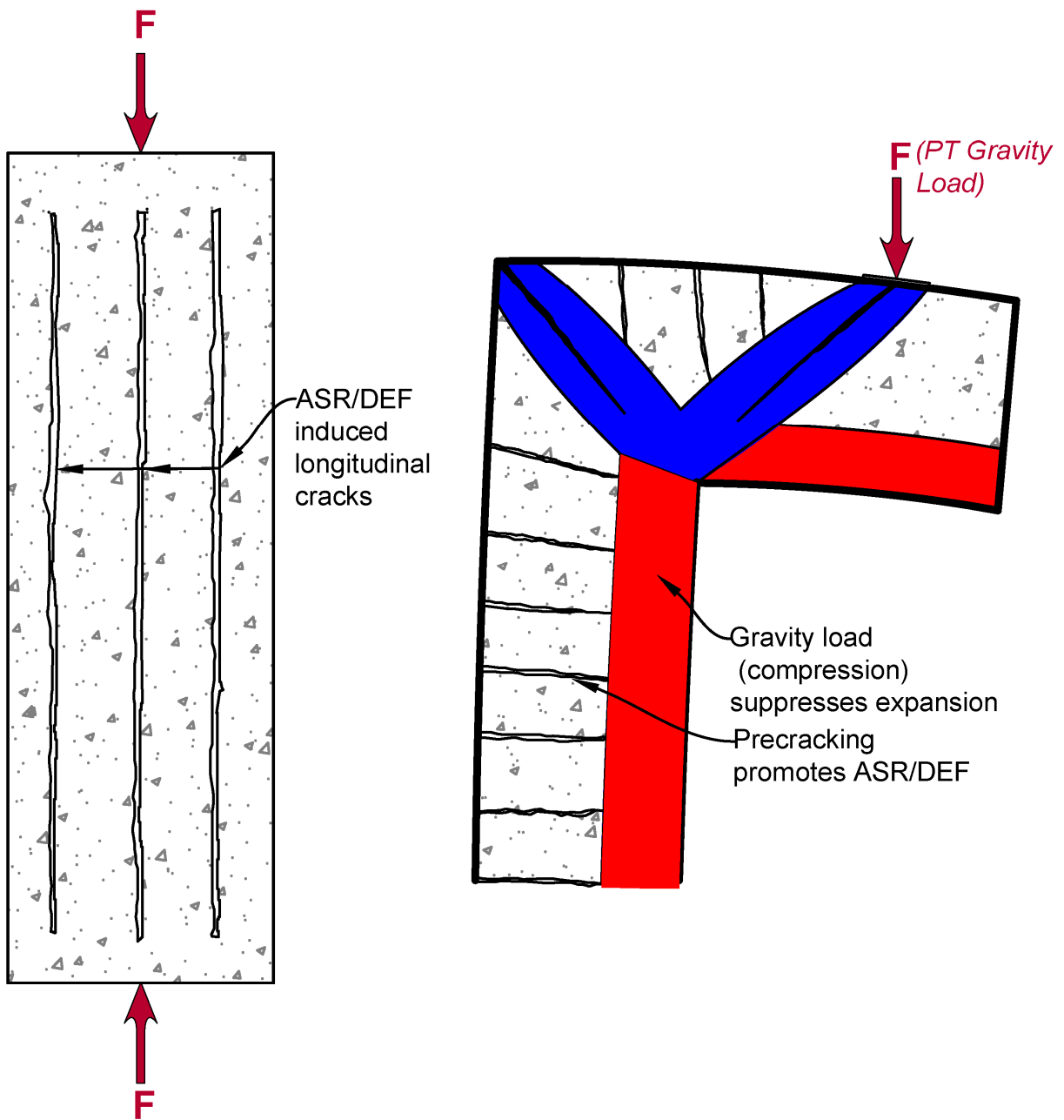
For  $\varepsilon_s < \varepsilon_y$

$$\varepsilon_\rho^{\max} = \frac{\varepsilon_t}{2\rho n} \left[ \sqrt{1 + 4\rho n \frac{\varepsilon_o^{\max}}{\varepsilon_t}} - 1 \right] \quad (4-7b)$$

in which  $\varepsilon_\rho^{\max}$  = the maximum expansion strain possible for a particular reinforcement ratio  $\rho$ . Substituting Eq. (4-7) into Eq. (4-1) gives the expression for ASR/DEF induced expansion strain with time. It is evident from Eqs. (4-1) and (4-7) that the proposed minimalist semi-empirical formulation requires only a few physical parameters, specifically  $\varepsilon_o^{\max}$ ,  $t_0$ , and  $t_r$ . The reinforcement ratio ( $\rho$ ) can be determined from the cross-section properties while the remaining parameters  $\varepsilon_y$  and  $\varepsilon_t$  can be determined knowing the reinforcing steel and concrete material properties.

However, in the presence of post-tensioning compressive loads or cracks induced by tensile loads as shown in Figure 4–3, contributions from the compressive/tensile loads towards ASR/DEF induced expansion need to be accounted for. The derivation of the related equations is presented in what follows.

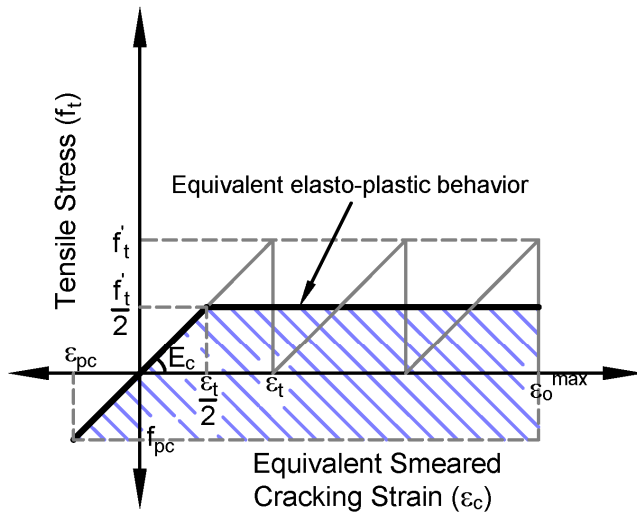
Figure 4–4a shows an equivalent elasto-plastic stress-strain relation of concrete in tension as explained earlier. In the presence of a constant compressive force ( $P$ ) applied across the section, by means of a constant axial load or post-tensioned prestress, the concrete experiences a compressive strain ( $\varepsilon_{pc}$ ) as shown in Figure 4–4a. This compressive effect essentially further increases resistance to the expansion caused by ASR/DEF in reinforced concrete. The concrete strain energy density which is the shaded area beneath the stress-strain curve shown in Figure 4–4a is given as:



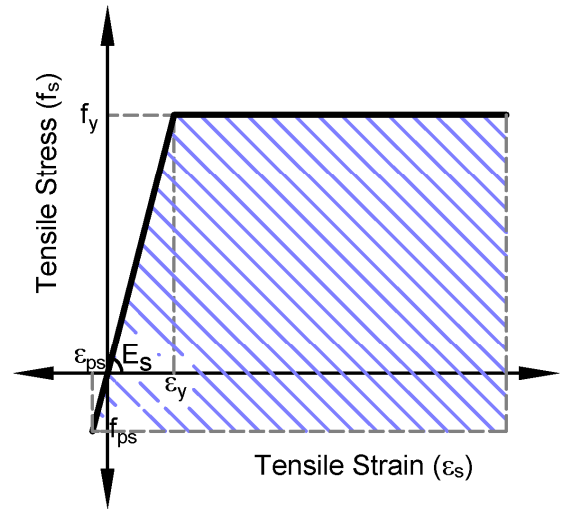
(a) Constant axial load due to PT suppresses expansion

(b) PT gravity load suppresses expansion on the compression side, and precracks promote expansion along the tension side

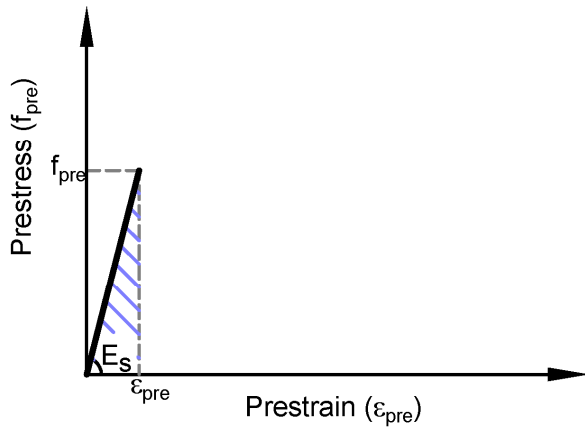
**Figure 4–3: Effects of Compressive and Tensile Loads on ASR/DEF Induced Expansion.**



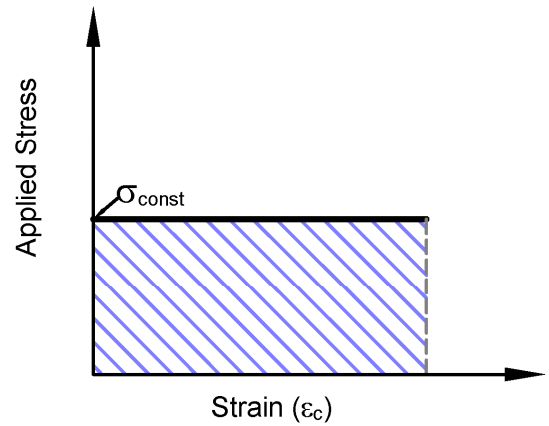
(a) *Elasto-Plastic Model of Concrete in Tension Subjected to Compressive Forces*



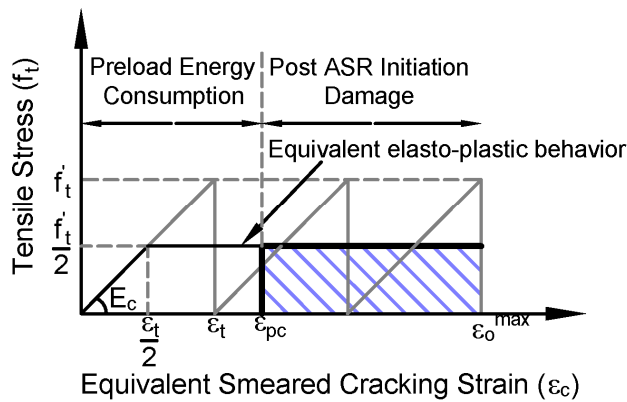
(b) *Elasto-Plastic Model of Reinforcing Steel Subjected to Compressive Forces*



(c) *Elasto-Plastic Model of Prestressing Steel*



(d) *Constant Applied Stress*



(e) *Elasto-Plastic Model of Precracked Concrete in Tension*

**Figure 4-4: Stress-Strain Models for Various Components.**

$$u_c = \frac{E_c}{2} \left[ (\varepsilon_{pc} + \varepsilon_c)^2 - \left\langle \varepsilon_c - \frac{\varepsilon_t}{2} \right\rangle^2 \right] \quad (4-8)$$

in which  $E_c$  = Young's modulus of concrete;  $\varepsilon_c$  = tensile strain in concrete;  $\varepsilon_t$  = strain corresponding to tensile strength of concrete ( $f'_t$ ), and  $\varepsilon_{pc}$  = compressive strain corresponding to the compressive stress in concrete  $f_{pc} = P/(E_c A_c)$  where  $A_c$  = cross-sectional area of concrete.

Figure 4–4b shows the elasto-plastic stress-strain relation of reinforcing steel. Here again, in the presence of applied compressive force the reinforcement experiences a compressive strain ( $\varepsilon_{ps}$ ). Depending on the reinforcement ratio and the compressive load applied on the reinforced concrete structure, two cases have to be considered. First, when the expansion strains caused by ASR/DEF expansion is greater than the yield strain of the reinforcing steel and second when the strains are below the yield strain. The strain energy density of steel which is the shaded area in Figure 4–4b is given by:

$$u_s = \frac{E_s}{2} \left[ (\varepsilon_{ps} + \varepsilon_s)^2 - \left\langle \varepsilon_s - \varepsilon_y \right\rangle^2 \right] \quad (4-9)$$

in which  $E_s$  = Young's modulus of steel;  $\varepsilon_s$  = tensile strain in steel;  $\varepsilon_y$  = yield strain of reinforcing steel, and  $\varepsilon_{ps}$  = compressive strain corresponding to the compressive stress in steel  $f_{ps} = P/E_s A_s$  where  $A_s$  = total cross-sectional area of reinforcing steel.

In the presence of prestressing strands, their contribution to the strain energy density of the structure also needs to be accounted for. The strands are tensioned well below their yield strength, and the area of the shaded region under the stress-strain curve in Figure 4–4c is given as:

$$u_{pre} = \frac{E_s}{2} \varepsilon_{pre}^2 \quad (4-10)$$

in which  $\varepsilon_{pre} = P/(E_s A_{pre})$  = prestrain in the strands where  $A_{pre}$  = area of prestressing strands.

Finally, the constant applied compressive force results in a constant compressive stress ( $\sigma_{const}$ ) across the concrete structure as shown in Figure 4–4d. The strain energy density due to the constant applied stress is given as:



$$u_{const} = \sigma_{const} \varepsilon_c \quad (4-11)$$

Multiplying Eqs. (4-8) through (4-11) with their respective concrete and steel volume gives the total strain energy of concrete ( $U_c$ ), reinforcing steel ( $U_s$ ), prestressing strands ( $U_{pre}$ ), and constant stress ( $U_{const}$ ). Using the principle of conservation of energy, the work done by ASR/DEF related expansion in plain concrete ( $U_{PC}$ ) is equal to the work done by ASR/DEF related expansion in reinforced concrete ( $U_{RC}$ ), which may or may not be subjected to a constant applied load, that is,

$$U_{PC} = U_{RC} = U_c + U_s + U_{pre} + U_{const} \quad (4-12)$$

The maximum strain in plain concrete is represented by  $\varepsilon_o^{\max}$  as shown in Figure 4-4a. Assuming strain compatibility in reinforced concrete results in the same strain in concrete and steel ( $\varepsilon_c = \varepsilon_s$ ). Making necessary substitutions in Eq. (4-12) and rearranging the terms gives the following conditional quadratic equation:

$$\frac{1}{2} \rho n \varepsilon_s^2 \left( 1 - \left\langle 1 - \frac{\varepsilon_y}{\varepsilon_s} \right\rangle^2 \right) + \varepsilon_s \left( \frac{\varepsilon_t}{2} - \varepsilon_{pc} - \rho n \varepsilon_{ps} - \frac{\sigma_{const}}{E_c} \right) - \frac{\varepsilon_t}{2} \varepsilon_o^{\max} + \frac{\varepsilon_{pc}^2}{2} + \frac{\rho n}{2} \varepsilon_{ps}^2 + \frac{\rho_{pre} n}{2} \varepsilon_{pre}^2 = 0 \quad (4-13)$$

in which  $\rho = A_s/A_c =$  reinforcement ratio;  $\rho_{pre} = A_{pre}/A_c =$  prestressing strand ratio; and  $n = E_s/E_c =$  modular ratio. Solving Eq. (4-13) for the two cases, Case I when the expansion strains are beyond the yield strain of the reinforcement and Case II where the expansion strains are lesser than the yield strain (then  $\varepsilon_y = \varepsilon_s$  in Eq. 4-13), respectively, gives rise to the following two equations:

For  $\varepsilon_s > \varepsilon_y$

$$\varepsilon_\rho^{\max} = \frac{\varepsilon_o^{\max} \varepsilon_t + \rho n (\varepsilon_y^2 - \varepsilon_{ps}^2) - \varepsilon_{pc}^2 - \rho_{pre} n \varepsilon_{pre}^2}{2 \left( \frac{\varepsilon_t}{2} - \varepsilon_{pc} + \rho n (\varepsilon_y - \varepsilon_{ps}) - \frac{\sigma_{const}}{E_c} \right)} \quad (4-14a)$$

For  $\varepsilon_s < \varepsilon_y$

$$\varepsilon_\rho^{\max} = \frac{\frac{\varepsilon_t}{2} - \varepsilon_{pc} - \rho n \varepsilon_{ps} - \frac{\sigma_{const}}{E_c}}{\rho n} \left( \pm \sqrt{1 - \frac{\rho n (\varepsilon_{pc}^2 + \rho n \varepsilon_{ps}^2 + \rho_{pre} n \varepsilon_{pre}^2 - \varepsilon_t \varepsilon_o^{\max})}{\left( \frac{\varepsilon_t}{2} - \varepsilon_{pc} - \rho n \varepsilon_{ps} - \frac{\sigma_{const}}{E_c} \right)^2}} - 1 \right) \quad (4-14b)$$

In Eq. (4-13) and (4-14)  $\varepsilon_{pc}$ ,  $\varepsilon_{ps}$ , and  $\sigma_{const}$  are positive for tensile strains induced by tensile loads and negative for compressive strains induced by compressive loads. In the case where no prestressing strands are present,  $\rho_{pre} = 0$ . The parameters  $\varepsilon_{pc}$ ,  $\varepsilon_{ps}$ ,  $\varepsilon_{pre}$ , and  $\sigma_{const}$  can be determined from the applied axial load  $P$  and corresponding cross-sectional areas. In the case of a reinforced concrete member without constant applied loads or prestress the terms  $\varepsilon_{pc}$ ,  $\varepsilon_{ps}$ ,  $\varepsilon_{pre}$ , and  $\sigma_{const}$  are zero.

The work done by ASR/DEF expansion on concrete is further reduced if the concrete is pre-cracked due to tensile prestrains, that is,  $\varepsilon_{pc} > \varepsilon_t$ . In this case the concrete strain energy density which is the shaded area beneath the stress-strain curve shown in Figure 4–4e is given by:

$$u_c = \frac{E_c}{2} \left[ \varepsilon_t (\varepsilon_c - \varepsilon_{pc}) \right] \quad (4-15)$$

Equating the work done by ASR/DEF related expansion in plain concrete and reinforced concrete as before, the maximum expansion can be computed using the following equations:

For  $\varepsilon_s > \varepsilon_y$

$$\varepsilon_\rho^{\max} = \frac{\varepsilon_o^{\max} \varepsilon_t + \rho n (\varepsilon_y^2 - \varepsilon_{ps}^2) + \varepsilon_t \varepsilon_{pc} - \left(\frac{\varepsilon_t}{2}\right)^2}{2 \left( \frac{\varepsilon_t}{2} + \rho n (\varepsilon_y - \varepsilon_{ps}) - \frac{\sigma_{const}}{E_c} \right)} \quad (4-16a)$$

For  $\varepsilon_s < \varepsilon_y$

$$\varepsilon_\rho^{\max} = \frac{\frac{\varepsilon_t}{2} - \rho n \varepsilon_{ps} - \frac{\sigma_{const}}{E_c}}{\rho n} \left( \pm \sqrt{1 - \frac{\rho n \left( \rho n \varepsilon_{ps}^2 + \rho_{pre} n \varepsilon_{pre}^2 - \varepsilon_t \varepsilon_o^{\max} - \varepsilon_t \varepsilon_{pc} + \left(\frac{\varepsilon_t}{2}\right)^2 \right)}{\left( \frac{\varepsilon_t}{2} - \rho n \varepsilon_{ps} - \frac{\sigma_{const}}{E_c} \right)^2}} - 1 \right) \quad (4-16b)$$

In Eqs. (4-14b) and (4-16b) it is important to consider only the positive value of  $\varepsilon_\rho^{\max}$  as it is an expansive strain and cannot be negative. Substituting the relevant expression for  $\varepsilon_\rho^{\max}$  into Eq. (4-1) gives the expression for ASR/DEF induced expansion strain with time.

The validation of the proposed expansion model for ASR and DEF related expansion in small scale laboratory tests is presented in Mander et al. (2015).

### 4.3. MODIFICATIONS TO ACCOUNT FOR TEMPERATURE AND MOISTURE VARIATIONS

It is well known that the reactive material content, and various environmental factors such as temperature and humidity, stress conditions, boundary restraint, and moisture supply, all affect the extent of expansion strain caused by the ASR/DEF in concrete. Of these the reactive material content is implicitly taken into account when estimating the parameters  $\varepsilon_o^{\max}$ ,  $t_o$ , and  $t_r$ . The effects of the restraints are also taken into account in the expression proposed for maximum expansion  $\varepsilon_\rho^{\max}$ . To account for the effects of the other two important factors, temperature and moisture content (degree of saturation), necessary modifications to the proposed expansion equation are considered here. Implicit in the earlier development of the proposed equations were: (i) constant temperature; and (ii) saturated conditions (water bath) were used for curing. However, the temperature and moisture content conditions of an actual structure subjected to ASR/DEF

expansion may vary on a daily basis. To account for these real field temperature and moisture variations, modifications are proposed to Eq. (4-1) to include their effects.

Eq. (4-1) can be slightly modified to include the effects of temperature ( $T$ ):

$$\varepsilon_{t,T} = \varepsilon_{\rho}^{\max} \tanh \left\langle \frac{t-t_o}{t_{r,T}} \right\rangle \quad (4-17)$$

where the parameters are defined as before and  $\varepsilon_{\max}(\rho)$  is given by Eqs. (4-14) or (4-16).

Ulm et al. (2000), defined the characteristic time ( $\tau_c$ ) associated with ASR product formation as:

$$\tau_c(\theta) = \tau_c(\theta_o) \exp \left[ \frac{U_c}{\theta\theta_o} (\theta_o - \theta) \right] \quad (4-18)$$

in which  $\tau_c(\theta_o)$  = characteristic time at standard temperature of  $\theta_o = 311^\circ\text{K} = T_o = 38^\circ\text{C}$  ( $100^\circ\text{F}$ ) and  $U_c = 5400 \pm 500 \text{ K} =$  activation energy constant of the characteristic time  $\tau_c$ .  $(\theta_o - \theta)^\circ\text{K}$  can be re-written as  $(T_o - T) = -\Delta T^\circ\text{C}$  (say). By the definition of the two terms  $\tau_c$  and  $t_r$ ,  $t_r \approx 2\tau_c$ . Therefore, the rise time of the tangent line ( $t_r$ ) is assumed to follow the same relation as Eq. (4-18) proposed by Ulm et al. (2000) i.e.,

$$t_r(\theta) = t_r(\theta_o) \exp \left[ \frac{U_c}{\theta\theta_o} (\theta_o - \theta) \right] \quad (4-19)$$

Substituting for  $\theta = \theta_o + \Delta T$ ,  $U_c = 5400^\circ\text{K}$  and as  $\Delta T \ll \theta_o (=311^\circ\text{K})$  then  $\Delta T/\theta_o \rightarrow 0$ , thus Eq. (4-19) may be simplified to give

$$t_{r,T} = t_{r,T_o} \exp \left( \frac{T_o - T}{18} \right) \quad (4-20)$$

Finally substituting  $T_o = 38^\circ\text{C}$  in Eq. (4-20) leads to

$$t_{r,T} = t_{r,T_o} \exp \left( \frac{38 - T}{18} \right) \quad (4-21)$$

which may now be substituted into Eq. (4-17) to give

$$\varepsilon_{t,T} = \varepsilon_{\rho}^{\max} \tanh \left( \exp \left( \frac{T-38}{18} \right) \left\langle \frac{t-t_o}{t_{r,T_o}} \right\rangle \right) \quad (4-22)$$

Eq. (4-22) gives the modified expression for the expansion caused by ASR/DEF in reinforced concrete taking into consideration the temperature variations.

To account for the variations in moisture content, necessary modifications to Eq. (4-22) needs to be made. Figure 4-5 shows the variation of characteristic time ( $\tau_c$ ) at 311°K with the degree of saturation ( $S$ ), where the data points are adapted from Ulm et al. (2000). The experimental data can be reasonably well represented by the exponential function  $e^{1-S}$ . Incorporating this into the modified equation Eq. (4-22) leads to the following overall time-dependent expansion strain model.

$$\varepsilon_{t,T,S} = \varepsilon_{\rho}^{\max} \tanh \left( \exp \left( \frac{T}{18} + S - 3.11 \right) \left\langle \frac{t-t_o}{t_{r,T_o}} \right\rangle \right) \quad (4-23)$$

Eq. (4-23) represents the proposed model modified for temperature and moisture content variations, for expansion strains in reinforced concrete caused by ASR/DEF expansion. Note that at standard temperature of 38°C (100°F) and degree of saturation of  $S = 1$ , Eq. (4-23) reverts back to Eq. (4-1).

Differentiating Eq. (4-23) with respect to time gives the expansion strain rate as follows:

$$\dot{\varepsilon}_{t,T,S} = \frac{\varepsilon_{\rho}^{\max}}{t_{r,T_o}} \exp \left( \frac{T}{18} + S - 3.11 \right) \left[ 1 - \left( \frac{\varepsilon_{t,T,S}}{\varepsilon_{\rho}^{\max}} \right)^2 \right] \quad (4-24)$$

which is an ordinary differential equation with variable coefficients dependent on temperature and degree of saturation,  $T$  and  $S$ . Because in field conditions  $T$  and  $S$  vary constantly, Eq. (4-24) requires a numerical solution as follows:

$$\varepsilon_{i+1} = \varepsilon_i + \left( \dot{\varepsilon}_{t,T,S} \right)_i \Delta t \quad (4-25)$$

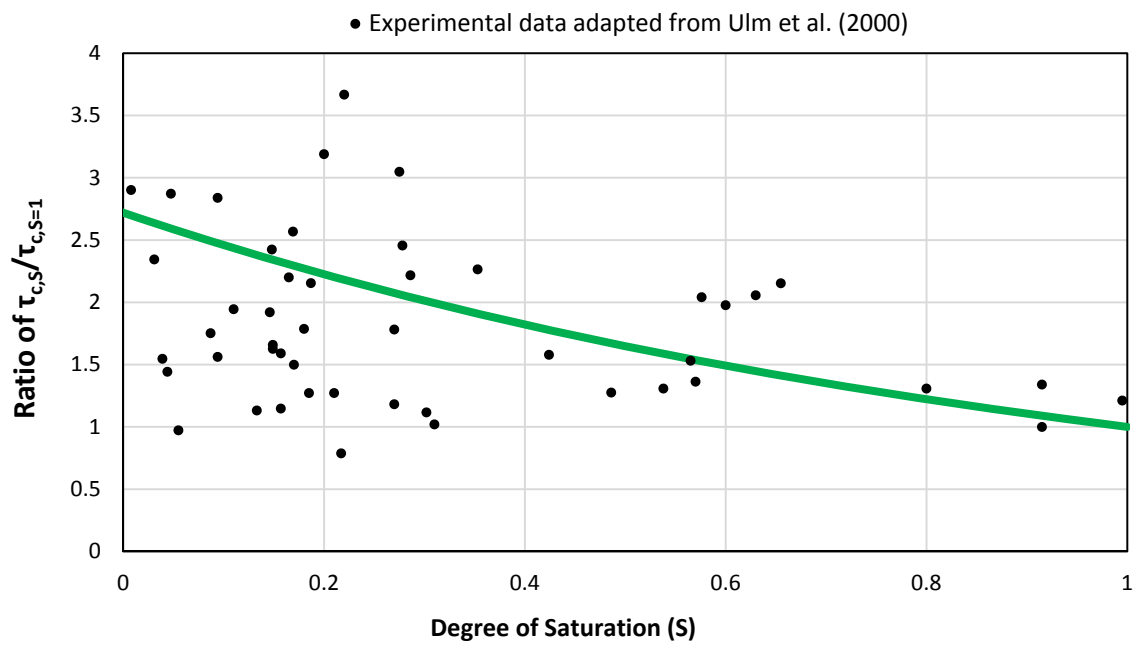


**Figure 4-5: Variation of Characteristic Time with Relative Weight Increase.**

in which  $\Delta t$  = time increment and the parameters with subscript ‘ $i$ ’ denote their value at the  $i^{th}$  time interval; and  $(\dot{\epsilon}_{i,T,S})$  is the temperature and saturation dependent strain rate given by Eq. (4-24). Eq. (4-25) can be easily solved computationally in an incremental time-stepping fashion. Daily temperatures and degree of saturation (assessed from rainfall records) are used directly in Eq. (4-24).

The validation of the developed theory is presented in Mander et al. (2015), where the theory is used to model the expansion strains in post-tensioned reinforced concrete members which were exposed to environmental conditions and as a result subjected to the daily variations in temperature and moisture content.

#### **4.4. CLOSURE AND KEY FINDINGS**

The existing models on predicting the expansion caused by ASR/DEF are limited mainly to plain concrete. Additionally, they are complex and typically require a finite element model to implement their effects on structures. In this chapter a semi-empirical minimalist model was proposed which is capable of estimating the expansion in reinforced concrete structures caused by ASR/DEF. The model requires only a limited number of input factors that are related to the expansion characteristics and the material properties. The key findings from this study are summarized below:

- The proposed model can simulate the expansion caused by ASR and/or DEF in laboratory specimens cured under standard laboratory conditions to accelerate ASR/DEF expansion.
- It is necessary to extend the basic laboratory-based model to take into account the widely varying field conditions in temperature and moisture (degree of saturation).
- The effects of compressive and tensile pre-strains are included in the model. This is an important aspect as compressive forces suppress the expansion caused by the ASR/DEF mechanisms, whereas tensile forces and initial cracking further promote and accelerate the ASR/DEF induced expansion.
- By taking into account the appropriate reinforcement ratios, the proposed model can simulate the expansion strains in both the longitudinal and transverse directions.

Detailed example on the application of ASR/DEF expansion model to the C-Beam specimens is presented in Chapter 5.



## **5. WORKED EXAMPLE: DETERMINING EXPANSION STRAINS CAUSED BY ASR/DEF**

### **5.1. INTRODUCTION**

As part of a large scale experimental program described in the Phase I report of this research (Mander et al., 2012b), reinforced concrete C-Beam specimens representing cantilever and straddle bent bridge piers were cast and cured to promote ASR/DEF induced expansion in reinforced concrete. The reinforcement layout and the cross-section details of the C-Beam specimen are presented in Figure 5–1. To promote ASR in the specimen, high alkali content cement and aggregates with reactive silica along with sodium hydroxide mixed in water were used. The specimens were subjected to curing temperatures in excess of 160°F by means of an electrical resistive wiring setup to promote DEF related expansion in the specimen. The specimens were then transported outdoors and subjected to environmental conditions, as any actual bridge under service would be exposed to. To accelerate the expansion caused by ASR/DEF for purposes of the experimental study, a sprinkler system was installed and the specimens were sprinkled with water at regular intervals. Of the four specimens constructed, Specimen 1 was the control specimen and was stored indoors, while Specimens 2, 3, and 4 were conditioned outdoors and subjected to ASR/DEF deterioration for varying periods of time.

Of the three deteriorated C-Beam specimens, Specimen 3 was conditioned in the field for five years with significant effects of ASR and DEF deterioration observed. The data from the strain and concrete gages embedded in the specimen, and DEMEC points on the surface of the specimen were collected on a regular basis. This chapter shows the application of the proposed expansion model to C-Beam Specimen 3. A comparison of the modeled expansion results with the field data is presented in Mander et al. (2015).

### **5.2. PARAMETERS FOR MODELING EXPANSION IN C-BEAM SPECIMEN**

To represent the expansion strains in the C-Beam specimen in a meaningful and logical way, the C-Beam specimen was divided into different regions. Figure 5–2a identifies the various regions of the C-Beam specimen used in this study to model expansion strains. The C-Beam specimen is

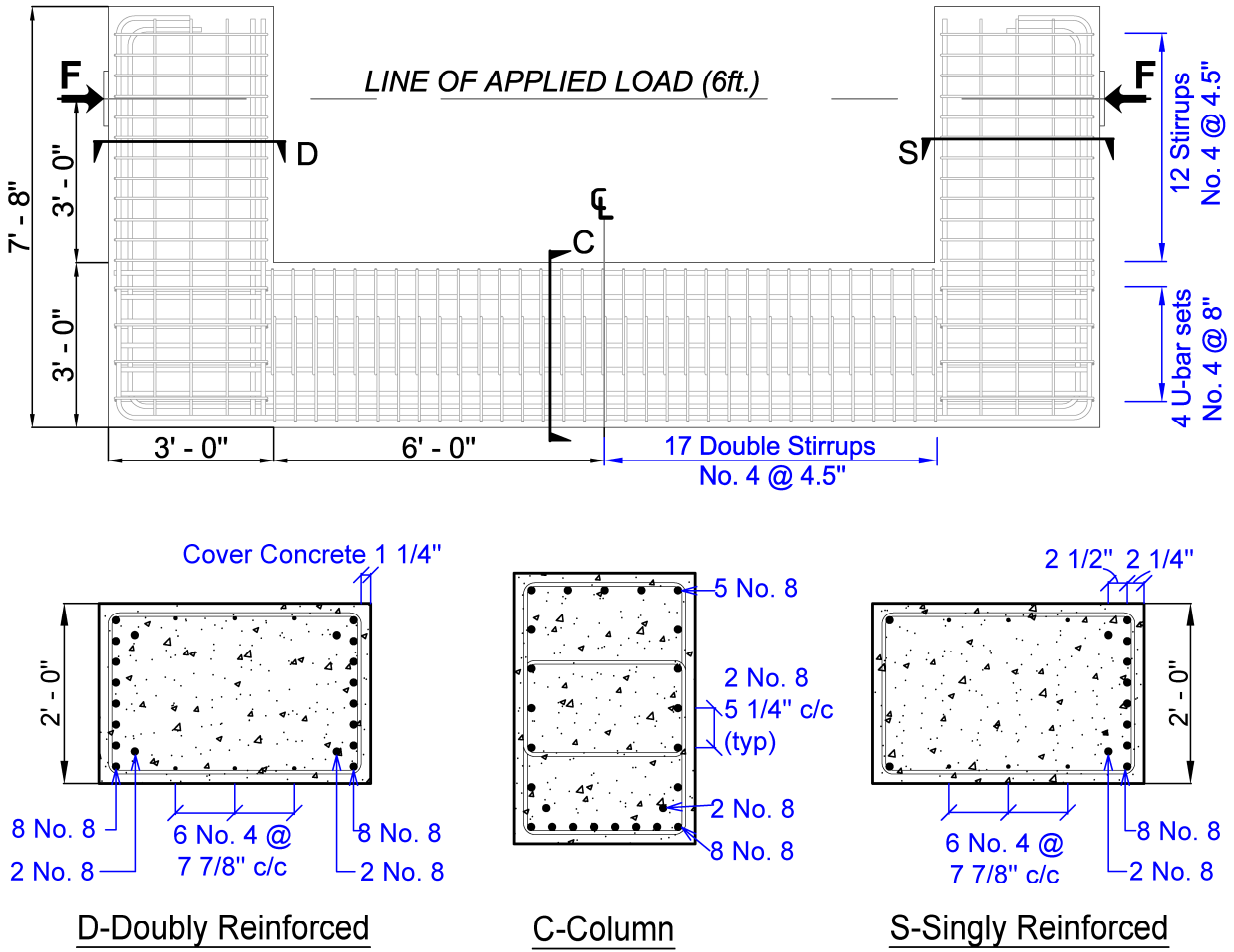
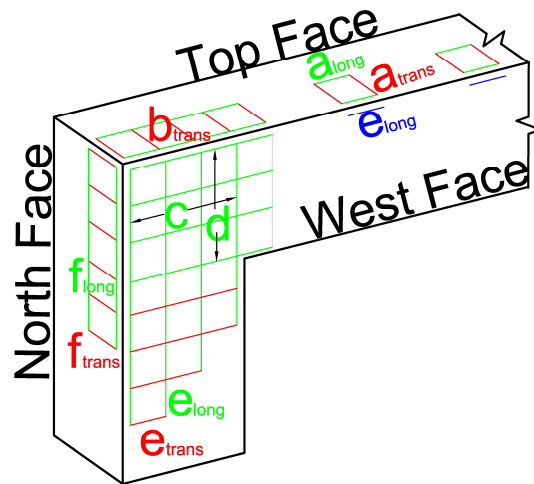


**Figure 5-1: Reinforcement Layout of C-Beam Specimen.**

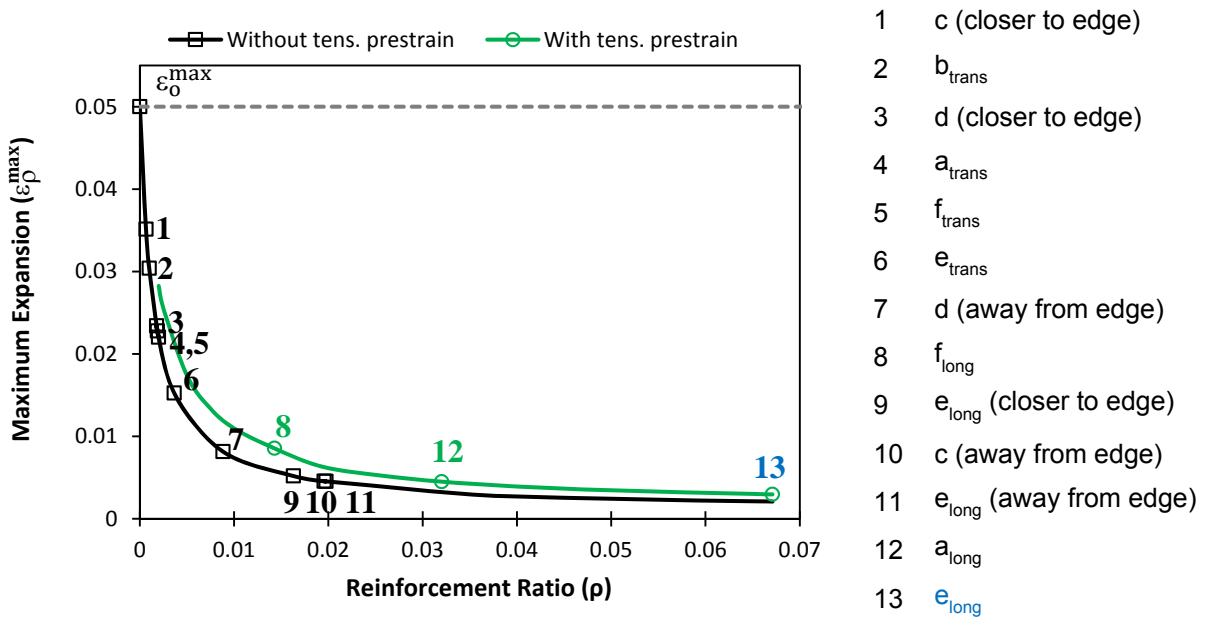
divided into the top face where the exposure face is horizontal, and the west and north side faces where the exposure face is vertical. Figure 5–2a also shows the location and orientation of DEMEC points on the surface of the C-Beam specimen.

The C-Beam specimens were subjected to both ASR and DEF expansion. Since no clear evidence was available on when and how much each of the two expansion mechanisms contributed toward the total expansion strains in the specimen, the proposed expansion equation was applied once, considering the overall expansion properties. From the experimental results presented in Mander et al. (2012b, 2015), the time ( $t_o$ ) when expansion strains initiate was taken as 60 days. The rise time of the tangent line ( $t_r$ ) was deduced to be 120 days from the expansion data of Specimen 3. Since no data was available on the expansion caused by ASR/DEF expansion in plain concrete ( $\epsilon_o^{\max}$ ), this parameter was inferred from the largest crack observed from an unreinforced part of the specimen. The largest crack that was observed at the knee joint of the C-Beam specimen was about 1.18 inches wide. It is to be noted that the top face of the column in the joint region was essentially unreinforced. A crack width of 1.18 inches across a total section width of 24 inches, resulted in an expansion strain of approximately 0.05. Therefore, for this study the value of  $\epsilon_o^{\max} = 0.05$  was adopted.

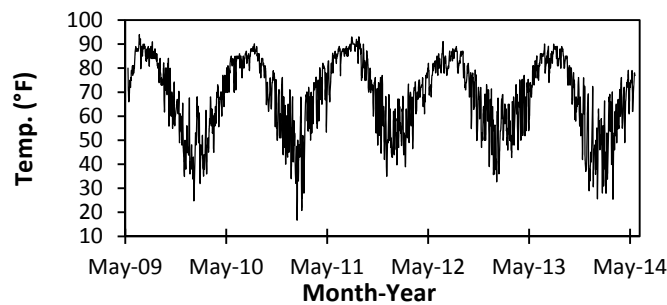
Figure 5–2b shows the relation between the reinforcement ratio and the maximum expansion strain computed for the various regions of the C-Beam specimen. As expected the maximum expansion strain in the C-Beam specimen decreases with increasing reinforcement ratio. The C-Beam specimen was subjected to tie-bar forces to simulate the effects of gravity loads on the structure. These induce tensile stresses promote cracking. These effects are also taken into account while computing the maximum expansion strain  $\epsilon_\rho^{\max}$ . In Figure 5–2b two curves are presented, one where there are no tensile prestrain effects on the expansion strain and the other with the tensile prestrain effects considered. It is clear that for the same reinforcement ratio, the maximum expansion strain is greater when the tensile prestrain effects are considered. This is complimentary to the case where compressive strains cause lower expansion strains. The computation of the reinforcement ratio is discussed later in this section. To account for the variation in expansion due to temperature and moisture content, the average daily temperature and rainfall amounts were obtained from the closest weather station to the site where the



(a) DEMEC Layout of C-Beam Specimen



(b) Variation of Maximum Expansion with Reinforcement Ratio



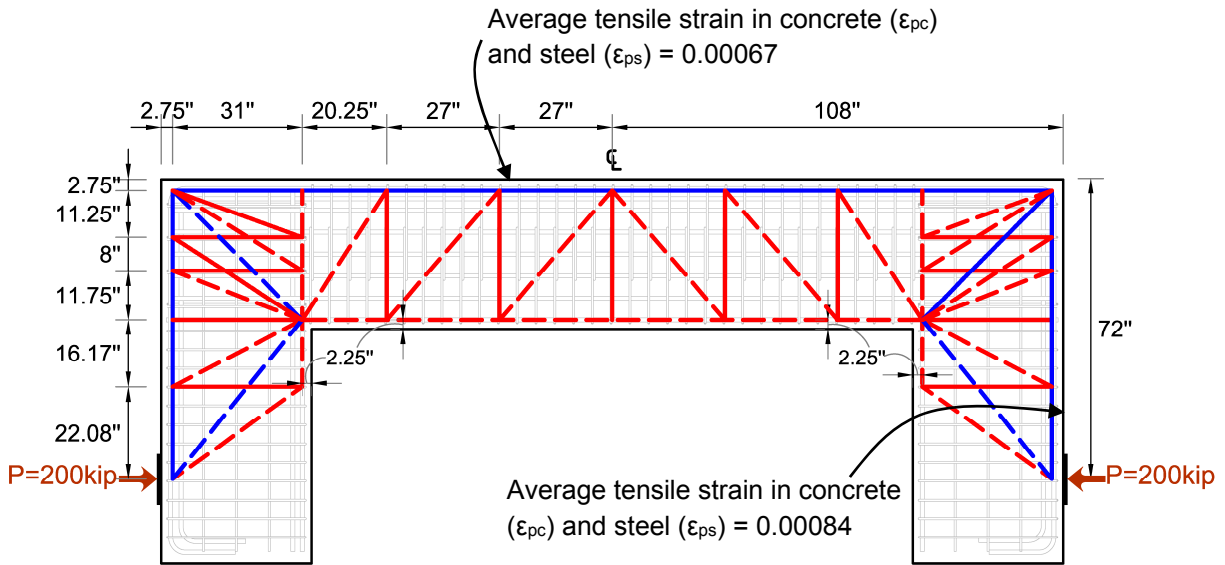
(c) Observed Average Daily Temperature

Figure 5–2: Information Pertinent to Model Expansion Strains in C-Beam Specimen.

specimens were conditioned. Additionally, to obtain a reasonable estimate of the actual amount of moisture that the specimens were subjected to due to supplemental water from the sprinkler system, a series of rain gages were installed at various locations on Specimen 3. For this study a degree of saturation of  $S = 0.1$  was assumed for the horizontal exposure surfaces and for strains measured in the horizontal direction caused by cracks in the vertical direction. The vertical cracks allow better ingress of moisture into the specimen, and the related expansion causes horizontal strains. For strains measured in the vertical direction caused by horizontal cracks on the vertical exposure face, a degree of saturation of  $S = 0.05$  was adopted as the horizontal cracks do not allow for moisture ingress into the specimen as well as the vertical cracks. The temperature and moisture content data were used in the computation of expansion strains in the reinforced concrete C-Beam specimen. Figure 5–2c shows the variation of the daily average temperature recorded at the closest weather station to the site for the period when Specimen 3 was exposed to field conditions.

Also taken into account in the computation of the maximum expansion strain, are the tensile strains induced by the applied tie-bar force used to mimic gravity loads on the specimen. The C-STM model of the C-Beam specimen that was developed by Mander et al. (2012b) was used to determine the initial strains. As shown in Figure 5–3 a 200 kip load corresponding to the tie-bar force was applied, and the corresponding tensile strains were obtained from the model. The values of the tensile strains in concrete and steel are shown in Figure 5–3. The applied tie-bar force caused tensile stresses in the longitudinal direction along the outer edges of the specimen, which resulted in a tensile prestrain. However, there were no stresses applied in the out-of-plane direction of the specimen, hence there are no prestrains that contribute to the expansion in the out-of-plane direction. However, the presence of transverse reinforcement restrains the expansion in the out-of-plane direction.

Another important parameter that is required for the implementation of the proposed expansion model is the reinforcement ratio of the specimen. As the DEMEC points were located on the surface of the specimen, the influence of reinforcing steel are different at the various DEMEC locations. Hence, it is essential to carefully compute the reinforcement ratio for the different regions of the specimen. In this study, various reinforcement ratios were computed based on the location and direction of the DEMEC strain measurements. Table 5–1 presents the properties of C-Beam Specimen 3 that were used in calculating the reinforcement ratios, where



**Figure 5–3: Computation of Average Tensile Loads from C-STM in the C-Beam Specimen due to Post-Tension Load.**

**Table 5–1: Properties for C-Beam Specimen 3.**

	<b>Specimen 3</b>
$f'_c$ (ksi)	5.93
$kd_{col}$ (in.)	13.98
$kd_{beam}$ (in.)	11.31
$l_d$ (in.) for #8 bars	42.20
$l_d$ (in.) for #4 bars	16.88

$kd_{col}$  and  $kd_{beam}$  are the depth of the neutral axis from the extreme compression fiber for the column and the beam, respectively, and  $l_d$  is the development length of the reinforcement. A detailed computation of the reinforcement ratio for C-Beam Specimen 3 is presented in Sheet 5-1–Sheet 5-8.

Sheet 5-1	COMPUTATION OF REINFORCEMENT RATIO ( $\rho$ ) AND MAXIMUM EXPANSION STRAIN ( $\epsilon_p^{max}$ ) FOR C-BEAM SPECIMEN 3.	1 8												
GENERAL NOTES														
<p><u>General parameters used:</u></p> <table style="width: 100%; border: none;"> <tr> <td><math>f'_c = 5.93 \text{ ksi}</math></td> <td><math>E_c^{actual} = 4390 \text{ ksi}</math></td> <td><math>f'_t = 0.580 \text{ ksi}</math></td> <td><math>\epsilon_t = 0.000132</math></td> </tr> <tr> <td><math>f_y = 65 \text{ ksi}</math></td> <td><math>E_s = 29000 \text{ ksi}</math></td> <td><math>\epsilon_y = 0.00224</math></td> <td></td> </tr> <tr> <td><math>t_r(\theta_o) = 120 \text{ days}</math></td> <td><math>\epsilon_{pc}^{ASR} = 0.05</math></td> <td><math>n = \frac{E_s}{E_c/3} = 19.82</math></td> <td></td> </tr> </table>			$f'_c = 5.93 \text{ ksi}$	$E_c^{actual} = 4390 \text{ ksi}$	$f'_t = 0.580 \text{ ksi}$	$\epsilon_t = 0.000132$	$f_y = 65 \text{ ksi}$	$E_s = 29000 \text{ ksi}$	$\epsilon_y = 0.00224$		$t_r(\theta_o) = 120 \text{ days}$	$\epsilon_{pc}^{ASR} = 0.05$	$n = \frac{E_s}{E_c/3} = 19.82$	
$f'_c = 5.93 \text{ ksi}$	$E_c^{actual} = 4390 \text{ ksi}$	$f'_t = 0.580 \text{ ksi}$	$\epsilon_t = 0.000132$											
$f_y = 65 \text{ ksi}$	$E_s = 29000 \text{ ksi}$	$\epsilon_y = 0.00224$												
$t_r(\theta_o) = 120 \text{ days}$	$\epsilon_{pc}^{ASR} = 0.05$	$n = \frac{E_s}{E_c/3} = 19.82$												
<p><u>Maximum Expansion Strain</u></p> <p>The C-Beam specimen were subjected to tie-bar force to simulate gravity loads on the structure. This resulted in the specimen being precracked, which further accelerated the expansion process as these cracks provided a pathway for moisture ingress. To take into account the precracked nature of the specimen, Eq. 3-16a (which is repeated below for convenience) was used in the computation of the expansion strains (<math>\epsilon_p^{max}</math>).</p> $\epsilon_p^{max} = \frac{\epsilon_o^{max} \epsilon_t + \rho n (\epsilon_y^2 - \epsilon_{ps}^2) + \epsilon_t \epsilon_{pc} - \left(\frac{\epsilon_t}{2}\right)^2}{2 \left( \frac{\epsilon_t}{2} + \rho n (\epsilon_y - \epsilon_{ps}) - \frac{\sigma_{const}}{E_c} \right)} \quad 3-16a$														
<p><u>Development Length (ACI Equations)</u></p> <p>It was established by Mander et al. (2011) that to develop the full yield strength of the reinforcement, the reinforcing bars transverse to the member edge should be longer than the bar development length (<math>l_d</math>).</p> <p>#8 bars: <math>(l_d) = \left( \frac{f_y \psi_t \psi_e}{20 \lambda \sqrt{f'_c}} \right) d_b = \left( \frac{65000(1)(1)}{20(1)\sqrt{f'_c}} \right) d_b = 3250 \frac{d_b}{\sqrt{f'_c}} = 42.20''</math></p> <p>#4 bars: <math>(l_d) = \left( \frac{f_y \psi_t \psi_e}{25 \lambda \sqrt{f'_c}} \right) d_b = \left( \frac{65000(1)(1)}{25(1)\sqrt{f'_c}} \right) d_b = 2600 \frac{d_b}{\sqrt{f'_c}} = 16.88''</math></p>														

Sheet 5-2	COMPUTATION OF REINFORCEMENT RATIO ( $\rho$ ) AND MAXIMUM EXPANSION STRAIN ( $\epsilon_p^{max}$ ) FOR C-BEAM SPECIMEN 3.	2 8
-----------	--	--------

**COLUMN TOP FACE MEMBER REGION**

Section depth ( $d$ ) = overall depth ( $D$ ) - depth to neutral axis ( $kd_{col}$ ) =  $36 - 13.98 = 22.02$ "

**Direction: Transverse (a)**

Reinforcement type: #4 bars with c/s area  $A_s = 0.19635 \text{ in}^2$  @ 4.5" c/c spacing

Reinforcement ratio  $\rho = A_s / (sd) = 0.00198$

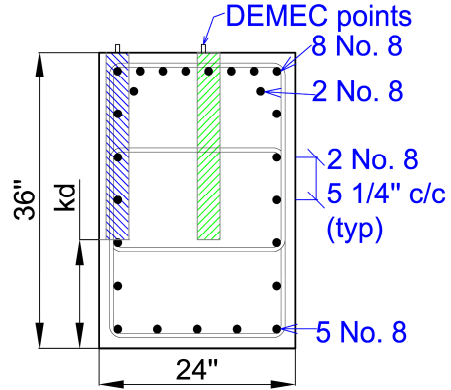
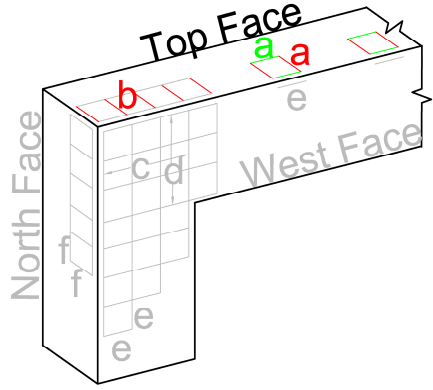
Additionally, as there are no tensile prestrains in the transverse direction,  $\epsilon_{pc} = \epsilon_{ps} = 0$ .

Maximum expansion strain  $\epsilon_p^{max} = 0.02202$

**Direction: Longitudinal (a)**

DEMEC measurements are made along two lines, one close to the edge of the column, and the other closer to the middle of the column cross-section. As the DEMEC readings are limited to the two lines, the strains measured could be more localized. Therefore narrow strips under the DEMEC points are considered to compute the reinforcement ratio. Because of their localized effects the average reinforcement ratio is considered.

Width of strip ( $b$ ) = 2.785" (shaded blue and green)  
 c/s area of concrete  $A_c = (22.02)(2.785) = 61.33 \text{ in}^2$



DEMEC points location	Close to column edge (shaded blue)	Close to column center (shaded green)
$A_s$ ( $\text{in}^2$ )	3.1416 (4-#8 bars)	0.7854 (1-#8 bar)
$\rho = A_s / (bd)$	0.05122	0.01281
Average $\rho$	0.03202	

$\epsilon_{pc} = \epsilon_{ps} = 0.00067$  obtained from C-STM model.

$\epsilon_p^{max} = 0.0045$

Figure 5-4a shows the expansion results obtained in the transverse and longitudinal direction on the member region of the column top face of the C-Beam specimen.



Sheet 5-3	COMPUTATION OF REINFORCEMENT RATIO ( $\rho$ ) AND MAXIMUM EXPANSION STRAIN ( $\epsilon_p^{\max}$ ) FOR C-BEAM SPECIMEN 3	3 8
-----------	--	--------

COLUMN TOP FACE JOINT REGION

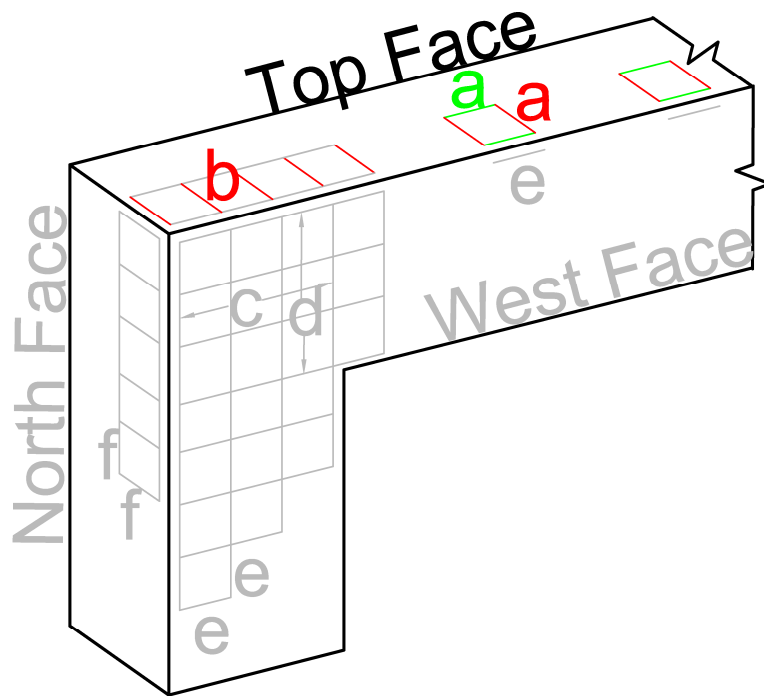
Direction: Transverse (b)

There are no transverse hoops on the column top face in the joint region. Therefore,  $\rho = 0$  is considered for the region close to the edge. However, in the region away from the edge and close to the column member region, the influence of transverse reinforcement in the column member region is considered. A  $\rho = 0.00198/2 = 0.00099$  is assumed.

Since there are no tensile prestrains in the transverse direction,  $\epsilon_{pc} = \epsilon_{ps} = 0$ .

$$\epsilon_p^{\max} = 0.0304$$

Figure 5-4b shows the transverse expansion strains in the joint region of the C-Beam specimen top face.



Sheet 5-4	COMPUTATION OF REINFORCEMENT RATIO ( $\rho$ ) AND MAXIMUM EXPANSION STRAIN ( $\epsilon_p^{max}$ ) FOR C-BEAM SPECIMEN 3	4 8
-----------	---	--------

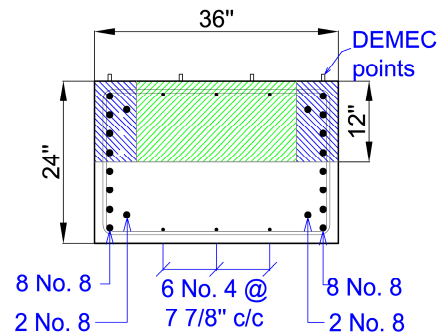
**BEAM COLUMN JOINT REGION**

Concrete and steel volume in half the section depth ( $d = 12"$ ) is considered for calculating the reinforcement ratio.

Direction: Vertical DEMEC Points Along Beam Longitudinal Steel

Depending on the location of the DEMEC points on the face of the beam cross-section, two separate reinforcement ratios are computed.

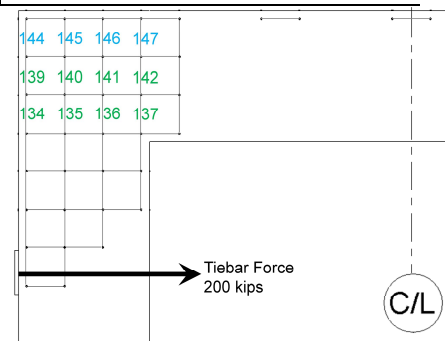
DEMEC location	Close to member edges (shaded blue)	For interior DEMEC points (shaded green)
Area of steel, $A_s$	3.9270 in <sup>2</sup> (5-#8 bars)	0.5890 in <sup>2</sup> (3-#4 bars)
Area of concrete, $A_c$	(12)(6.1875) = 74.25 in <sup>2</sup>	(12)(23.625) = 283.5 in <sup>2</sup>
$\rho$	0.0529	0.00208



The reinforcement ratio is scaled down for the DEMEC points close to the C-Beam specimen edges.

Scaled reinforcement ratio for:	DEMEC 145 and 146 close to specimen top edge	DEMEC 139-142, still within the development length
$l$	5.25"	15.75"
$\rho_{reduced} = \rho(l/l_d)$	$0.00208(5.25/16.88) = 0.000647$	$0.0529(15.75/42.20) = 0.01974$
With ( $\epsilon_{pc} = \epsilon_{ps} = 0$ ), $\epsilon_p^{max} =$	0.03514	0.00453

Figure 5-4c shows two curves for the expansion results from the model. Curve A corresponds to the case where the expansion strains are computed closer to the top edge of the specimen (within development length zone close to top edge) and Curve B for expansion strains computed away from the top edge (within development length zone away from top edge).



Sheet 5-5	COMPUTATION OF REINFORCEMENT RATIO ( $\rho$ ) AND MAXIMUM EXPANSION STRAIN ( $\epsilon_p^{max}$ ) FOR C-BEAM SPECIMEN 3	5 8
-----------	---	--------

**BEAM COLUMN JOINT REGION**

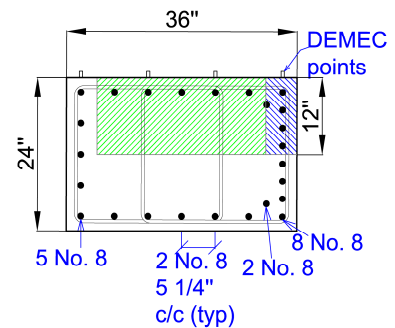
Concrete and steel volume in half the section depth ( $d = 12''$ ) is considered for calculating the reinforcement ratio.

**Direction: Horizontal DEMEC Points Along Column Longitudinal Steel**

Depending on the location of the DEMEC points on the face of the beam cross-section, two separate reinforcement ratios are computed.

For DEMEC within the development length zone and close to the specimen edges (first layer of DEMEC points 158, 162, 166, 170) the portion shaded in green is used to compute the reinforcement ratio as the influence of the reinforcement at the extremes (shaded blue) is unlikely to influence the expansion close to the specimen edge.

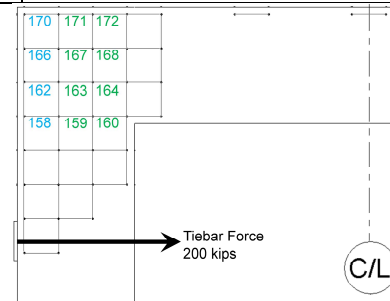
DEMEC location	Close to member edges (shaded blue)	For interior DEMEC points (shaded green)
Area of steel, $A_s$	10.21 in <sup>2</sup> (12-#8 and 4-#4 u-bars, not shown)	4.7124 in <sup>2</sup> (5-#8 and 4-#4 u-bars, not shown)
Area of concrete, $A_c$	(12)(36) = 432 in <sup>2</sup>	(12)(26.25) = 315 in <sup>2</sup>
$\rho$	0.0236	0.01496



The reinforcement ratio is scaled down for DEMEC points close to C-Beam specimen edges.

Scaled reinforcement ratio for:	DEMEC 159, 163, 167 and 171, still within the development length	DEMEC 158, 162, 166 and 170 close to specimen edge
$l$	15.75"	5.25"
$\rho_{reduced} = \rho(l/l_d)$	$0.0236(15.75/42.20) = 0.00881$	$0.01496(5.25/42.20) = 0.001861$
With ( $\epsilon_{pc} = \epsilon_{ps} = 0$ ), $\epsilon_p^{max} =$	0.00816	0.02278

Figure 5-4d shows the expansion strains, close and away from the specimen edge, obtained from the model.



Sheet 5-6	COMPUTATION OF REINFORCEMENT RATIO ( $\rho$ ) AND MAXIMUM EXPANSION STRAIN ( $\epsilon_p^{max}$ ) FOR C-BEAM SPECIMEN 3	6
		8

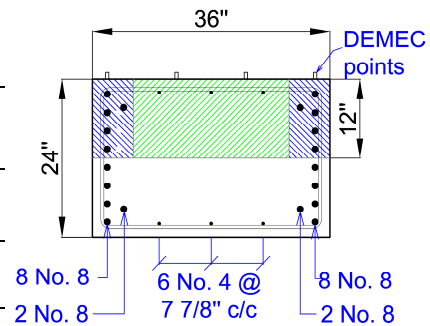
**BEAM WEST FACE**

Concrete and steel volume in half the section depth ( $d = 12''$ ) is considered for calculating the reinforcement ratio.

**Direction: Longitudinal**

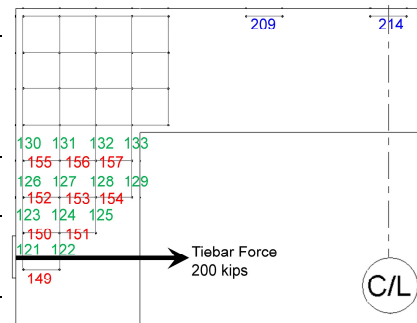
As the DEMEC points are considerably away from the specimen edge, the reinforcement in the entire half-depth of the cross-section ( $d = 12''$ ) is considered as localized effects near the edges are eliminated.

Area of steel, $A_s$	8.44 in <sup>2</sup> (10-#8 and 3-#4 bars)
Area of concrete, $A_c$	(12)(36) = 432 in <sup>2</sup>
$\rho$	0.01954
With ( $\epsilon_{pc} = \epsilon_{ps} = 0$ ), $\epsilon_p^{max} =$	0.00456



The reinforcement ratio is scaled down for the DEMEC points within the development length zone.

Scaled reinforcement ratio for:	DEMEC 123-125 within the development length zone
$l$	35.15''
$\rho_{reduced} = \rho(l/l_d)$	0.01954 (35.15/42.20) = 0.01628
With ( $\epsilon_{pc} = \epsilon_{ps} = 0$ ), $\epsilon_p^{max} =$	0.00519



**Direction: Transverse**

Reinforcement type: #4 bars with c/s area  $A_s = 0.19635 \text{ in}^2 @ 4.5'' \text{ c/c spacing}$

Reinforcement ratio  $\rho = A_s / (sd) = 0.00364$

As there are no tensile prestrains in the transverse direction,  $\epsilon_{pc} = \epsilon_{ps} = 0$ .

Maximum expansion strain  $\epsilon_p^{max} = 0.01526$

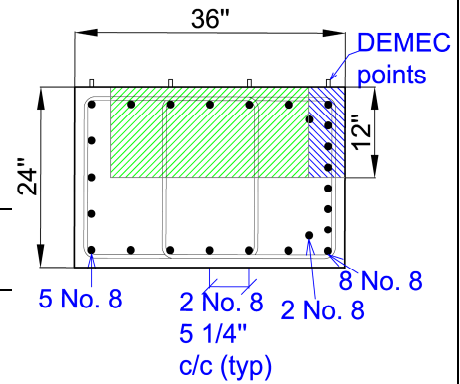
Figure 5-4e shows the expansion strain  $s$  in the longitudinal and transverse direction on the beam west face.

Sheet 5-7	COMPUTATION OF REINFORCEMENT RATIO ( $\rho$ ) AND MAXIMUM EXPANSION STRAIN ( $\epsilon_p^{max}$ ) FOR C-BEAM SPECIMEN 3	7 8
-----------	---	--------

COLUMN WEST FACE

Direction: *Longitudinal*

The DEMEC points in the column of the specimen west face were located close to the specimen top edge, therefore the reinforcement ratio is calculated considering the area shaded in blue.



Area of steel, $A_s$	3.927 in <sup>2</sup> (5-#8 bars)
Area of concrete, $A_c$	(12)(4.875) = 58.5 in <sup>2</sup>
$\rho$	0.0671

$\epsilon_{pc} = \epsilon_{ps} = 0.00067$   
 obtained from C-STM  
 model.  $\epsilon_p^{max} = 0.00296$

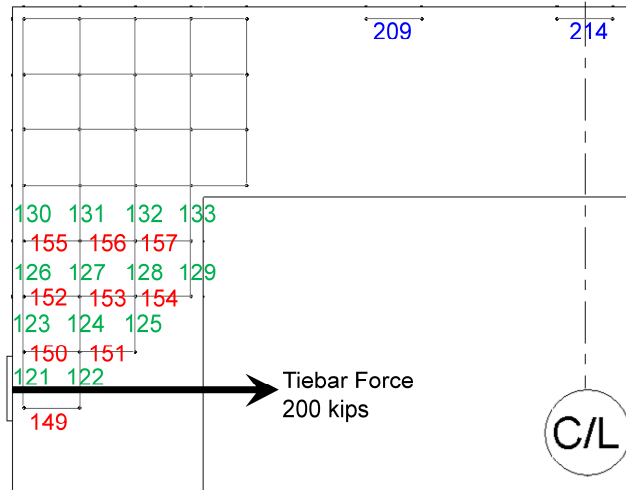


Figure 5-4e shows the expansion strain  $\epsilon$  in the longitudinal direction on the column west face

Sheet 5-8	COMPUTATION OF REINFORCEMENT RATIO ( $\rho$ ) AND MAXIMUM EXPANSION STRAIN ( $\epsilon_p^{max}$ ) FOR C-BEAM SPECIMEN 3	8 8
-----------	---	--------

**BEAM NORTH FACE**

Section depth ( $d$ ) = overall depth ( $D$ ) - depth to neutral axis ( $kd_{beam}$ ) =  $36 - 11.31 = 24.69$ "

**Direction: Transverse (f)**

Reinforcement type: #4 bars with c/s area  $A_s = 0.19635 \text{ in}^2$  @ 4.5" c/c spacing

Reinforcement ratio  $\rho = A_s / (sd) = 0.00177$

As there are no tensile prestrains in the transverse direction,  $\epsilon_{pc} = \epsilon_{ps} = 0$ .

Maximum expansion strain  $\epsilon_p^{max} = 0.0234$

**Direction: Longitudinal (f)**

DEMEC measurements are made along two lines, one close to the edge of the beam, and the other closer to the middle of the beam cross-section. As the DEMEC readings are limited to the two lines, the strains measured could be more localized. Therefore narrow strips under the DEMEC points are considered to compute the reinforcement ratio. Because of their localized effects, the average reinforcement ratio is considered.

Width of strip ( $b$ ) = 2.785" (shaded blue and green)

c/s area of concrete  $A_c = (24.69)(2.785) = 68.76 \text{ in}^2$

DEMEC points location	Close to beam edge (shaded blue)	Close to beam center (shaded green)
$A_s$ (in <sup>2</sup> )	1.1781 in <sup>2</sup> (1-#8 and 2-#4 bars)	0.7854 in <sup>2</sup> (1-#8 bar)
$\rho = A_s / (bd)$	0.01713	0.01142
Average $\rho$	0.01428	

$\epsilon_{pc} = \epsilon_{ps} = 0.00084$  obtained from C-STM model.

Maximum expansion strain  $\epsilon_p^{max} = 0.00855$

Figure 5-4f shows the expansion strain results on the north face of the C-Beam specimen.

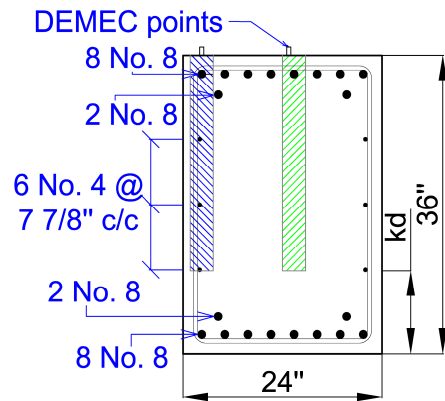
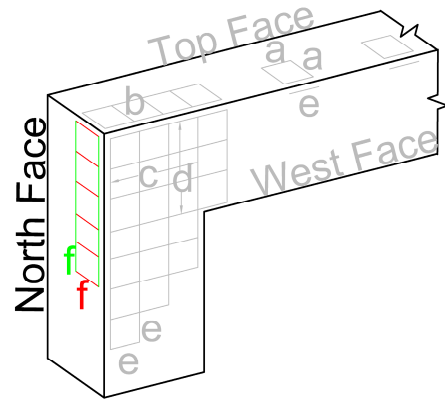


Table 5–2 presents a summary of the reinforcement ratio and the maximum expansion strains for the various regions of C-Beam Specimen 3.

### 5.3. MODELING ASR/DEF EXPANSION IN C-BEAM SPECIMEN

Figure 5–4a and b, respectively, considers the member region and the joint region of the C-Beam specimen top face. In the top face member region, the expansion strains in the transverse and longitudinal directions were considered. The concrete and steel volume from the extreme tension fiber to the neutral axis were used in the computation of the reinforcement ratio. In the longitudinal direction, DEMEC measurements were made along two lines, one close to the edge of the column, and the other closer to the middle of the column cross section as shown in Figure 5–4i. As the DEMEC readings were limited to two lines, the measured strains could be more localized, and the reinforcement ratios were computed accordingly as shown in Sheet 5-2. The tensile strains due to the tie-bar force computed from the C-STM analysis as shown in Figure 5–3 resulted in a tensile concrete and steel strain of 0.00067 and were appropriately incorporated into computing the maximum expansion strain  $\varepsilon_{\rho}^{\max}$ . Figure 5–4a shows the expansion results obtained in the transverse and longitudinal direction on the column top face member region of the C-Beam specimen.

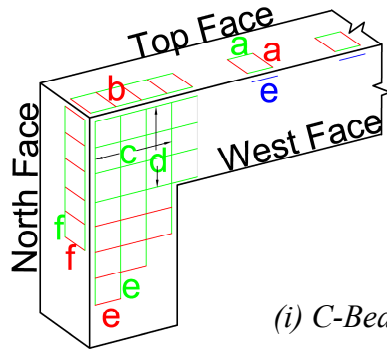
Figure 5–4b considers the transverse expansion strains in the joint region of the C-Beam specimen top face. As there were no transverse U-bars in the joint region, this region is essentially unreinforced in the transverse direction. Therefore a reinforcement ratio of  $\rho = 0$  was considered for this case. However, the transverse reinforcement in the column region can likely influence the expansion strains caused in the joint region away from the edge of the joint. Therefore, a case with half the transverse reinforcement ratio in the column region is also presented in Figure 5–4b.

Figure 5–4c and d, respectively, considers the expansion strain in the vertical and horizontal direction in the beam-column joint region of the C-Beam specimen's west face. Concrete and steel volume in half the section depth (12 in.) were considered for calculating the reinforcement ratio.

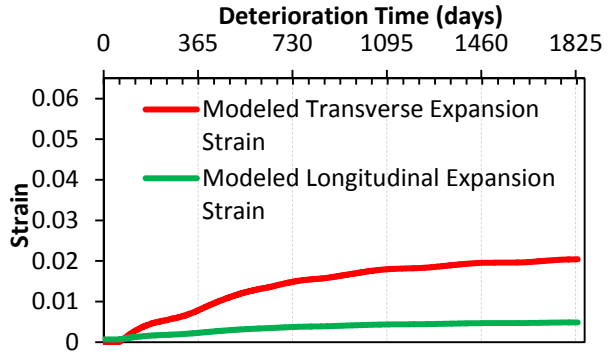
**Table 5–2: Computation of Reinforcement Ratio and Maximum Expansion Strain for C-Beam Specimen 3.**

Region	Dir.	Section Depth (in)	Concrete Width (in)	Rebar Considered		$\rho$	Max. Expansion Strain	Eq. No.	Comments
				No.	Bar (#)				$f'_c=5.93$ ksi; $kd_{col}=13.98"$ ; $kd_{beam}=11.31"$
(a) Column Top-Member	Long.	22.02	2.785			0.03202	0.0045	3-16a	Average $\rho$ of edge (4-#8, $\rho=0.05122$ ) and interior (1-#8, $\rho=0.01281$ ) strips. $\epsilon_{pc}=\epsilon_{ps}=0.00067$ .
	Trans.	22.02	---	---	4	0.00198	0.02202	3-16a	
(b) Column Top-Joint	Trans.					0.00099	0.03040	3-16a	$\rho=0$ close to edge and $\rho$ =half of (a) Column Top-Member Trans. (0.00191) away from edge.
(c) West Face Joint Vertical	Long.	12	6.1875	5	8	0.01974	0.004532	3-16a	Considering edge and scaled for 2 <sup>nd</sup> level of DEMEC points. $l_d=42.20"$ , $x=15.75"$ , $\rho=0.0529$ .
	Long.	12	23.625	3	4	0.00065	0.03514	3-16a	Considering interior and scaled for 1 <sup>st</sup> level of DEMEC points. $l_d=16.88"$ , $x=5.25"$ , $\rho=0.00208$ .
(d) West Face Joint Horizontal	Long.	12	36	12 4	8 4	0.00881	0.00816	3-16a	Scaled for 2 <sup>nd</sup> level of DEMECs. $l_d=42.20"$ , $x=15.75"$ , $\rho=0.0236$ .
	Long.	12	36	5 4	8 4	0.00186	0.02278	3-16a	Considering interior region and scaled for 1 <sup>st</sup> level of DEMEC points. $l_d=42.20"$ , $x=5.25"$ , $\rho=0.01496$ .
(e) West Face-Beam	Long.	12	36	10 3	8 4	0.01954	0.00456	3-16a	Considering steel and concrete in 12" depth
						0.01628	0.00519		Scaled for 2 <sup>nd</sup> level of DEMECs. $l_d=42.20"$ , $x=35.15"$ , $\rho=0.01954$
	Trans.	12	---	---	4	0.00364	0.01526	3-16a	
(e) West Face-Column	Long.	12	4.875	5	8	0.0671	0.00296	3-16a	
(f) North Face-Beam	Long.	24.69	2.785			0.01428	0.00855	3-16a	Average $\rho$ of edge (1-#8 and 2-#4, $\rho=0.01713$ ) and interior (1-#8, $\rho=0.01142$ ) strips. $\epsilon_{pc}=\epsilon_{ps}=0.00084$ .
	Trans.	24.69	---	---	4	0.00177	0.02341	3-16a	

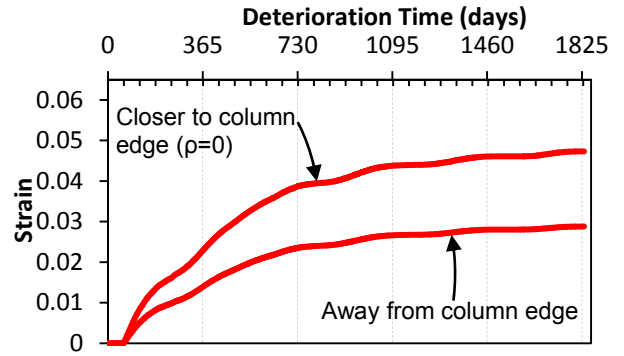




(i) C-Beam Specimen DEMEC Locations

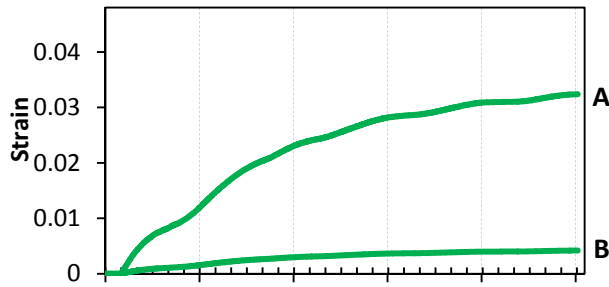


(a) Member

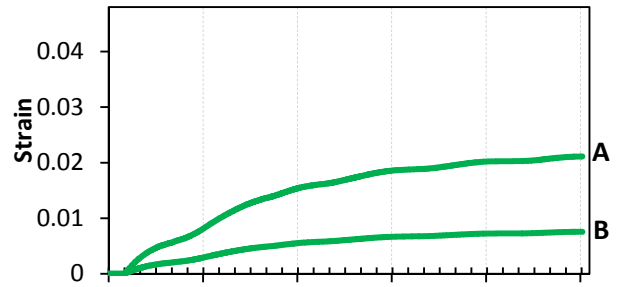


(b) Joint

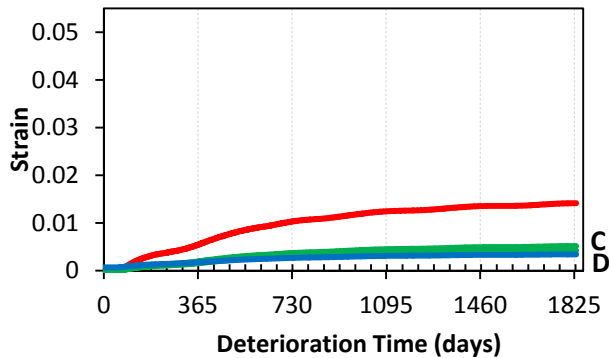
Top Face (Horizontal Exposure Face)



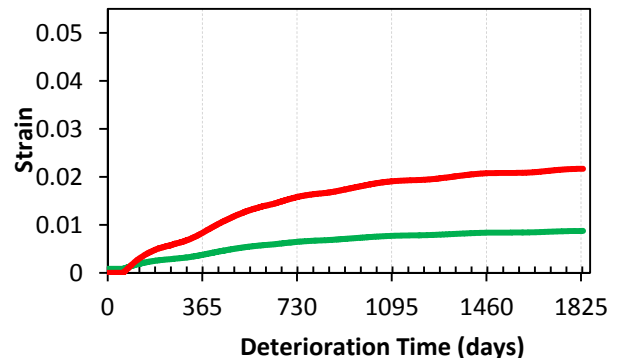
(c) Joint Vertical Direction



(d) Joint Horizontal Direction



(e) West Face



(f) North Face

Side Faces (Vertical Surface Exposed)

Note: A/B: Within Dev. Length Zone Closer/Away from Edge; C/D: Inside/Outside Dev. Length Zone

**Figure 5-4: Observed and Computed Expansion Strain—Specimen 3.**

Depending on the location of the DEMEC points in the vertical direction of the beam-column joint, separate reinforcement ratios were computed as shown in Sheet 5-4. Additionally, it was shown by Mander et al. (2011) that to develop the full yield strength of the reinforcement, the reinforcing bars transverse to the member edge should be longer than the bar development length ( $l_d$ ). Therefore, scaled reinforcement ratios were considered for DEMEC points within the development length zone. Figure 5-4c shows two curves for the expansion results from the model. Curve A corresponds to the case where the expansion strains were computed closer to the top edge of the specimen (within development length zone close to top edge) and Curve B for expansion strains computed away from the top edge (within development length zone away from top edge).

Figure 5-4d shows the modeled expansion strains in the direction of the column longitudinal reinforcement in the joint region. As in the earlier case, half section depth of 12 in. was used for the computation of reinforcement ratio (Sheet 5-5), and they were scaled down accordingly within the development length zone. In Figure 5-4d, Curve A and Curve B, respectively, corresponds to the case where the expansion strains were computed closer to the top edge and away from the top edge of the specimen, both still within the development length zone.

Figure 5-4e shows the longitudinal expansion strains in the column, and the longitudinal and transverse expansion strains in the beam of the C-Beam specimen's west face. The reinforcement ratios were computed considering half-depth (12 in.) of the cross section (Sheets 5-6 and 5-7). The DEMEC points in the column of the specimen west face were located close to the specimen top edge, and the reinforcement ratio was computed accordingly to account for the localized nature of the DEMEC readings (Sheet 5-7). The tensile concrete and steel strains due to the applied tie-bar force were computed to be 0.00067 from the C-STM model shown in Figure 5-3 and they were incorporated into computing the maximum expansion strains. For longitudinal expansion strains in the beam of the C-Beam specimen west face, scaled reinforcement ratios were considered for DEMEC points within the development length zone (Sheet 5-6). Figure 5-4e shows the expansion results from the model, where curve C and D, respectively, represent the expansion strains inside and outside the development length zone. In this case it is observed that there is not much difference between the two cases, as the DEMEC measurements were made relatively away from the specimen edges.

Figure 5–4f shows the modeled expansion strains in the longitudinal and transverse direction of the C-Beam specimen’s north face. The depth of the beam cross section from the extreme tension fiber to the neutral axis was considered for the computation of the reinforcement ratios. As in the case of the column top face, the longitudinal DEMEC measurements in the beam were made along two lines, one close to the edge of the beam, and the other closer to the middle of the beam cross section as shown in Figure 5–4i. The strains measured could be more localized as the DEMEC readings were limited to two lines, and the reinforcement ratios were computed accordingly as shown in Sheet 5-8. The tensile strains due to the tie-bar force computed from the C-STM analysis as shown in Figure 5–3, resulted in a tensile concrete and steel strain of 0.00084 and were appropriately incorporated in computing the maximum expansion strain. Figure 5–4f shows the simulated transverse and longitudinal expansion strain on the C-Beam specimen north face.

#### **5.4. DISCUSSION**

A comparison of the simulated expansion results with the field observations presented in Mander et al. (2015) shows that the proposed model can be used to simulate the expansion strains in reinforced concrete reasonably well, considering the complex nature of ASR/DEF related expansion in reinforced concrete and the vagaries associated with the expansion data gathered from the field. In most cases the simulated results were within the range of measured field expansion data for the specimens.

The effects of tensile strains caused by gravity loads on ASR/DEF expansion were also taken into account in the model to simulate the expansion results with good accuracy. The tie-bar force that was applied to simulate gravity loads in the C-Beam specimens caused tensile stresses along the tension side of the specimen. These tensile stresses caused pre-cracking which promoted ASR/DEF expansion. The tensile pre-strains along the direction of the longitudinal reinforcement were considered in the model. However, the tie-bar force did not cause any stresses in the transverse (out-of-plane) direction of the specimen, and hence the tensile prestrains were not considered in modeling the strains along the direction of the transverse reinforcement. As demonstrated in the chapter, it is extremely important to compute the relevant reinforcement ratio, as it affects the extent of expansion that can be caused by ASR/DEF.

Due to the orientation of the specimen during its field conditioning, different parts of the specimen were subjected to various amounts of moisture and hence different degrees of saturation. To account for this, the degree of saturation for the horizontal exposure faces and for strains caused by vertical cracks on the vertical exposure faces were assumed to be greater than the degree of saturation for the strains caused by horizontal cracks in the vertical exposure face. This assumption was also backed by the field expansion data. In an actual structure, many of these parameters cannot be determined realistically, and therefore it is important to assume relevant values based on sound reasoning.

The results of this investigation show that if appropriate values are assigned to the limited input parameters required for the model, the proposed minimalist semi-empirical model can be effectively used to model the ASR/DEF induced expansion in reinforced concrete members that are exposed to field conditions.

## **5.5. CLOSURE AND KEY FINDINGS**

By taking into account the appropriate input parameters for the proposed expansion model, the expansion strains caused by ASR/DEF in reinforced concrete specimen can be estimated within reasonable bounds as demonstrated in this chapter. The model predicts the general expansion behavior reasonably well. The key observations and findings from this chapter are summarized below:

- Depending on the region of the specimen that is being considered, the moisture content and hence the degree of saturation can be different. Especially, on the horizontal exposure faces, water tends to pool/stand for longer when compared to the vertical exposure face, where the water runs off almost immediately.
- The orientation of the cracks can also lead to differences in the expansion strain behavior. On vertical exposure faces, vertical cracks which cause horizontal expansion strains allow for more rapid water ingress into the specimen through the cracks, when compared to horizontal cracks which results in vertical strains.
- The proposed model takes into account the tensile prestrains caused by the tie-bar force (which simulates gravity loads) in the direction of the longitudinal reinforcement.

- Considering the complex nature of the C-Beam specimen, and ASR/DEF induced expansion strains, the proposed model captures the expansion strains caused by ASR/DEF quite well.



## **6. WORKED EXAMPLE: ANALYSIS SCHEMA FOR C-BEAM SPECIMENS**

### **6.1 SCOPE**

In this section a reinforced concrete bridge pier tested by the authors in order to investigate the effect of premature concrete deterioration in bridge bents currently used in practice, specifically cantilever bents and straddle bents, is selected to illustrate the procedure of analysis detailed in Chapter 2. Additionally, the structure is modeled using the C-STM technique without and with the effects of ASR/DEF. All results are then compared with the experimental results.

### **6.2 THE STRUCTURE**

The experimental specimen was designed as a 'C' shape sub-assembly such that two large-scale bridge bent components were placed back-to-back so they could be tested as a self-reacting system. The C-Beam specimen had a constant cross-section of 3 ft. deep and 2 ft. wide that was symmetrical with the exception of the beam compression steel. More specifically the physical model scale factors representing the singly reinforced cantilevered bent and the doubly reinforced straddle bent were approximately 0.5 and 0.75, respectively.

Figure 6–1 presents the reinforcing layout and cross-section of C-Beam Specimen. The longitudinal reinforcement consisted of 10 No. 8 bars running continuously around the outside and hooked at the end of each beam. The singly reinforced beam had two No. 8 straight compression bars for construction purposes. The doubly reinforced beam had symmetrical compression and tension reinforcement.

The longitudinal beam distribution steel (distributed along the beam web) consisted of three sets of No. 4 straight bars equally spaced. Transverse beam reinforcement consisted of closed stirrups with a center-to-center spacing of 4.5 in. starting at the column face. The longitudinal column distribution steel consisted of five sets of No. 8 bars equally spaced. Transverse column reinforcement had overlapping No. 4 stirrups spaced 4.5 in. centers. The beam-column joint was reinforced with four No. 4 U-bars at 8 in. centers continuing from the transverse beam reinforcement.

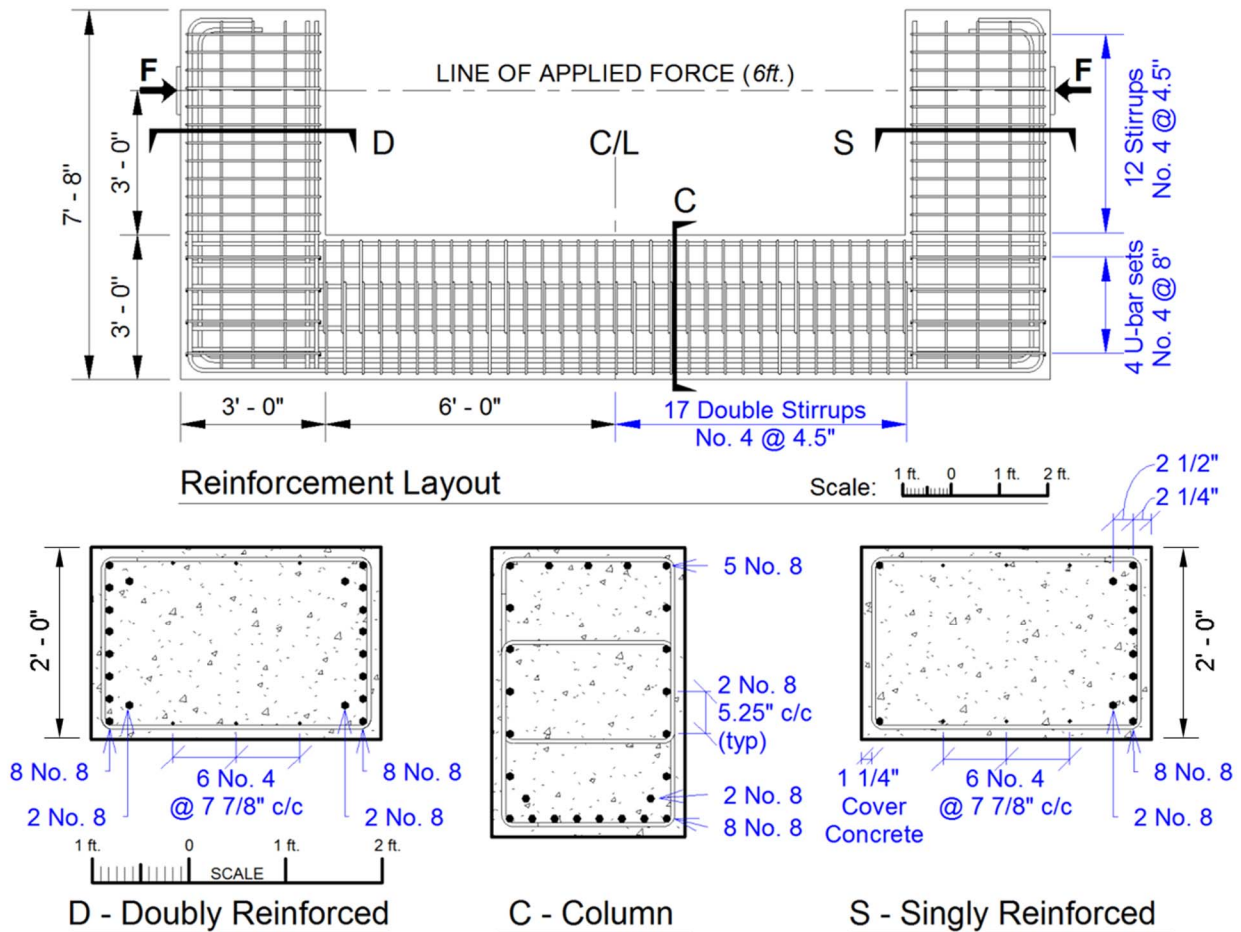


**Figure 6-1: Elevation and Cross-Section of the C-Beam Specimens.**



Table 6–1 presents the reported material strength data on the test day and experimental test results. Specimen 1 was the control specimen and does not have any ASR/DEF induced damage, whereas Specimens 4 and 3 showed a 'moderate' and 'heavy' amount of damage due to ASR/DEF effects. The experimental setup, procedure, and general observations from the test can be found in Mander et al. (2012b, 2015).

**Table 6–1: Material Properties and Test Results.**

		<b>Specimen 1</b>	<b>Specimen 4</b>	<b>Specimen 3</b>
<b>Material properties</b>	$f'_c$ (ksi)	5.40	4.00	5.93
	$f'_t$ (ksi)	0.30	---	---
	$E_c$ (ksi)	4190	3605	4390
	$n^*$	6.92	8.04	6.61
<b>Experimental results</b>	$P_{Yield}^{Expt}$ (kip)	440	440	---
	$P_{Failure}^{Expt}$ (kip)	474	503	498
	$\Delta_{Yield}^{Expt}$ (in.)	1.49	1.1	---
	$\Delta_{Failure}^{Expt}$ (in.)	1.69	2.17	0.80
	$\mu$	1.13	1.97	---

\*Modular ratio = Young's modulus of steel to concrete, where  
 $E_s = 29000ksi = 200GPa$

### 6.3 STAGE 1: STRENGTH ANALYSIS USING BEAM THEORY

The code-based design approaches that were described in detail in Chapter 2 are used to predict the response of C-Beam Specimens 1, 4, and 3. Results from the application of each of these approaches are presented as follows. Computations are presented in Appendix A.

**Step 1:** Determine first yield flexural capacity,  $M_y^b$ .

The yield moment and the external load causing first yield are calculated using Eqs. (2-1) and (2-3), respectively. The parameters required by the analysis of Specimens 1, 4, and 3 are presented in Table 6–2. For Specimen 1 the analysis resulted in a yield moment of  $M_y^b = 1290$  kip-ft and a yield force of  $P_y^b = 430$  kip for the doubly reinforced beam.

**Table 6–2: Results of Stage 1 Flexure Analysis (Without Deterioration).**

	Specimen 1		Specimen 4		Specimen 3		
	Doubly	Singly	Doubly	Singly	Doubly	Singly	
$k$	0.271	0.299	0.285	0.317	0.267	0.293	<i>Eq. (2-2)</i>
$C_c(kip)$	-377	-480	-366	-474	-382	-478	
$C_s(kip)$	-132	-34	-144	-37	-128	-33	
$T(kip)$	511	511	511	511	511	511	
$M_y^b(kip.ft)$	1290	1276	1285	1269	1291	1279	<i>Eq. (2-1)</i>
$P_y^b(kip)$	<b>430</b>	<b>425</b>	<b>428</b>	<b>423</b>	430	426	<i>Eq. (2-3)</i>
$\beta_1$	0.78	0.78	0.85	0.85	0.75	0.75	<i>Eq. (2-5)</i>
$M_n^f(kip.ft)$	1442	1416	1428	1383	1446	1425	<i>Eq. (2-4)</i>
$P_n^f(kip)$	<b>481</b>	<b>472</b>	<b>476</b>	<b>461</b>	<b>482</b>	<b>475</b>	<i>Eq. (2-6)</i>

**Steps 2:** Determine nominal flexural moment,  $M_n^f$ .

The nominal flexural moment ( $M_n^f$ ) was calculated based on Eq. (2-4). The flexural capacity,  $M_n^f = 1442$  kip-ft for the doubly reinforced beam of Specimen 1.

**Step 3:** Determine externally applied load based on beam flexure,  $P_n^f$ .

Based on the nominal flexural moment ( $M_n^f$ ), and knowing that the shear span to the face of the column  $L_b = 36$  inches, the external load causing beam flexure on the bent cap is found to be  $P_n^f = 481$  kip for the doubly reinforced beam of Specimen 1. The results for Specimens 1, 4, and 3 are presented in Table 6–2.

**Step 4:** Determine beam shear capacity,  $V_n^s$ .

The shear capacity ( $V_n^s$ ) is calculated from Eq. (2-7). Since there are no prestressing tendons, the component of shear carried by tendons  $V_p = 0$ . The parameters  $\beta$  and  $\theta$  are calculated based on Method 1. For the doubly reinforced side of Specimen 1 the shear capacity for the beam was found

to be  $V_n^s = 281$  kip and for the joint was found to be  $V_n^j = 532$  kip. The results of this analysis for Specimens 1, 4, and 3 are presented in Table 6–3.

**Table 6–3: Results of Stage 1 Shear Analysis.**

	Specimen 1		Specimen 4		Specimen 3		
$A_{sh}(in^2)$	0.393		0.393		0.393		
$f'_c(ksi)$	5.40		4.00		5.93		
$f_y(ksi)$	65		65		65		
$s^b(in.)$	4.5		4.5		4.5		
$s^j(in.)$	8		8		8		
	Singly	Doubly	Singly	Doubly	Singly	Doubly	
$jd(in.)$	31	30.5	31	30.5	31	30.5	
$V_c(kip)$	109	108	94	93	115	113	<i>Eq. (2-8)</i>
$V_s(kip)$	176	173	176	173	176	173	<i>Eq. (2-9)</i>
$V_{arch}(kip)$	437	430	376	370	458	451	<i>Eq. (2-17)</i>
$V_{truss}(kip) = \sum A_{sv}f_y$	102	102	102	102	102	102	
$V_n^s(kip)$	<b>285</b>	<b>281</b>	<b>270</b>	<b>266</b>	<b>291</b>	<b>286</b>	<i>Eq. (2-7)</i>
$V_n^j(kip)$	<b>539</b>	<b>532</b>	<b>478</b>	<b>472</b>	<b>560</b>	<b>553</b>	<i>Eq. (2-16)</i>

**Step 5:** Check strength hierarchy.

The strength reduction factor for shear and flexure are  $\phi_v = 0.90$  and  $\phi_f = 0.90$ , respectively. It is observed that for the doubly reinforced beam of Specimen 1,  $\phi_v V_n^s = 0.90 \times 281 = 253$  kip is less than  $\phi_f P_n^f = 0.90 \times 481 = 433$  kip. This result shows that the factored shear capacity for the beam is insufficient, which can lead to a shear failure in the beam. Similar observations are made for Specimens 4 and 3.

**Step 6:** Determine the shear capacity of the beam-column joint regions.

The beam-column joint shear can be found from the shear force diagram of the equivalent beam model of the C-Beam specimen shown in Figure 6–2. The joint shear was found to be  $V_{jv} = 558$  kip. The joint shear capacity of the joint is calculated based on Eq. (2-16) and is found to be  $V_n^j = 532$  kip. For the joint, it is observed that  $\phi_v V_n^j = 0.90 \times 532 = 479$  kip is less than  $\phi_f V_{jv} = 0.90 \times 558 = 502$  kip.

From this analysis it can be concluded that the factored shear capacity for both the beam and the joint is insufficient. This is true for Specimens 1, 4, and 3, and hence warrants further investigation, and a strut-and-tie analysis is performed.

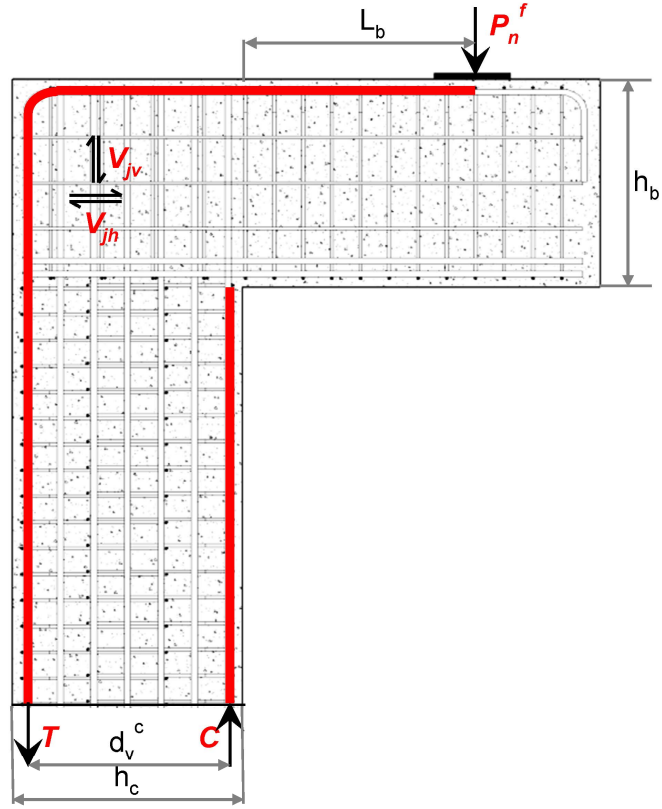
#### 6.4 STAGE 2: STRENGTH ANALYSIS USING STRUT-AND-TIE MODELING

The strut-and-tie model developed for C-Beam Specimen 1 is shown in Figure 6–3. The steps involved in the construct and analysis of the strut-and-tie method are shown below.

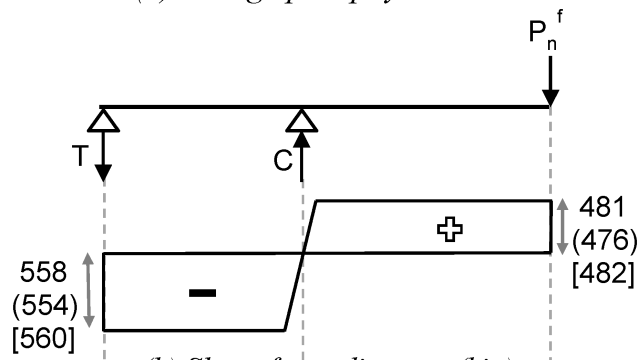
**Step 1:** Determine the truss and node geometry.

The width of the bottom face of the CCC node is equal to the depth of compression zone of the column ( $kd$ ), which is determined based on the equation for the elastic compression zone coefficient  $k$  (Eq. 2-2) and was found to be equal to 9.53 in. The bottom face of the CCC node can be proportioned based on the ratio of  $V_{jv} / P_n^f = 558 / 481 = 1.16$  (from the shear force diagram in Figure 6–2). The width of the CCT node is taken to be equal to the width of the bearing pad, which is 12 in. The width of the CTT node is based on the bar bending radius ( $R = 4$  in.) and the radius ( $d_b / 2$ ) of the longitudinal column reinforcement.

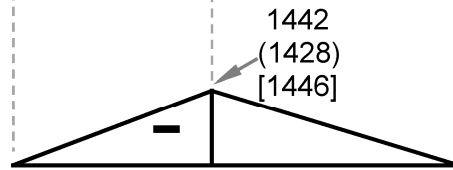
The height of the CCC node is assumed to be equal to the depth of the back face of the CCT node (which equals two times the distance from the tension face to the centroid of the tension reinforcement). The crack angle in the beam-column joint is assumed to be  $45^\circ$ . After the node geometries are determined, all the SAT model dimensions and inclination angle can be obtained.



(a) Bridge pier physical model



(b) Shear force diagram (kip)



(c) Bending moment diagram (kip-ft) of cap beam

**Figure 6–2: Shear Force and Bending Moment Diagram of the Equivalent Beam Model of C-Beam Specimen 1 (Specimen 4) and [Specimen 3].**

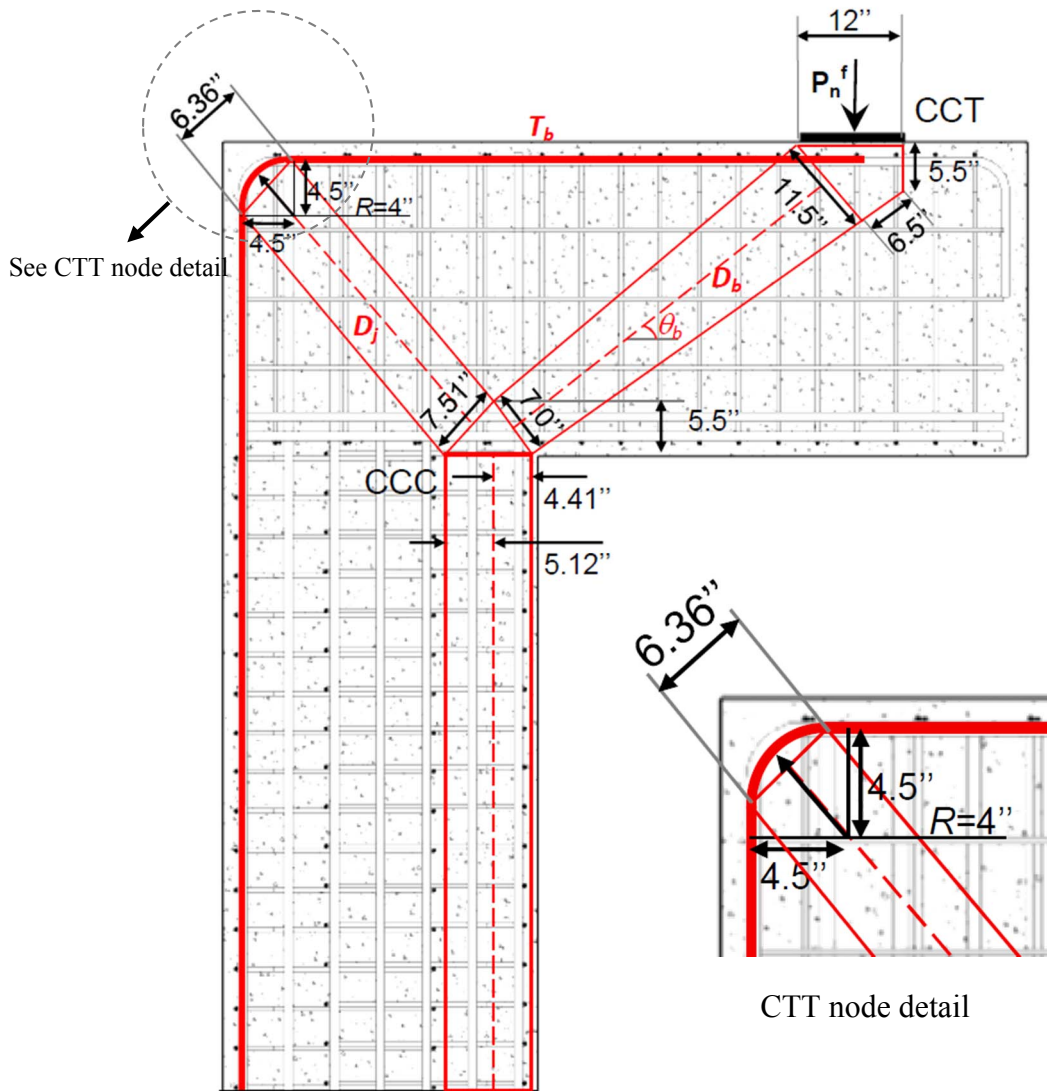


Figure 6-3: Strut-and-Tie Model for C-Beam Specimen 1.

**Step 2:** Solve the determinate truss.

All the member forces can be determined based on joint equilibrium assuming that the tension tie has yielded, that is  $T = A_s f_y$ . The externally applied load based on steel yield was found to be  $P_y^{SAT} = 429$  kip. However, this is most unlikely to be the critical load, as the critical node needs to be identified as follows.

**Step 3:** Determine critical node.

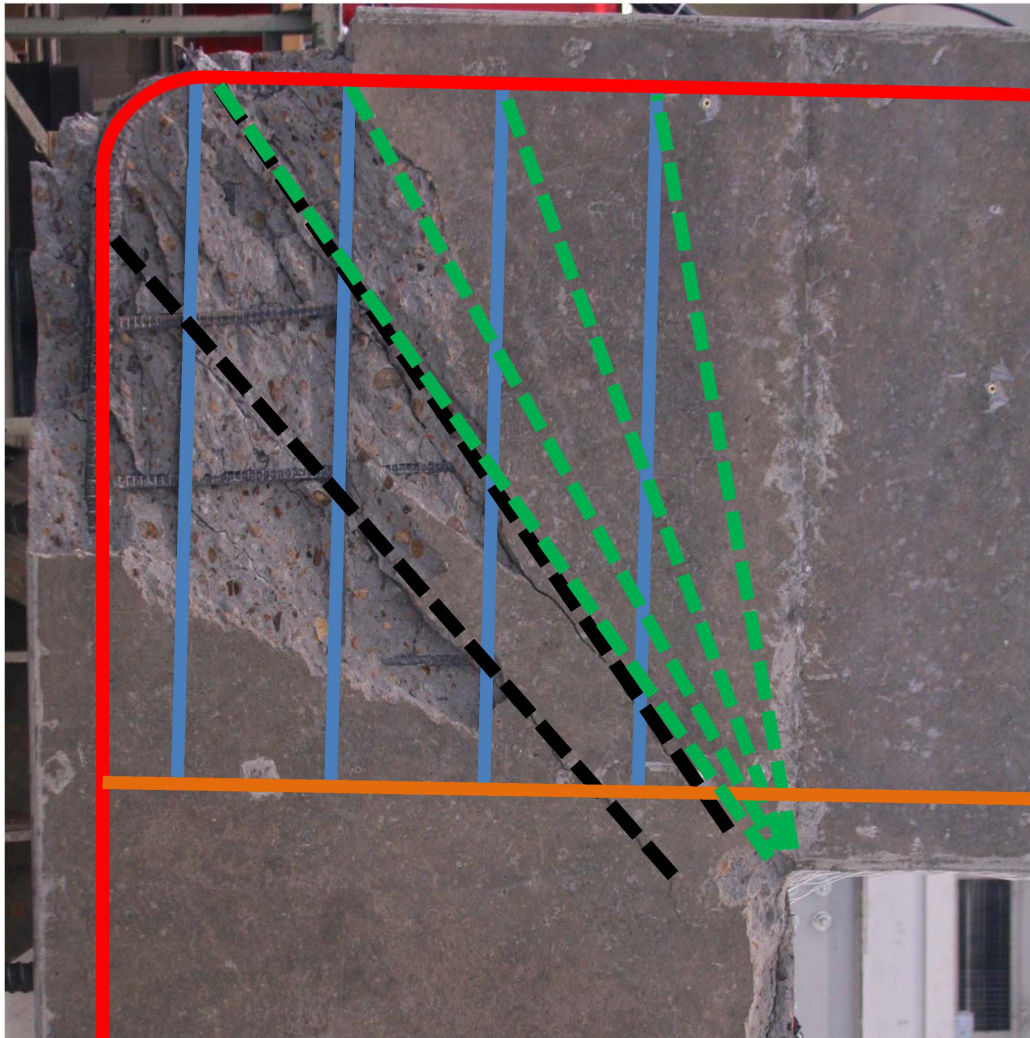
Based on the geometry of the nodes it is determined that the CTT node is the most critical node with allowable stress in this node given as  $0.65 f'_c$  (Eq. 2-19). The node strength of the CTT node is found to be  $F_{cu} = 536$  kip, 397 kip, and 588 kip for Specimen 1, 4, and 3, respectively.

**Step 4:** Determine external load causing node failure.

The external load causing node failure for Specimen 1 based on the node capacity of the CTT node can be back calculated and is found to be  $P_n^{SAT} = 318$  kip. It is noted that for both the specimen  $P_n^{SAT} < P_n^f$  and also the factored capacities  $\phi_n P_n^{SAT} < \phi_n P_n^f$ . Therefore, joint capacity is technically undependable. The results of the strut-and-tie analysis are summarized in Table 6–4.

Figure 6–4 shows that indeed the beam-column joint is most critical and that the CTT node is the most critical node. The joint is overlaid with the truss and the arch members as was observed from the crack pattern.

The results show that it is somewhat inconclusive as to what the failure mode for Specimen 1 will be because the joint capacity is technically undependable. It is observed that the specimen also have undependable joint capacity. Additionally, the SAT analysis does not take into account the effects of ASR/DEF damage. This justifies the use of an advanced analysis technique where the C-STM method comes in handy.



- Tension ties
- Beam chord
- Transverse ties
- - - Truss action
- - - Arch action

**Figure 6-4: Failure Pattern Observed at the Beam-Column Joint of C-Beam Specimen 1.**



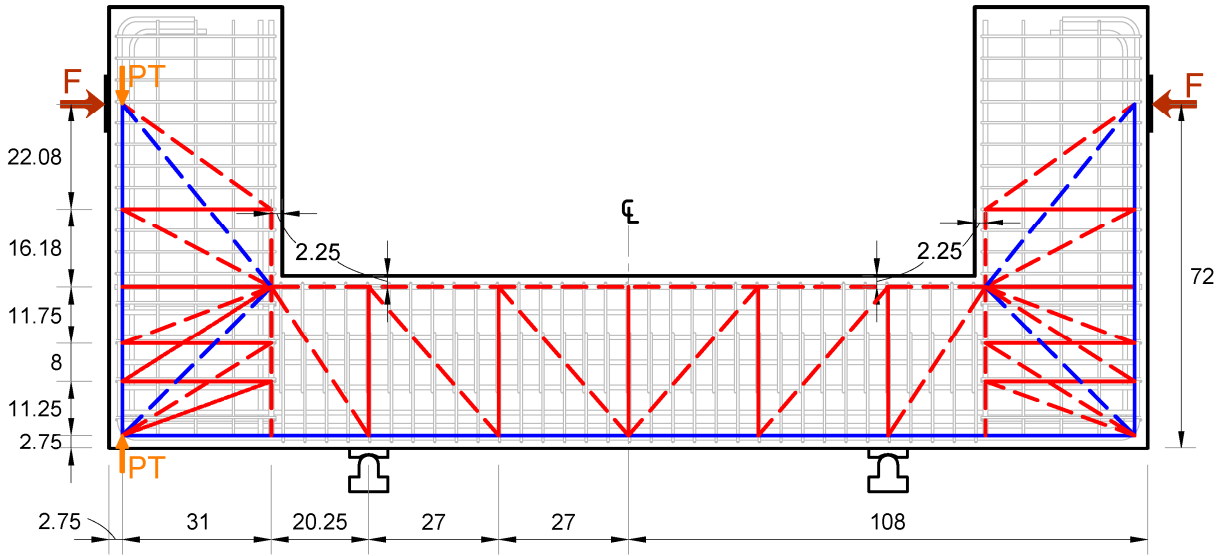
**Table 6–4: Results for Stage 2 SAT Analysis.**

	<b>Specimen 1</b>	<b>Specimen 4</b>	<b>Specimen 3</b>	<b>Comments</b>
$D_b$ (kip)	667	667	667	
$D_j$ (kip)	723	723	723	
$\theta_b$ (degrees)	40	40	40	
$\theta_j$ (degrees)	45	45	45	
$P_y^{SAT}$ (kip)	429	429	429	Based on longitudinal steel yield.
$\phi_v P_y^{SAT}$ (kip)	300	300	300	
$P_n^{SAT}$ (kip)	<b>318*</b>	<b>236*</b>	<b>349*</b>	Based on node capacity.
$\phi_v P_n^{SAT}$ (kip)	223	165	244	
$\phi_f P_n^f$ (kip)	433	428	434	

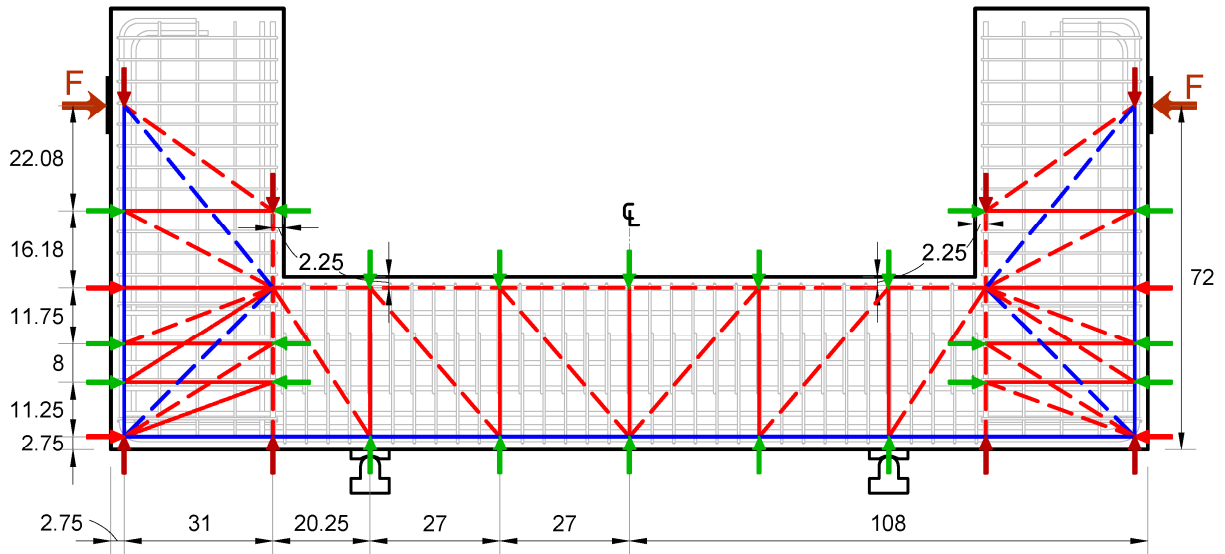
\*Expected critical failure mode capacity.

### **6.5 STAGE 3: STRENGTH AND DEFORMATION CAPACITY USING COMPATIBILITY STRUT-AND-TIE COMPUTATIONAL MODELING**

Figure 6–5 shows the C-STM model for C-Beam specimen (a) without and (b) with ASR/DEF damage. The cantilever beams were modeled using a single-point Gauss quadrature model. The joints were modeled using a two-point Gauss model (Kim and Mander, 1999) where the transverse ties were aligned with the U-bar reinforcement to provide a more exact representation of the reinforcement. The representative areas of reinforcement for the tension chord were defined as the sum of longitudinal steel and three sets of web distribution steel for tension. The compression chord was defined as the compression longitudinal steel. Rows 2, 3, and 4 of Figure 6–6, respectively, show the different nonlinear concrete stress-strain relationships that were derived for C-Beam Specimens 1, 4, and 3 from the material properties presented in Table 6–1.



(a) Specimen 1: Without ASR/DEF damage



(b) Specimen 2,3 & 4: With ASR/DEF damage

- Primary tension reinforcement
- Ties representing bundles of hoops
- - - Concrete struts for "truss"
- - - Central concrete "arch"
- Initial confinement effect in hoops and longitudinal steel due to concrete swelling, modeled as a set of externally applied nodal forces
- 

**Figure 6-5: Modeling the C-Beam Specimens without and with ASR/DEF Damage.**

Note: The additional forces in (b) represent the prestress effect actively induced in the reinforcing steel caused by ASR/DEF induced concrete swelling.

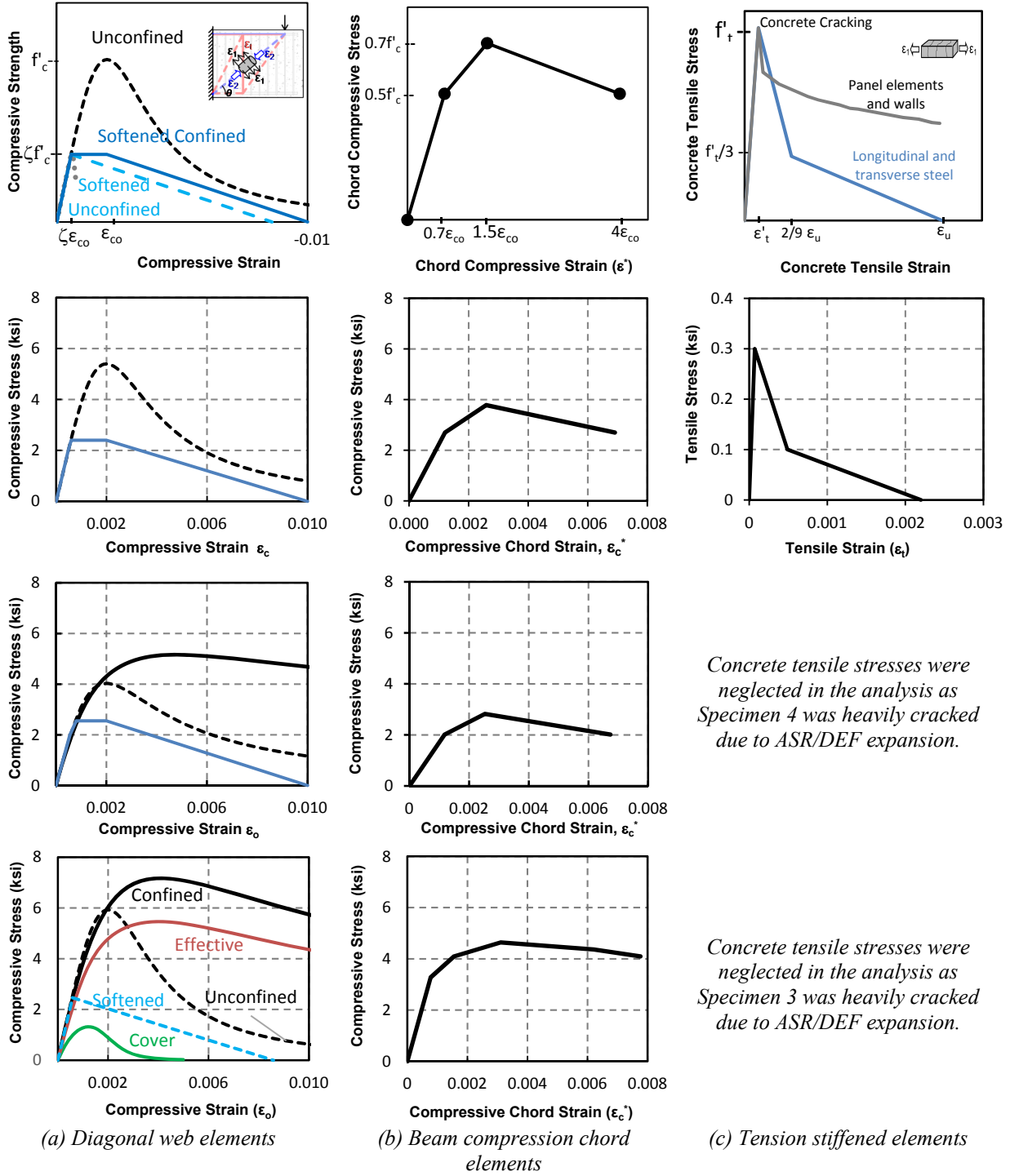


**Figure 6-6: Cracked Reinforced Concrete Material Properties.**

- Row 1: Theoretical nonlinear behavior**
- Row 2: Specimen 1 modeled behavior**
- Row 3: Specimen 4 modeled behavior**
- Row 4: Specimen 3 modeled behavior**

### Stage 3.1: C-STM without ASR/DEF damage

Figure 6–5a shows the C-STM model that was developed for C-Beam Specimen 1. Specimen 1, the control specimen, had no ASR/DEF induced damages. To simulate the experimental test setup as accurately as possible, initial loads (shown as PT in Figure 6–5a) were applied to the tension chord members of the protected beam in order to replicate post-tensioning effects in accordance with Phase I and Phase II testing. Note that this model essentially represents the C-STM analysis *without* any ASR/DEF effects.

### Stage 3.2: C-STM with ASR/DEF damage

Figure 6–5b shows the C-STM model for C-Beam Specimens 4 and 3, which respectively, showed '*moderate*' and '*heavy*' damage due to ASR/DEF. In order to account for the effects of ASR/DEF expansion, the confinement ratio for Specimen 4 was calculated to be  $K_{cc} = 1.28$  and  $1.35$  for the beam and the column core concrete, respectively. Similarly for Specimen 3 the confinement ratio was calculated as  $K_{cc} = 1.21$  for the beam and  $K_{cc} = 1.31$  for the column. The computation of confinement ratio for Specimen 3 is presented in Sheet 6-1. Based on the theory presented in section 3.6.5 the cover concrete strength reduction factors  $\lambda = 0.40$  and  $\lambda = 0.30$  were adopted for Specimens 4 and 3 with '*moderate*' and '*heavy*' damage. As both the cover and core concrete areas contribute to the area of the strut in the C-STM model, a weighted average value of concrete compressive strength was used in the C-STM model. The computation of the effective concrete compressive strength for Specimen 3 is presented in detail in the Sheet 6-2.

The prestress in the longitudinal and transverse reinforcement were deduced from the ASR/DEF expansion model presented in Chapter 4 and applied to the C-Beam specimens in Chapter 5, unlike in the earlier work (Mander et al., 2012b) where recommendations were made for the prestrains based on the level of damage. Detailed prestrain computations for the different longitudinal and transverse members of Specimen 3 are presented in Sheet 6-3–Sheet 6-7.

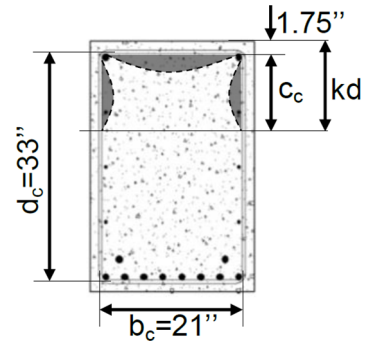
Sheet 6-1	Computation of material properties to perform the C-STM analysis for C-Beam Specimen 3.	1 2
-----------	---	--------

**1. Computation of Confinement Ratio for Beam and Column**

Concrete compressive strength obtained experimentally from cylinder tests,  $f'_c = 5.93$  ksi  
 As the strains in the steel were much higher than the yield strain,  $f_y = 75$  ksi is considered for the following computations.

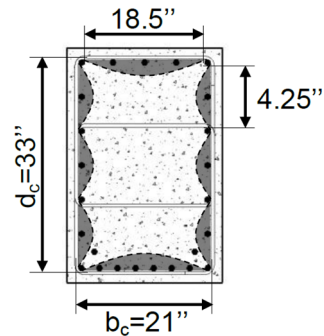
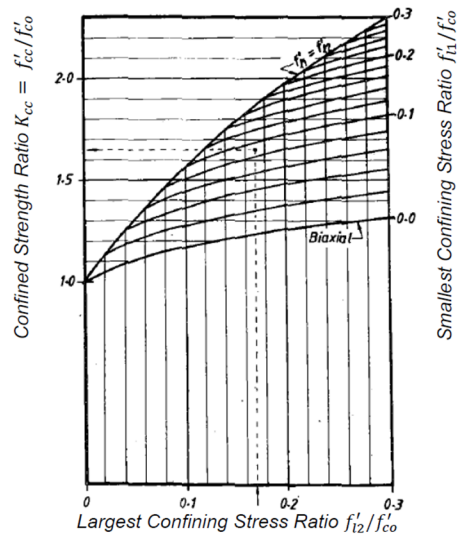
Computation of concrete confinement ratio: beam

$kd$ (in.)	11.31
$A_{cc}$ (in <sup>2</sup> ) = $(c_c + d_s / 2) \times b_c$	206
$A_e$ (in <sup>2</sup> ) = $(c_c + d_s / 2) \times b_c$ - area of shaded region	124.58
$k_e = A_e / A_{cc}$	0.605
$f_{lx}$ (ksi) = $k_e \frac{A_{str} f_y}{(c_c + d_{str}) s}$	0.201
$f_{ly}$ (ksi) = $k_e \frac{2 A_{str} f_y}{b_c s}$	0.188
Smallest confining stress ratio $f_{ly} / f'_c$	0.032
Largest confining stress ratio $f_{lx} / f'_c$	0.034
$K$ (from chart)	1.21



Computation of concrete confinement ratio: column

$kd$ (in.)	13.98
$A_{cc}$ (in <sup>2</sup> ) = $(c_c + d_s / 2) \times b_c$	693
$A_e$ (in <sup>2</sup> ) = $(c_c + d_s / 2) \times b_c$ - area of shaded region	560.85
$k_e = A_e / A_{cc}$	0.81
$f_{lx}$ (ksi) = $k_e \frac{(A_{str})_x f_y}{s d_c}$	0.321
$f_{ly}$ (ksi) = $k_e \frac{(A_{str})_y f_y}{s b_c}$	0.252
Smallest confining stress ratio $f_{ly} / f'_c$	0.042
Largest confining stress ratio $f_{lx} / f'_c$	0.054
$K$ (from chart)	1.31



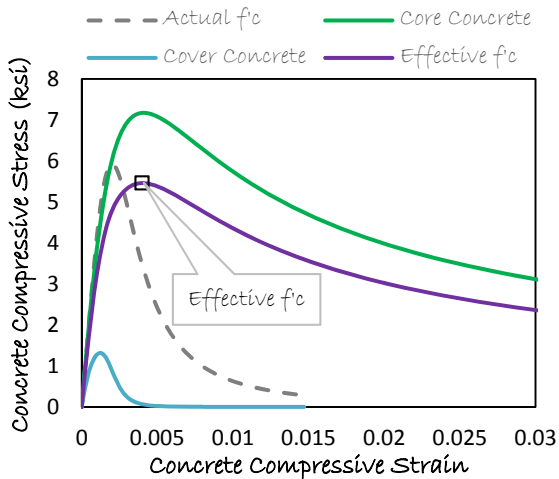
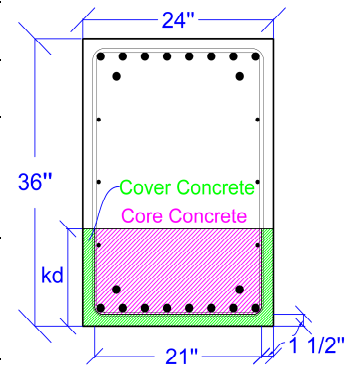
Sheet 6-2	Computation of material properties to perform the C-STM analysis for C-Beam Specimen 3.	2 2
-----------	---	--------

## 2. Computation of effective concrete strength

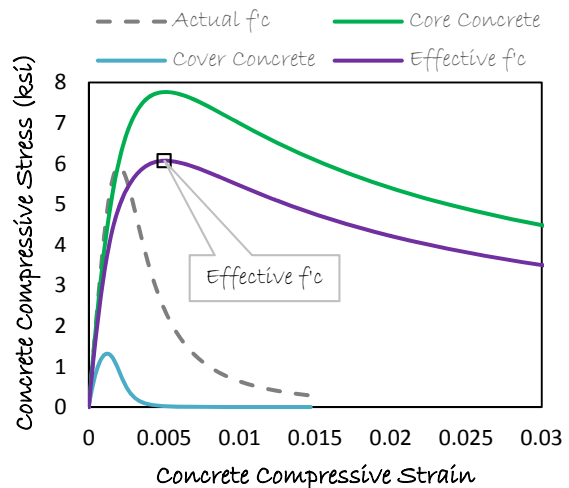
$kd$  = depth from the compression face to the neutral axis

Total area of concrete assigned to the chord members = breadth  $\times$  depth to neutral axis from compression face,  $A_{total} = b \times kd = 24 \times kd$

	Beam	Column
$kd$ (in)	11.31	13.98
Area of cover concrete (in <sup>2</sup> )	65.43	73.44
$A_{cover} = 2(1.5) \times kd + [b - 2(1.5)]1.5$		
Area of core concrete (in <sup>2</sup> )	206	262.1
$A_{core} = [24 - (2 \times 1.5)](kd - 1.5)$		
Contribution of cover concrete to the total area = $A_{cover} / A_{total}$	0.241	0.219
Contribution of core concrete to the total area = $A_{core} / A_{total}$	0.759	0.781
Effective $f'_c$ from graph (ksi)	5.46	6.07



Concrete Stress-Strain Relation for Beam



Concrete Stress-Strain Relation for Concrete

Sheet 6-3	Computation of prestains in the various members of the C-STM model for Specimen 3	1 5
-----------	---	--------

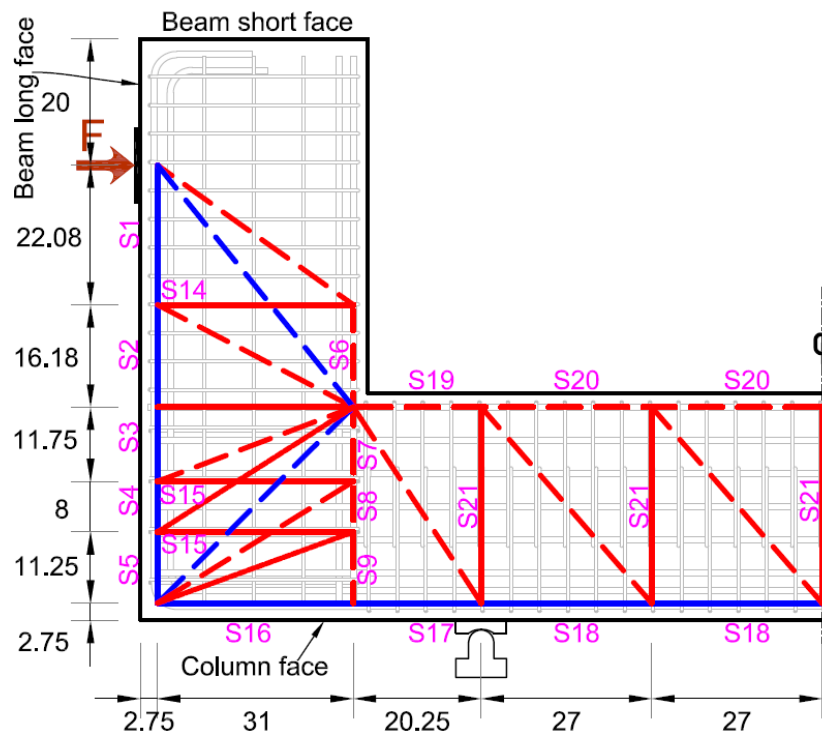
General notes

Development length for Specimen 3 #8 bars (DL) = 42.20"

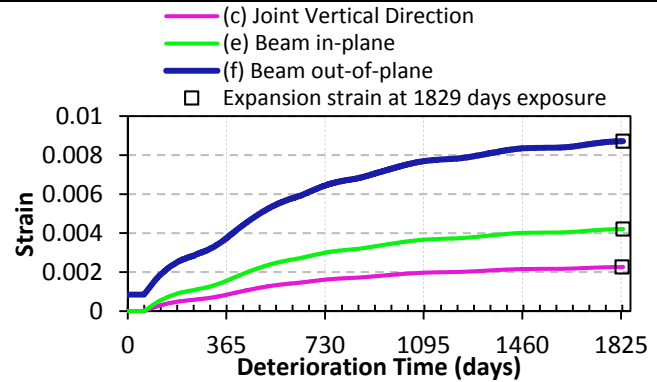
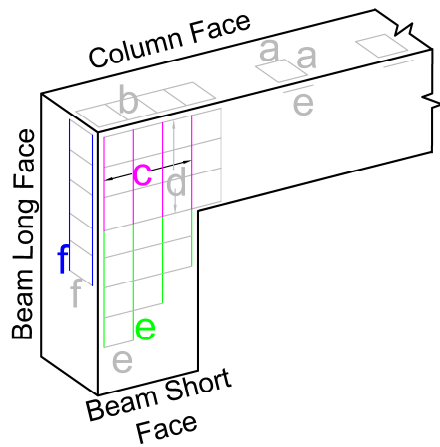
Distance to center of C-STM members (l)

Member	from beam short face (in.)	from column face (in.)
S1	31.04	58.22
S2/S6	50.17	39.09
S3/S7	64.135	25.125
S4/S8	74.01	15.25
S5/S9	83.635	5.625
	from beam long face (in.)	
S16	15.5	
S17/S19	41.125	

Note: values in blue are less than the development length.



Longitudinal beam members (S1-S5)



Modeled Expansion Strains Outside Development Length Zone

The prestrains in the longitudinal beam members (S1-S5) are computed considering the average of modeled expansion strains at the end of the exposure period (1829 days) in the joint vertical direction (c presented as Case III in Appendix I) or longitudinal beam in-plane direction (e presented as Case V in Appendix I) and longitudinal beam out-of-plane direction (f presented as Case VII in Appendix I).

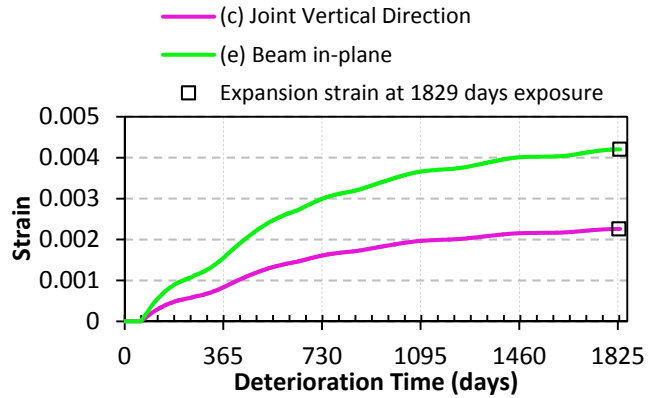
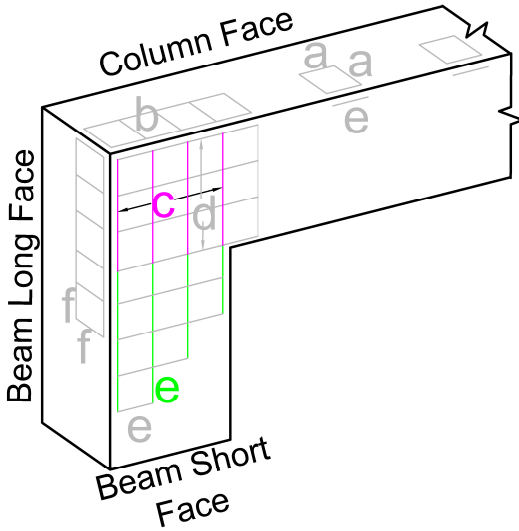
Note:  $\rho_{eff} = (l/DL)\rho$  and  $\epsilon_{\rho_{eff}}^{1829}$  = expansion strain at 1829 days of exposure.

		Joint vertical direction c (Case III, Appendix I)		Longitudinal beam out-of-plane direction f (Case VII, Appendix I)		Average prestrain
Outside DL		$\rho = 0.0529$		$\rho = 0.01428$		
		$\epsilon_{\rho}^{1829} = 0.00226$		$\epsilon_{\rho}^{1829} = 0.00871$		
C-STM Member	l from column face (in.)	$\rho_{eff}$	$\epsilon_{\rho_{eff}}^{1829}$	$\rho_{eff}$	$\epsilon_{\rho_{eff}}^{1829}$	Average prestrain
S5	5.625	0.00705	0.00884	0.0019	0.0274	
S4	15.25	0.01912	0.00427	0.00516	0.01652	0.01040
S3	25.125	0.0315	0.00305	0.00850	0.01214	0.00759
S2	39.09	0.0490	0.00235	0.01323	0.00914	0.00575
		Longitudinal beam in-plane e (Case V, Appendix I)		Longitudinal beam out-of-plane direction f (Case VII, Appendix I)		Average prestrain
l from beam short face		$\rho = 0.01954$		$\rho = 0.01428$		
S2	Outside DL	$\epsilon_{\rho}^{1829} = 0.0042$		$\epsilon_{\rho}^{1829} = 0.00871$		0.00646
S1	31.04"	$\rho_{eff} = 0.01437$	$\epsilon_{\rho_{eff}}^{1829} = 0.00523$	$\rho_{eff} = 0.01050$	$\epsilon_{\rho_{eff}}^{1829} = 0.01060$	0.00792

Note: Prestrain values presented in blue are adopted for the corresponding C-STM member.



**Longitudinal Beam Members (S6-S9)**



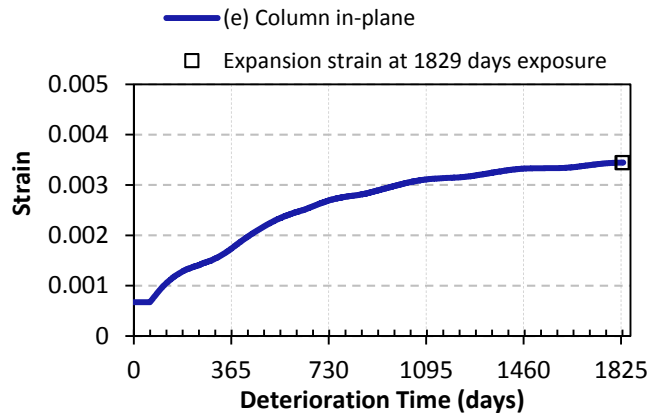
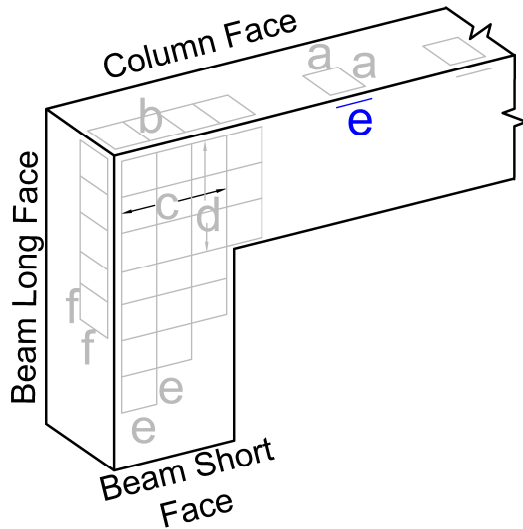
Modeled Expansion Strains Outside Development Length Zone

The prestains in the longitudinal beam members (S6-S9) are computed considering the modeled expansion strains at the end of the exposure period in the joint vertical direction (c presented as Case III in Appendix I) or longitudinal beam in-plane direction (e presented as Case V in Appendix I).

		Joint vertical direction c (Case III, Appendix I)	
Outside DL		$\rho = 0.0529 \quad \epsilon_p^{1829} = 0.00226$	
C-STM Member	l measured from column face (in.)	$\rho_{eff}$	$\epsilon_{p(eff)}^{1829}$
S9	5.625	0.00705	0.00884
S8	15.25	0.01912	0.00427
S7	25.125	0.0315	0.00305
S6	39.09	0.0490	0.00235
		Longitudinal beam in-plane e (Case V, Appendix I)	
S6	Outside DL	$\rho = 0.01954 \quad \epsilon_p^{1829} = 0.0042$	

Note: Prestrain values presented in blue are adopted for the corresponding C-STM member.

Longitudinal column members (S16-S20)



Modeled Expansion Strains Outside Development Length Zone

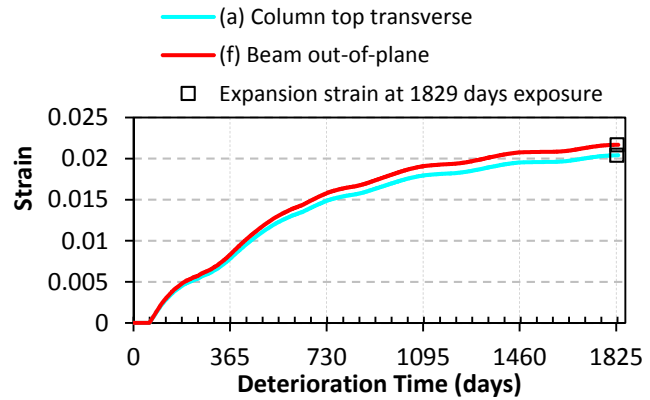
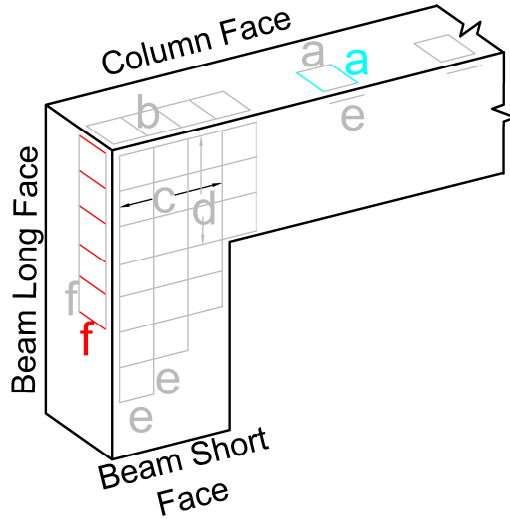
The prestains in the longitudinal column members (S16-S20) are computed considering the modeled expansion strains at the end of the exposure period (1829 days) in the column longitudinal face (e presented as Case VI in Appendix I).

Note:  $\rho_{eff} = (l/DL)\rho$  and  $\epsilon_{\rho_{eff}}^{1829}$  = expansion strain at 1829 days of exposure.

C-STM Member	l measured from beam long face (in.)	Column longitudinal direction e (Case VI, Appendix I)	
S18/S20	Outside DL	$\rho = 0.0671 \epsilon_p^{1829} = 0.0034$	
		$\rho_{eff}$	$\epsilon_{\rho_{eff}}^{1829}$
S17/S19	41.125	0.06539	0.0034
S16	15.5	0.02465	0.00565

Note: Prestrain values presented in blue are adopted for the corresponding C-STM member.

Transverse members (S14, S15, S21)



Modeled Expansion Strains Outside Development Length Zone

The prestrains in the transverse members in the beam (S14) and the beam-column joint (S15) are computed considering the modeled expansion strains at the end of the exposure period (1829 days) in the beam out-of-plane region (f presented as Case I in Appendix I). Similarly, the prestrains in the column transverse members (S21) are computed from the modeled expansion strains in the column top transverse region (a presented as Case II in Appendix I).

Note:  $\rho_{eff} = (l / DL) \rho$  and  $\epsilon_{\rho_{eff}}^{1829} =$  expansion strain at 1829 days of exposure.

C-STM Member	$\rho$	$\epsilon_{\rho}^{1829} =$
S14/S15	0.00177	0.02166
S21	0.00198	0.02038

Note: Prestrain values presented in blue are adopted for the corresponding C-STM member.

Table 6–5 presents a summary of the prestrains for Specimen 3 and 4. Based on the prestrains and the area of the steel member, the prestress force on the C-STM members were backcalculated. The modified stress-strain relation of longitudinal and transverse reinforcing steel due to prestressing effects (for Specimen 4) is shown in Figure 6–7.

## 6.6 C-STM RESULTS AND DISCUSSION

Figure 6–8a shows the modeled results for the C-STM response for C-Beam Specimens 1, 4, and 3. The stiffness change in the control Specimen 1 at about 130 kip was due to the first cracking of concrete. For Specimens 4 and 3, the major stiffness changes were at 450 kip and 465 kip, respectively. This change in stiffness occurred when the decompression of the prestress effect occurred at the critical cross sections.

Figure 6–8b presents the experimental performance of the C-Beam specimens. The behavior of the specimens during the initial prestress process were not captured accurately. Therefore, the initial displacement of the experimental results are offset based on the C-STM observations.

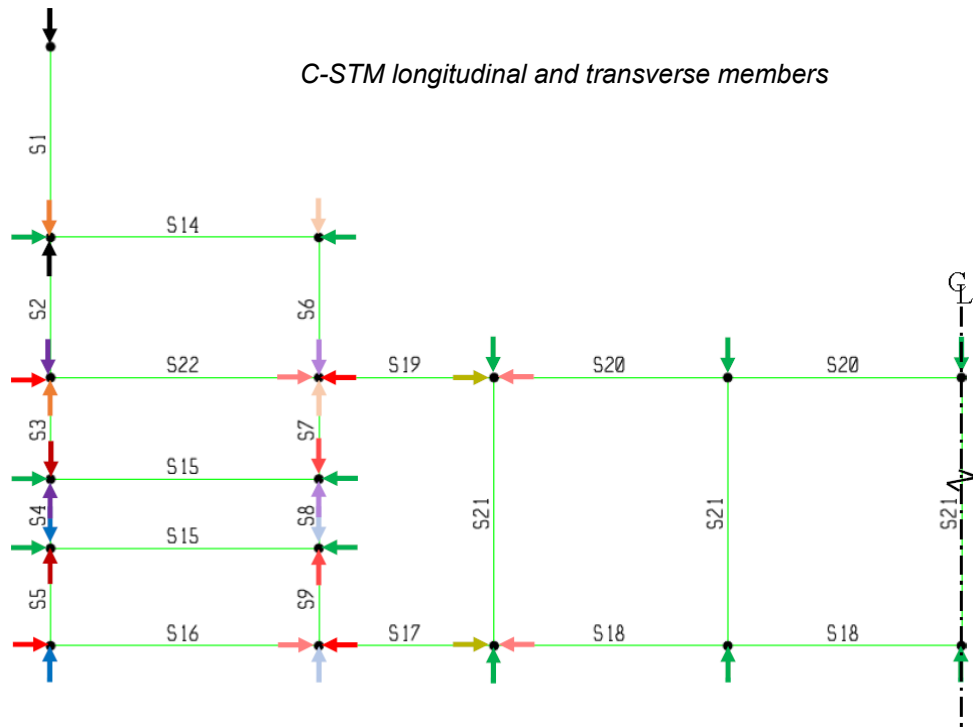
It is evident from Figure 6–8 that the computationally modelled C-STM results are in good agreement with the experimental observations from the C-Beam specimens. A comparison between the C-STM and experimental ultimate load capacity for the C-Beam specimens shows that the C-STM results are within 5% from the experimental results.

The various levels of deterioration caused by ASR/DEF expansion on the concrete structure were also successfully modeled into the C-STM, and the results are in good agreement with the experimental observations.

All the nonlinear mechanisms that developed progressively in the various constituent members of the C-STM are presented in Figure 6–9. The left column of Figure 6–9 shows the development of nonlinear hinges formed during the C-STM analysis of the C-Beam specimens. When this information is combined with the overall force-deformation behavior of the specimens (the graphs in Figure 6–9), some insight into the progression of nonlinear hinge formation with respect to the global force-deformation behavior of the structure is obtained. These modeled outcomes shown in Figure 6–9 agree well with the visual observations made during each experiment.

**Table 6-5: Prestrains in C-STM Members for C-Beam Specimens.**

Member	Specimen 4	Specimen 3
S1	0.0044	0.0079
S2	0.0036	0.0065
S3	0.0038	0.0076
S4	0.0046	0.0104
S5	0.0068	0.0181
S6	0.0027	0.0042
S7	0.0021	0.0031
S8	0.0027	0.0043
S9	0.0043	0.0088
S14/S15	0.0075	0.0217
S16/S22	0.0044	0.0057
S17/S19	0.0028	0.0034
S18/S20	0.0025	0.0034
S21	0.0133	0.0204



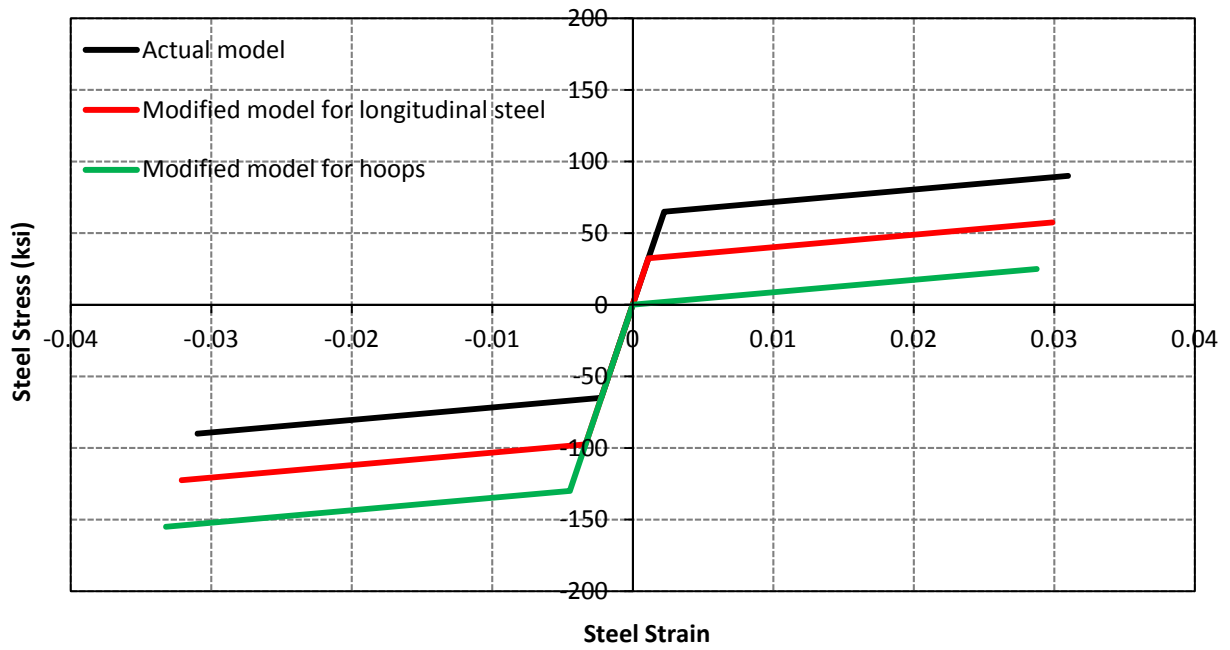
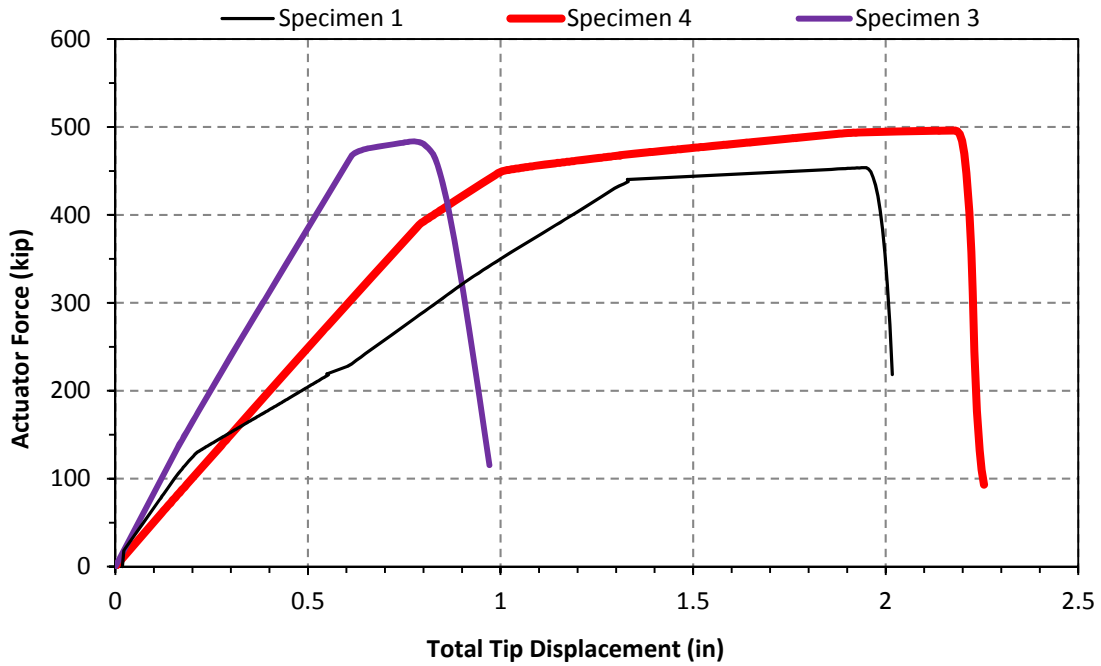
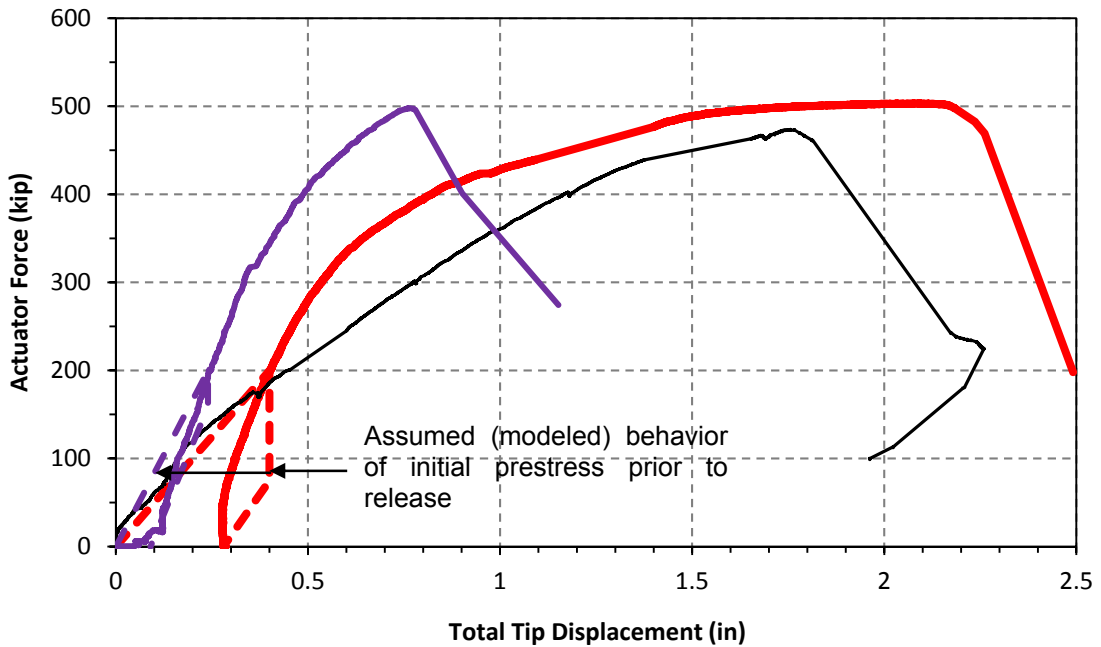


**Figure 6-7: Actual and Modified Stress-Strain Models for Reinforcing Steel to Account for Prestressing Effects in C-Beam Specimen 4.**



(a) C-STM Results



(b) Experimental Performance

Figure 6-8: Force-Deformation Results for Specimens 1, 4, and 3.

Figure 6–9a shows the order of nonlinear hinge formation observed from the C-STM analysis of Specimen 1, in addition to the force-deformation of C-Beam Specimen 1 along with the points that correspond to the formation of nonlinear hinges. The chronological progression of nonlinear behavior for C-Beam Specimen 1 is as follows.

- Longitudinal cracking first occurred in the beam. This is when the member stress exceeds the concrete tensile strength, thus initiating flexural cracking in the beam at the column face, and along the column, respectively. Tension softening refers to the concrete's ability to resist tensile strains after the development of the primary cracks.
- Transverse cracking then occurred in the transverse concrete elements, starting in the beam-column joint and then in the beam. This corresponds with diagonal shear cracking observed as a result of the flexure-shear interaction and is in agreement with experimental observations.
- Chord compression occurred in the diagonal arch and column compression chord elements indicating that the concrete had exceeded the elastic limit of  $0.5f'_c$ .
- Longitudinal yielding occurred in the longitudinal beam reinforcement when the stress exceeds the specified yield stress  $f_y$ .
- Transverse steel yielding in the beam-column joint U-bars were the next member in the C-STM to respond nonlinearly.
- With the yielding of transverse reinforcement in the beam-column joint the load-carrying capacity of the truss mechanism is limited, and the stress flow occurs through the corner-to-corner arch diagonal in the beam-column joint.
- The final event, which results in the collapse of the concrete bridge pier, is compression softening of the main corner-to-corner (arch) strut in the beam-column joint.

It should be noted that Specimens 3 and 4 were heavily cracked due to the effects of ASR/DEF related expansion. Therefore, for Specimens 3 and 4 the concrete tensile strength was neglected in the C-STM analysis. As noted earlier, prestress forces were applied to the C-STM model to simulate the effects of expansion caused by ASR/DEF on the structure. Concrete decompression in Figure 6–9 refers to the stage when the effects of the applied prestress are overcome by the applied loading and the concrete strains become tensile (positive).



× Concrete Cracking ◆ Concrete Compression ■ Concrete Decompression ● Steel Yield × Concrete Crushing

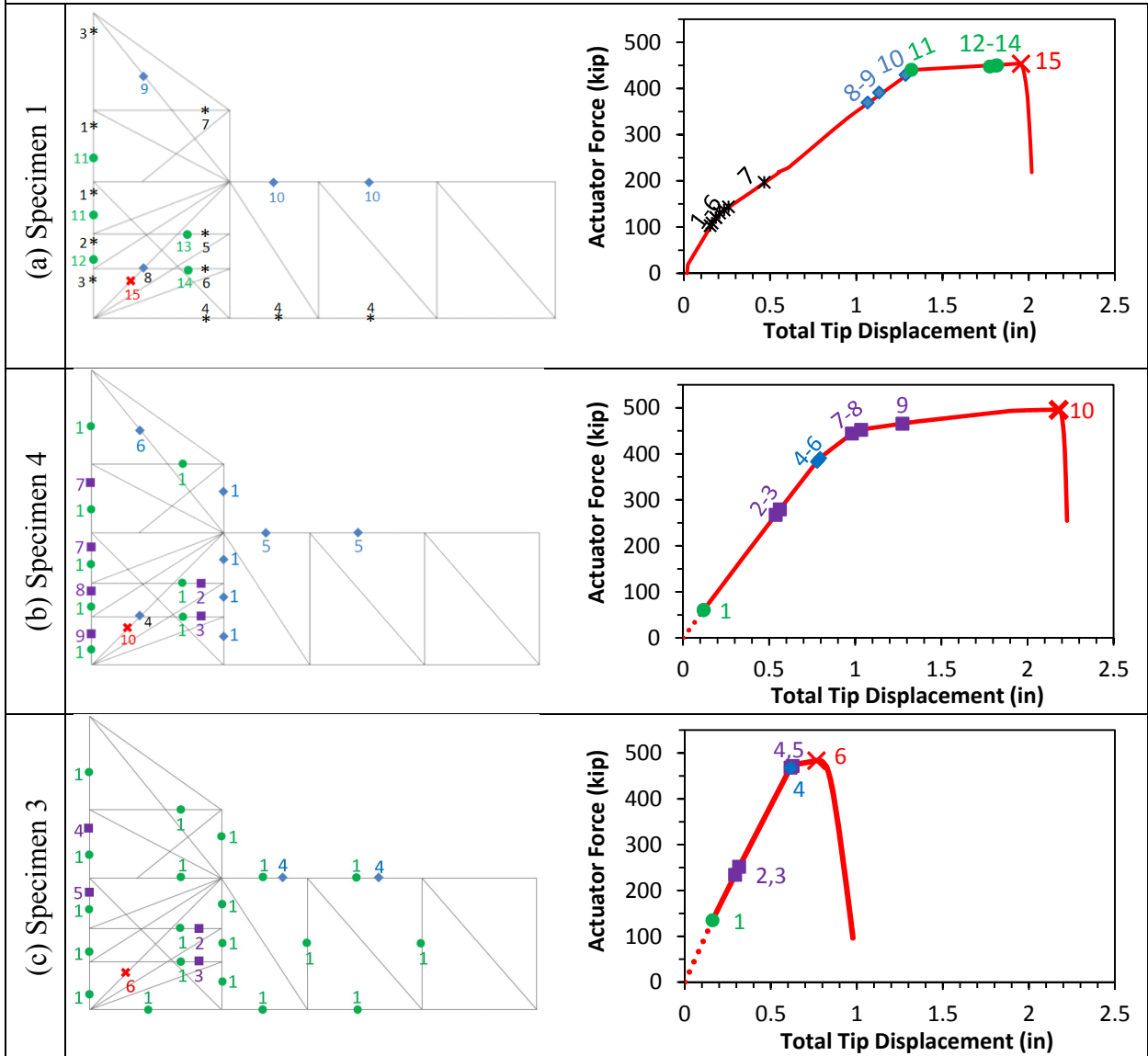


**Figure 6-9: Computed Sequence of Non-Linear Behavior Events.**

(Note: Specimens 1, 4, and 3 respectively, had no, moderate, and heavy ASR/DEF damage.)

In Specimens 3 and 4, from the strain data obtained from the field, it was noted that reinforcement had yielded prior to testing. Similar observations are made in the C-STM analysis. In Specimen 4 the major change in stiffness of the force-deformation behavior occurred when decompression occurred in concrete in the beam and the beam-column region of the specimen (events 7-8 in Figure 6–9c). Similar observations were also made for Specimen 3 where the major change in stiffness occurred during the decompression of longitudinal reinforcement in the beam and beam-column region (events 4-5 in Figure 6–9d) just before the failure of the specimen.

From Figure 6–9 it is evident that by overlaying the commencement of formation of non-linear hinges in the different members of the C-STM on the overall force-deformation behavior of the specimen, a deep insight into the internal mechanism of the specimen behavior can be obtained. Also it is clear that the final event which resulted in the collapse of the C-Beam specimens with and without ASR/DEF damage was the compression softening of the corner-to-corner (arch) strut in the beam-column joint and the CTT node failure was an outcome of that failure mechanism.

## **6.7 CONCLUDING REMARKS ON WORKED EXAMPLE**

The results of the analysis are summarized in Table 6–6.

From the results presented in Table 6–6 and the C-STM results presented in Figure 6–8, it is observed that the flexural analysis predicts the yield force accurately. However, the sectional shear approach had the largest discrepancy and did not accurately represent the specimen capacity. These predictions are unduly harsh because the shear capacity is calculated in a D-region where the theory breaks down. It is for this reason a SAT analysis needs to be conducted. This analysis would imply that the joint would fail even before the beam yielded, thus suggesting that the structure fails in a very brittle manner. However, this is not the case as can be seen from the experimental results (Figure 6–8). The effects of ASR/DEF damage cannot be analyzed using any of these techniques.

On the other hand, the C-STM simulates the behavior of the specimen quite well and also overcomes the difficulties associated with trying to model the failure mechanism using present conventional strength-based analysis techniques used in AASHTO LRFD (2010) for design. The

Table 6–6: Result for C-Beam Specimens 1, 4, and 3.

		Specimen 1		Specimen 4		Specimen 3		
Stage		Capacity (kip)	Factored Capacity (kip)	Capacity (kip)	Factored Capacity (kip)	Capacity (kip)	Factored Capacity (kip)	Comments
Stage 1: Beam Theory	$P_y^b$	430	---	428	---	430	---	External load based on yield flexural of the beam.
	$P_n^f$	481	433	476	428	482	434	External load based on nominal flexural capacity of the beam.
	$V_n^s$	281	253	266	239	286	257	Beam shear capacity.
	$V_n^j$	532	479	472	425	553	498	Joint shear capacity.
Stage 2: SAT	$P_n^{SAT}$	318	223	236	165	349	244	External load based on critical CTT node.
	$P_y^{SAT}$	429	N/A	429	N/A	429	N/A	External load based on yield of longitudinal steel in beam.
Stage 3: C-STM	$P_{C-STM}$	<b>454*</b>	318 <sup>+</sup>	<b>496*</b>	347	<b>484*</b>	339	Compression failure due to diagonal splitting/compression in the beam-column joint zone. $\phi = 0.70$ (assumed).
Experiment	$P_{Failure}^{Expt}$	474	---	503	---	498	---	Maximum load at incipient failure due to failure in beam-column joint zone.

\* Bold typeface = critical case.

<sup>+</sup> Value assumed for overall structural load rating.

effects of ASR/DEF were modeled into the C-STM analysis technique, and the results are in good agreement with the experimental observations. Additionally, the C-STM provides additional insight in terms of the sequence of behavior and whether the behavior is ductile or brittle.

Finally, providing the applied factored loads  $1.25D+1.75(L+I)$  are less than  $\phi P_{C-STM} = 318$  kip then the load carrying performance of the structure can be deemed acceptable. However, it is to be noted that ‘heavy’ damage due to ASR/DEF considerably affects the ductility of the structure. Additionally, the cracks act as a pathway for moisture ingress into the core of the specimen which in turn promotes a considerable amount of corrosion of the exposed reinforcing bars. It is unknown what the combined effects of ASR/DEF expansion and corrosion would be on the structure.

## 7. CLOSURE

The model for ASR/DEF related expansion in reinforced concrete, is an effective means of predicting the expansion strain in the various regions of a structure. Knowing the expansion strains, the amount of prestress to be applied on the structure to simulate the effects of ASR/DEF expansion can be computed.

From the analysis of the C-Beam specimens presented in the earlier sections, it can be seen that the strength-based analysis does not give a conclusive estimate of the ultimate strength of bridge piers. Also, none of these analysis techniques takes the effects of ASR/DEF damage into account. However, the compatibility based strut-and-tie model that was developed as a computational method of analyzing the nonlinear flexure-shear interaction of deep beams and other disturbed regions gives a good estimate of the behavior of shear critical concrete bridge piers. The highlights of the expansion modeling and computational truss modeling technique are as follows:

### *ASR/DEF Expansion Model:*

- The proposed minimalist model needs limited input parameters, which can be deduced from expansion observations and material properties.
- In addition to the effects of varying temperature and moisture on ASR/DEF induced expansion, the effects of compressive and tensile stresses were also included in the formulation.
- By taking into account the appropriate reinforcement ratios, the model was able to simulate the expansion strains in the longitudinal and transverse directions. Considering the complex nature of the ASR/DEF expansion mechanism, and the wide scatter of field recorded data, the model was able to simulate the expansion strains quite well.

### *C-STM Analytical Modeling:*

- Incorporates a method for apportioning the interaction of different truss and arch shear resisting mechanisms.
- Incorporates the contribution of both flexural steel and concrete in compression chord members transformed from conventional stress block methods, which in turn defines nodal coordinates.

- Incorporates a direct method of modeling the softened constitutive relations of cracked reinforced concrete struts, which does not require an iterative process to obtain convergence.
- Enables to model the effects of ASR/DEF into the analysis.
- Accurately simulates the global force-deformation response of the structure without and with ASR/DEF damage.
- Enables to “see” the nonlinear mechanism that progressively develops in the structure and precisely pinpoints the failure point and mechanism.

## REFERENCES

- AASHTO. (2010). "LRFD Bridge Design Specifications and Commentary." Third edition, *American Association of State Highway and Transportation Officials*, Washington DC, 1264 pp.
- ACI Committee 318. (2011). "Building Code Requirements for Structural Concrete (ACI 318-11) and Commentary." *American Concrete Institute*, Farmington Hills, MI, 2008.
- Arnold, D.M. (2004). "Development and Experimental Testing of a Seismic Damage Avoidance Designed Beam to Column Connection Utilizing Draped Unbonded Post-tensioning." M.S. Thesis, University of Canterbury, Christchurch, New Zealand.
- Belarbi, A., and Hsu, T.T.C. (1995). "Constitutive Laws of Softened Concrete in Biaxial Tension-Compression." *ACI Structural Journal*, 92(5), 562-573.
- Bentz, E.C., Vecchio, F.J., and Collins, M.P. (2006). "Simplified Modified Compression Field Theory for Calculating Shear Strength of Reinforced Concrete Elements." *ASCE J Struct Div*, 104(4), 649-666.
- Bouzabata, H., Multon, S., Sellier, A., and Houari, H. (2012). "Effects of Restraint on Expansion due to Delayed Ettringite Formation." *Cement and Concrete Research*, 42(7), 1024-1031.
- Capra B., and Sellier A. (2003). "Orthotropic Modelling of Alkali-Aggregate Reaction in Concrete Structures: Numerical Simulations." *Mechanics of Materials*, 35(8), 817-830.
- Collins, M.P. (1978). "Towards a Rational Theory for RC Members in Shear." *ASCE J Struct Div*, 104(4), 649-666.
- Collins, M.P., and Mitchell, D. (1991). *Prestress Concrete Structures*. Prentice Hall, Englewood Cliffs, NJ.
- Dilger, W. (1966). "Veränderlichkeit der Biege- und Schubsteifigkeit bei Stahlbetontragwerken und ihr Einfluß auf Schnittkraftverteilung und Traglast bei statisch unbestimmter Lagerung." Deutscher Ausschuss für Stahlbeton, Heft 179, Berlin, Germany.

- Drucker, D.C. (1961). "On Structural Concrete and the Theorems of Limit Analysis." *International Association for Bridge and Structural Engineering (IABSE)*. Zürich, Abhandlungen 21.
- FIP-Commission 3. (1996). "Practical Design of Structural Concrete." SETO, distributed by FIP, London, UK.
- Hobbs, D.W. (1988). *Alkali-Silica Reaction in Concrete*. London: Thomas Telford.
- Holden, T., Restrepo, J., and Mander, J.B. (2003). "Seismic Performance of Precast Reinforced and Prestressed Concrete Walls." *Journal of Structural Engineering*, 129(3), 286-296.
- Hsu, T.T.C. (1996). "Toward a Unified Nomenclature for Reinforced-Concrete Theory." *Journal of Structural Engineering*, 122(3), 275-283.
- Hsu, T.T.C., and Zhang, L.X. (1997). "Nonlinear Analysis of Membrane Elements by Fixed-Angle Softened-Truss Model." *ACI Structural Journal*, 94(5), 483-492.
- Hwang, S.J., Lu, W.Y., and Lee, H.J. (2000) "Shear Strength Prediction for Deep Beams." *ACI Structural Journal*, 97(3), 367-376.
- Jones, A.E.K., and Clark, L.A. (1996). "The Effects of Restraint on ASR Expansion of Reinforced Concrete." *Magazine of Concrete Research*, 48(174), 1-13.
- Karthik, M.M., and Mander, J.B. (2011) "Stress-Block Parameters for Unconfined and Confined Concrete Based on a Unified Stress-Strain Model." *ASCE Journal of Structural Engineering*, 137(28), 270-273.
- Kim, J.H., and Mander, J.B. (1999). *Truss Modeling of Reinforced Concrete Shear-Flexure Behavior*. Technical Report MCEER - 99-0005, University at Buffalo, NY.
- Kim, J.H., and Mander, J.B. (2000). "Cyclic Inelastic Strut-Tie Modeling of Shear-Critical Reinforced Concrete Members." *American Concrete Institute*, V. SP Vol. 193, 707-728.
- Kim, J.H., and Mander, J.B. (2007). "Influence of Transverse Reinforcement on Elastic Shear Stiffness of Cracked Concrete Elements." *Engineering Structures*, 29(8), 1798-1807.



- Li, K. and Coussy, O. (2002). "Concrete ASR Degradation: from Material Modeling to Structure Assessment." *Concrete Science and Engineering*, 4, 35-46.
- MacGregor, J.G. (1992). *Reinforced Concrete Mechanics and Design*. 2<sup>nd</sup> Ed., Prentice-Hall, Englewood Cliffs, NJ.
- Mander, J.B. (1983). "Seismic Design of Bridge Piers." Ph.D. Thesis, Univ. of Canterbury, New Zealand.
- Mander, J.B., Priestley, M.J.N., and Park, R. (1988). "Theoretical Stress-Strain Model for Confined Concrete." *ASCE Journal of Structural Engineering*, 114(8), 1804-1826.
- Mander, J.B., Hurlbaas, S., Karthik, M.M., and Scott, R.M. (2012a). "Guidelines for Determining the Capacity of D-Regions with Premature Concrete Deterioration of ASR/DEF." Texas Transportation Institute, The Texas A&M University System.
- Mander, J.B., Bracci, J.M., Hurlbaas, S., Grasley, Z., Karthik, M.M., Liu, S.-H., and Scott, R.M. (2012b). "Structural Assessment of "D" Region Affected by Premature Concrete Deterioration: Technical Report." *Rep. No. FHWA/TX-12/0-5997-1*, Texas Transportation Institute, The Texas A&M University System.
- Mander, J.B., Bracci, J.M., Hurlbaas, S., and Karthik, M.M. (2015). "Structural Assessment of "D" Region Affected by Premature Concrete Deterioration: Technical Report." *Rep. No. FHWA/TX-15/0-5997-2*, Texas Transportation Institute, The Texas A&M University System.
- Mau, S.T., and Hsu, T.T.C. (1987). "Shear Strength Prediction for Deep Beams with Web Reinforcement." *ACI Structural Journal*, 84(6), 513-523.
- Mörsch, E. (1909). *Concrete-Steel Construction*, McGraw-Hill, NY.
- Multon, S., Seignol, J.F., and Toutlemonde, F. (2006). "Chemomechanical Assessment of Beams Damaged by Alkali-Silica Reaction." *Journal of Materials in Civil Engineering*, 18(4), 500-509.

- Park, R., and Paulay, T. (1975). *Reinforced Concrete Structures*. Wiley, NY.
- Paulay, T. (1971). "Coupling Beams of Reinforced Concrete Shear Walls." *Journal of the Structural Division, ASCE*, 97(ST3), 843-862.
- Petersson, P.E. (1980). "Fracture Energy of Concrete: Practical Performance and Experimental Results." *Cement and Concrete Research*, 10(1), 91-101.
- Ritter, W. (1899). "Die Bauweise Hennebique (The Hennebique system)." *Schweizerische Bauzeitung* (Zürich).
- Rots, J.G., Nauta, P., Kusters, G.M.A., and Blaauwendraad, J. (1985). "Smearred Crack Approach and Fracture Localization in Concrete." *Heron*, 30(1), 1-48.
- Salem, H.M., and Maekawa, K. (2006). "Computer-Aided Analysis of Reinforced Concrete Using a Refined Nonlinear Strut-and-Tie Model Approach." *Journal of Advanced Concrete Technology*, 4(2), 325-336.
- SAP2000™ (1995). Advanced 14.0.0, Computer and Structures, Inc, Berkeley, CA.
- Sritharan, S., and Ingham, J.M. (2003). "Application of Strut-and-Tie Concepts to Concrete Bridge Joints in Seismic Regions." *PCI Journal*, 48(4), 66-90.
- Thürlimann, B., Marti, P., Pralong, J., Ritz, P., and Zimmerli, B. (1983). "Application of the Theory of Plasticity to Reinforced Concrete (Anwendung der plastizitätstheorie auf stahlbeton)." *Institute of Structural Engineering, ETH Zürich*.
- Ulm, F.J., Coussy, O., Kefei, L., and Larive, C. (2000). "Thermo-Chemo-Mechanics of ASR Expansion in Concrete Structures." *Journal of Engineering Mechanics*, 126(3), 233-242
- Vecchio, F.J., and Collins, M.P. (1986). "The Modified Compression-Field Theory for Reinforced Concrete Elements Subjected to Shear." *Journal of the American Concrete Institute*, 83(2), 219-231.
- Vecchio, F.J., and Collins, M.P. (1993). "Compression Response of Cracked Reinforced Concrete." *Journal of Structural Engineering*, 119(12), 3590-3610.

Vecchio, F.J. (2000). "Analysis of Shear-Critical Reinforced Concrete Beams." *ACI Structural Journal*, 97(1), 102-110.

Yun, Y.M. (2000). "Nonlinear Strut-Tie Model Approach for Structural Concrete." *ACI Structural Journal*, 97(4), 581-590.

Zhu, R.R.H., Wanichakorn, W., Hsu, T.T.C., and Vogel, J. (2003). "Crack Width Prediction Using Compatibility-Aided Strut-and-Tie Model." *ACI Structural Journal*, 100(4), 413-421.



## APPENDIX A: STAGE 1–3 ANALYSIS–C-BEAM SPECIMENS

This appendix presents the analysis procedure followed for the C-Beam specimens. The computations for Stage 1 (beam theory), Stage 2 (SAT analysis), and Stage 3 (C-STM analysis) are included.

**Table A–1: Material Properties for C-Beam Specimens.**

	Specimen 1	Specimen 4
$f'_c$ (ksi) (at time of testing)	5.40	4.00
$f'_t$ (ksi)	0.30	0.23
$E_c$ (ksi)	4190	3605
$f_y$ (ksi)	65	65
$E_s$ (ksi)	29000	29000

### STAGE 1: ANALYSIS USING BEAM THEORY

Step 1: Determine first yield flexural capacity,  $M_y^b$ .

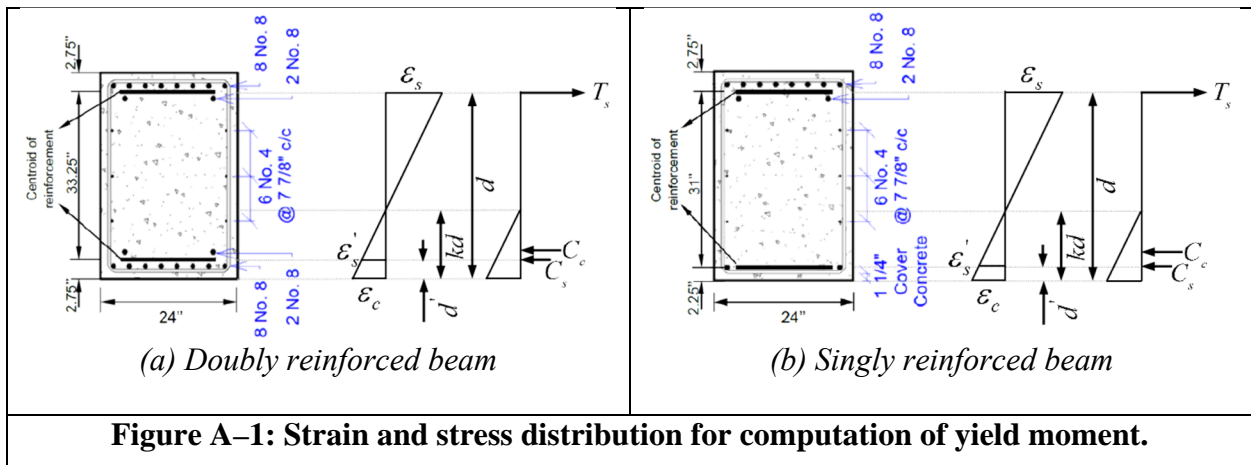


**Table A–2: Computation of First Yield Flexural Capacity and Corresponding Axial Load.**

	Specimen 1		Specimen 4	
	<i>Doubly reinforced</i>	<i>Singly reinforced</i>	<i>Doubly reinforced</i>	<i>Singly reinforced</i>
$A_s$ (in <sup>2</sup> )	7.854	7.854	7.854	7.854
$A'_s$ (in <sup>2</sup> )	7.854	1.571	7.854	1.571
$b$ (in.)	24	24	24	24
$d$ (in.)	33.25	33.25	33.25	33.25
$d'$ (in.)	2.75	2.25	2.75	2.25
$jd = d - d'$ (in.)	30.5	31	30.5	31
$\rho_L = \frac{A_s}{bd}$	0.00984	0.00984	0.00984	0.00984
$\rho'_L = \frac{A'_s}{bd}$	0.00984	0.00197	0.00984	0.00197
$n = E_s / E_c$	6.92		8.04	
$k = \sqrt{(\rho_L + \rho'_L)^2 n^2 + 2(\rho_L + \rho'_L d'/d)n} - (\rho_L + \rho'_L)n$				
$k$	0.271	0.299	0.285	0.317
$kd$ (in)	9.01	9.94	9.48	10.54
$\varepsilon_c = \frac{\varepsilon_y(kd)}{d - kd}$	0.00083	0.00096	0.00089	0.00104
$\varepsilon'_s = \frac{\varepsilon_y(kd - d')}{d - kd}$	0.00058	0.00074	0.00063	0.00082
$C_c$ (kip) = $\frac{1}{2} \varepsilon_c E_c (kd)b$	-377	-480	-366	-474
$C_s$ (kip) = $A'_s \varepsilon'_s E_s$	-132	-34	-144	-37
$T_s$ (kip) = $A_s f_y$	511	511	511	511
$M_y^b = T_s(d - kd/3) + C_s(kd/3 - d')$				
$M_y^b$ (kip.in)	15474	15319	15420	15228
$P_y^b = M_y^b / L_b$ where $L_b = 36$ in.				
$P_y^b$ (kip)	430	425	428	423

Step 2 and Step 3: Determine nominal flexural moment,  $M_n^f$  and externally applied load based on flexure,  $P_n^f$ .

For an accurate estimate of the nominal moment, calculations were performed in a spreadsheet considering the contribution of each layer of steel. The spreadsheets are presented below for both doubly and singly reinforced beam for both the specimens.

**Table A–3: Computation of Flexural Moment and Corresponding Axial Load Demand for Doubly Reinforced Beam: Specimen 1.**

Input Parameters						Calculated Variables	
<i>Section Properties</i>		<i>Reinforcement Details</i>		<i>Reinforcement Properties</i>		$\alpha$	0.85
Breadth (in)	24	Reinforcement	Diameter (in)	Es (ksi)	29000	$\beta$	0.78
a (shear span) (in)	36	Longitudinal	1	fy (ksi)	65		
<i>Concrete Properties</i>		Distribution	0.5			Assume NA depth for equilibrium, c (in)	4.145
$f_c$ (ksi)	5.4	Stirrups	0.5				
Analysis							
<i>Layer</i>	<i>No: of bars</i>	<i>Area (in<sup>2</sup>)</i>	<i>Dist to layers from bottom (in)</i>	<i>Strain</i>	<i>Stress in Steel (ksi)</i>	<i>Force in Concrete/ Steel (kip)</i>	<i>Moment (kip-in)</i>
Concrete (Bottom)	-----	-----	1.617	-0.0030	-----	-356.16	-575.75
1	8	6.28	2.250	-0.0014	-39.77	-249.91	-562.30
Steel 2	2	1.57	4.750	0.0004	12.70	19.95	94.75
Steel 3	2	0.39	10.125	0.0043	64.96	25.51	258.29
Steel 4	2	0.39	18.000	0.0100	64.96	25.51	459.18
Steel 5	2	0.39	25.875	0.0157	64.96	25.51	660.06
Steel 6	2	1.57	31.250	0.0196	64.96	102.04	3188.72
Steel 7	8	6.28	33.750	0.0214	64.96	408.16	13775.26
						$M_n^f$ (kip-ft)	<b>1441.52</b>
						$P_n^f$ (kip)	<b>480.51</b>

**Table A–4: Computation of Flexural Moment and Corresponding Axial Load Demand for Singly Reinforced Beam: Specimen 1.**

Input Parameters						Calculated Variables	
Section Properties		Reinforcement Details		Reinforcement Properties		$\alpha$	0.85
Breadth (in)	24	Reinforcement	Diameter (in.)	$E_s$ (ksi)	29000	$\beta$	0.78
a (shear span) (in)	36	Longitudinal	1	$f_y$ (ksi)	65		
Concrete Properties		Distribution	0.5			Assume NA depth for equilibrium, c (in)	5.845
$f'_c$ (ksi)	5.4	Stirrups	0.5				
Analysis							
Layer	No: of bars	Area (in <sup>2</sup> )	Dist to layers from bottom (in)	Strain	Stress in Steel (ksi)	Force in Concrete/ Steel (kip)	Moment (kip-in)
Concrete (Bottom)	-----	-----	2.280	-0.0030	-----	-502.23	-1144.86
1	2	1.57	2.250	-0.0018	-53.46	-83.97	-188.93
Steel 2	0	0.00	4.750	-0.0006	-16.30	0.00	0.00
Steel 3	2	0.39	10.125	0.0022	62.08	24.38	246.83
Steel 4	2	0.39	18.000	0.0062	64.96	25.51	459.18
Steel 5	2	0.39	25.875	0.0103	64.96	25.51	660.06
Steel 6	2	1.57	31.250	0.0130	64.96	102.04	3188.72
Steel 7	8	6.28	33.750	0.0143	64.96	408.16	13775.26
						$M_n^f$ (kip-ft)	<b>1416.36</b>
						$P_n^f$ (kip)	<b>472.12</b>



**Table A-5: Computation of Flexural Moment and Corresponding Axial Load Demand for Doubly Reinforced Beam: Specimen 4.**

Input Parameters						Calculated Variables	
<i>Section Properties</i>		<i>Reinforcement Details</i>		<i>Reinforcement Properties</i>		$\alpha$	0.85
Breadth (in)	24	Reinforcement	Diameter (in.)	$E_s$ (ksi)	29000	$\beta$	0.85
a (shear span) (in)	36	Longitudinal	1	$f_y$ (ksi)	65		
<i>Concrete Properties</i>		Distribution	0.5			Assume NA depth for equilibrium, c (in)	4.555
$f'_c$ (ksi)	4	Stirrups	0.5				
Analysis							
<i>Layer</i>	<i>No. of bars</i>	<i>Area (in<sup>2</sup>)</i>	<i>Dist to layers from bottom (in)</i>	<i>Strain</i>	<i>Stress in Steel (ksi)</i>	<i>Force in Concrete/ Steel (kip)</i>	<i>Moment (kip-in)</i>
Concrete	-----	-----	1.936	-0.0030	-----	-315.93	-611.61
(Bottom) 1	8	6.28	2.250	-0.0015	-44.02	-276.61	-622.38
Steel 2	2	1.57	4.750	0.0001	3.72	5.85	27.79
Steel 3	2	0.39	10.125	0.0037	64.96	25.51	258.29
Steel 4	2	0.39	18.000	0.0089	64.96	25.51	459.18
Steel 5	2	0.39	25.875	0.0140	64.96	25.51	660.06
Steel 6	2	1.57	31.250	0.0176	64.96	102.04	3188.72
Steel 7	8	6.28	33.750	0.0192	64.96	408.16	13775.26
						$M_n^f$ (kip-ft)	<b>1427.94</b>
						$P_n^f$ (kip)	<b>475.98</b>

**Table A-6: Computation of Flexural Moment and Corresponding Axial Load Demand for Singly Reinforced Beam: Specimen 4.**

Input Parameters						Calculated Variables	
Section Properties		Reinforcement Details		Reinforcement Properties		$\alpha$	0.85
Breadth (in)	24	Reinforcement	Diameter (in.)	$E_s$ (ksi)	29000	$\beta$	0.85
a (shear span) (in)	36	Longitudinal	1	$f_y$ (ksi)	65		
Concrete Properties		Distribution	0.5			Assume NA depth for equilibrium, c (in)	6.985
$f'_c$ (ksi)	4	Stirrups	0.5				
Analysis							
Layer	No. of bars	Area (in <sup>2</sup> )	Dist to layers from bottom (in)	Strain	Stress in Steel (ksi)	Force in Concrete/ Steel (kip)	Moment (kip-in)
Concrete (Bottom)	-----	-----	2.969	-0.0030	-----	-484.48	-1438.24
1	2	1.57	2.250	-0.0020	-58.58	-92.01	-207.03
Steel 2	0	0.00	4.750	-0.0010	-27.84	0.00	0.00
Steel 3	2	0.39	10.125	0.0013	39.11	15.36	155.50
Steel 4	2	0.39	18.000	0.0047	64.96	25.51	459.18
Steel 5	2	0.39	25.875	0.0081	64.96	25.51	660.06
Steel 6	2	1.57	31.250	0.0104	64.96	102.04	3188.72
Steel 7	8	6.28	33.750	0.0115	64.96	408.16	13775.26
						$M_n^f$ (kip-ft)	<b>1382.79</b>
						$P_n^f$ (kip)	<b>460.93</b>

Step 4: Determine beam shear capacity,  $V_n^s$ .

**Table A-7: Computation of Beam Shear Capacity.**

	Specimen 1		Specimen 4	
	<i>Doubly</i>	<i>Singly</i>	<i>Doubly</i>	<i>Singly</i>
$f'_c$ (ksi) (at time of testing)	5.40		4.00	
$f_y$ (ksi)	65		65	
$b_v$ (in.)	24		24	
$A_v$ (in <sup>2</sup> )	0.393		0.393	
$s$ (in)	4.5		4.5	
$\beta$ (per AASHTO Method 1)	2		2	
$\theta$ (degrees) (per AASHTO Method 1)	45		45	
$d_v = jd$ (in)	30.5	31	30.5	31
$V_c = 0.0316 \beta \sqrt{f'_c} b_v d_v$ (kip)	108	109	93	94
$V_s = A_v f_y \frac{d_v}{s} \cot \theta$ (kip)	173	176	173	176
$V_n^s = V_c + V_s$ (kip)	281	285	266	270

Step 5: Check strength hierarchy.

**Table A-8: Checking Strength Hierarchy.**

	Specimen 1		Specimen 4	
	<i>Doubly</i>	<i>Singly</i>	<i>Doubly</i>	<i>Singly</i>
$\phi$	0.90 (AASHTO 5.5.4.2)			
$V_n^s$ (kip)	281	285	266	270
$\phi_f$	0.90 (AASHTO 5.5.4.2)			
$P_n^f$ (kip)	481	472	476	461
$\phi V_n^s$ (kip)	253	256	239	243
$\phi_f P_n^f$ (kip)	433	425	428	415

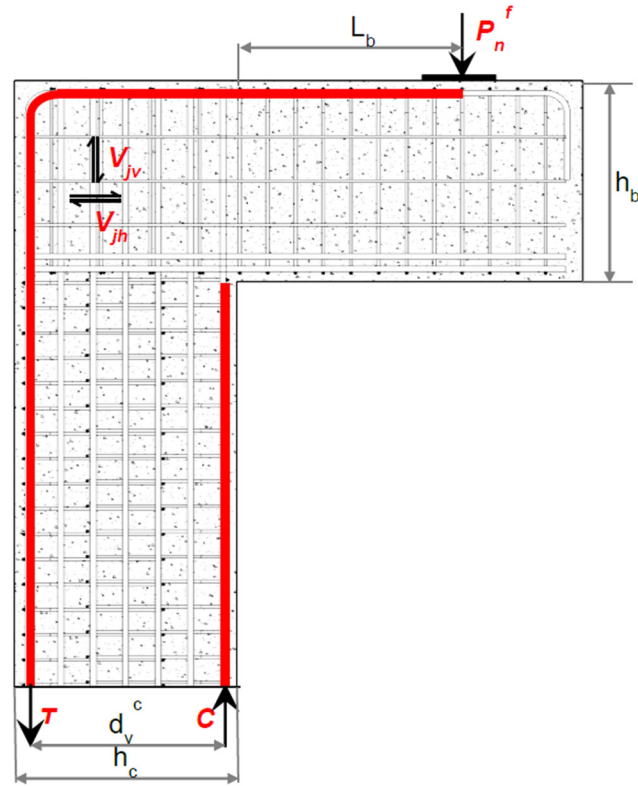
In all of the above cases  $\phi V_n^s < \phi_f P_n^f$ , which implies that the dependable shear capacity may be insufficient leading to a shear failure of the bridge pier.

*Step 6: Determine the shear capacity of the beam-column joint region.*

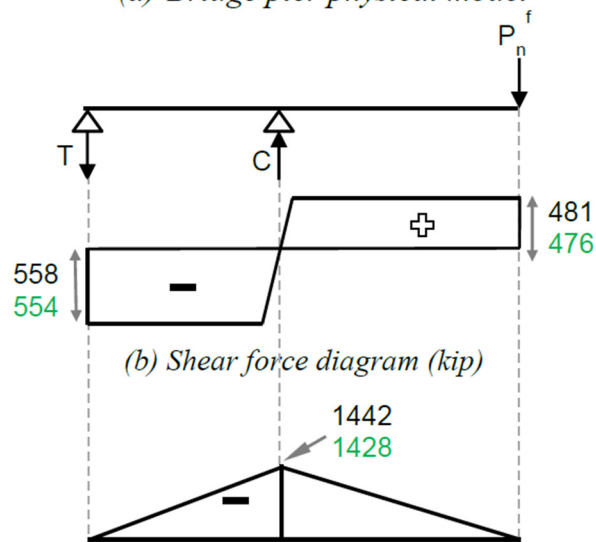
The vertical shear in the joint ( $V_{jv}$ ) caused by the axial load based on flexure can be determined from the shear force diagram of the equivalent beam model of the bridge pier shown in Figure A-2. The horizontal shear  $V_{jh}$  can be computed from  $V_{jv}$ .

**Table A-9: Computing the Vertical and Horizontal Shear in the Beam-Column Joint Caused by Flexural Axial Load Demand.**

	Specimen 1		Specimen 4	
	<i>Doubly</i>	<i>Singly</i>	<i>Doubly</i>	<i>Singly</i>
$P_n^f$ (kip)	481	472	476	461
$V_{jv}$ (kip)	558	548	554	535
$h_c = h_b$ (in.)	36		36	
$V_{jh} = \frac{h_c}{h_b} V_{jv}$ (kip)	558	548	554	535



(a) Bridge pier physical model



(c) Bending moment diagram  
(kip-ft) of cap beam

**Figure A-2: Approach to determine shear in the beam-column joint for Specimen 1 and Specimen 4.**

The computation for assessing the joint shear capacity is as follows:

**Table A–10: Assessing the Joint Shear Capacity.**

	Specimen 1		Specimen 4	
$\sum A_{sv} \text{ (in}^2\text{)}$ (total area of hoops/ties in the joint region)	1.571		1.571	
$f_y \text{ (ksi)}$	65		65	
$f'_c \text{ (ksi)}$	5.4		4.0	
$b_v \text{ (in)}$	24		24	
	<i>Doubly</i>	<i>Singly</i>	<i>Doubly</i>	<i>Singly</i>
$jd \text{ (in.)}$	30.5	31	30.5	31
$V_{truss} \text{ (kip)}$	102	102	102	102
$V_{arch} \text{ (kip)}$	430	437	370	376
$V_n^j \text{ (kip)} = V_{arch} + V_{truss}$	532	539	472	478
$\phi_v$	0.90			
$\phi_v V_n^j \text{ (kip)}$	479	485	425	430
$\phi_f$	0.90			
$\phi_f V_{jv} \text{ (kip)}$	502	493	498	481

In the above cases  $\phi_v V_n^j < \phi_f V_{jv}$ , which implies that the joint capacity is less than the demand, and hence there could be a shear joint failure.

From the above analysis it is determined that the beam and the beam-column joint are shear critical. Therefore a strut-and-tie analysis is performed. It is also required by the code to perform a SAT as the  $a/d$  ratio for the specimen is 1.08.

## STAGE 2: STRUT-AND-TIE ANALYSIS

*Step 1: Determine the node geometry.*

The computation of the node dimensions and geometry for the two specimens follows.

*CCT node:*

- The width of the CCT node is taken equal to the width of the bearing pad = 12".
- The depth of the back face of the CCT node =  $2 \times$  distance from the extreme tension face to the centroid of the tension reinforcement =  $2 \times 2.75 = 5.5$ ".

*CTT Node:*

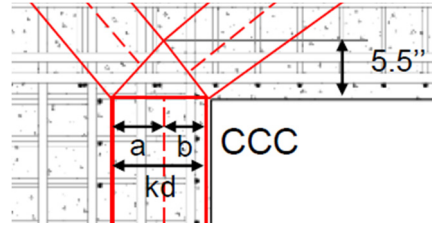
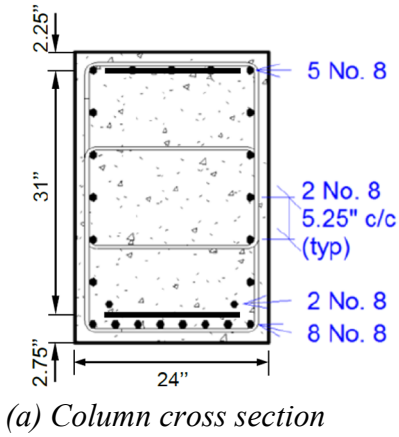
- Width of the CTT node =  $\sqrt{2 \times (R + d_b / 2)^2}$  where  $R$  = bar bending radius = 4" and  $d_b$  = diameter of the column longitudinal rebar = 1".

*CCC Node:*

- The width of the bottom face of the CCC node is equal to the depth of compression zone of the column ( $kd$ ), which is determined based on the equation for the elastic compression zone coefficient  $k$ .
- The bottom face is proportioned based on the ratio of  $a/b = V_{jv} / P_n^f$  (Figure in Table A-11) obtained from Stage 1 of the analysis.
- Since the horizontal force in the CCC node is equal to the horizontal force in the CCT node, the height of the CCC node is assumed to be equal to the depth of the back face of the CCT node =  $2 \times 2.75 = 5.5$ ".
- Knowing the above, the other sides of the CCC node can be determined.

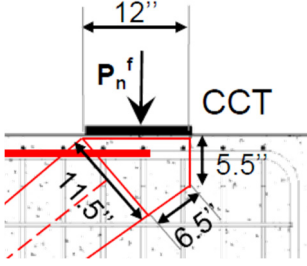
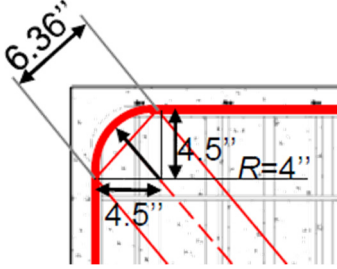
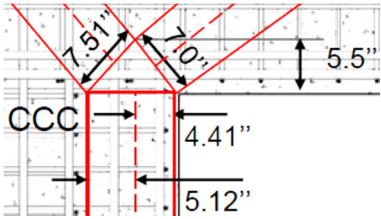
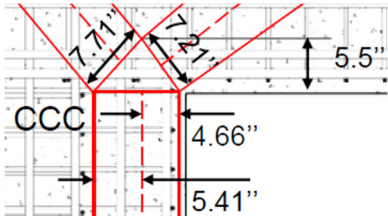
**Table A-11: Computations for Sizing the CCC Node.**

	<b>Specimen 1</b>	<b>Specimen 4</b>
$A_s$ (in <sup>2</sup> )	7.854	
$A'_s$ (in <sup>2</sup> )	3.927	
$b$ (in.)	24	
$d$ (in.)	33.25	
$d'$ (in.)	2.25	
$\rho_L = \frac{A_s}{bd}$	0.00984	0.00984
$\rho'_L = \frac{A'_s}{bd}$	0.00492	
$n = E_s / E_c$	6.92	8.04
$k = \sqrt{(\rho_L + \rho'_L)^2 n^2 + 2(\rho_L + \rho'_L d'/d)n - (\rho_L + \rho'_L)n}$		
$k$	0.287	0.303
$kd$ (in.)	9.5	10.1
$V_{jv}$ (kip)	558	554
$P_n^f$ (kip)	481	476
$V_{jv} / P_n^f$	1.16	1.16
$a$ (in)	5.12	5.41
$b$ (in)	4.41	4.66





**Table A-12: Geometry and Dimensions of Nodes.**

<b>CCT Node</b>		
<b>CTT Node</b>		
<b>CCC Node</b>	<p><b>Specimen 1</b></p> 	<p><b>Specimen 4</b></p> 

Step 2: Solve the determinate truss-determine strut and tie forces.

**Table A–13: Forces in the Struts and Ties of the SAT Model.**

<b>CCT Node</b>	<b>Node forces based on steel yield</b>		
	$A_s$ (in <sup>2</sup> )	7.854	
	$f_y$ (ksi)	65	
	$\theta_b$ (degrees)	40	
	$\theta_j$ (degrees)	45	
	$T = A_s f_y$ (kip)	511	
	$D_b = T / \cos(\theta_b)$ (kip)	667	
$P^{SAT} = D_b \sin(\theta_b)$ (kip) = $P_y^{SAT}$	429		
<b>CCC Node</b>	$C' = D_b \cos(\theta_b)$ (kip)	511	
	$D_j = C' / \cos(\theta_j)$ (kip)	723	
	$P_v^j = D_j \sin(\theta_j)$ (kip)	511	

Step 3 and Step 4: Determine minimum externally applied load causing node failure and determine shear demand.

Allowable stresses in the nodes based on AASHTO (2010) are presented in Table A–14. From the allowable node stresses, the CTT node is found to be the critical node. The axial load required to cause the failure of the CTT node can be backcalculated based on the allowable nodal stress and the area of the node. The results are presented in Table A–14.

**Table A-14: Allowable Node Stresses and Axial Load Required to Cause CTT Node Failure.**

	<b>Specimen 1</b>	<b>Specimen 4</b>
$f'_c(ksi)$	5.40	4.00
<b>Allowable Stresses</b>		
CCC Node $f_{cu} = 0.85 f'_c$	4.60	3.40
CCT Node $f_{cu} = 0.75 f'_c$	4.05	3.00
CTT Node $f_{cu} = 0.65 f'_c$	3.51	2.60
Node capacity $D_{j(node)} (kip) = F_{cu}$	536	397
Axial load that causes nodal failure, $P_n^{SAT} (kip) = P_y^{SAT} D_{j(node)} / D_j$	318	236

For both the specimens it is evident that  $P_n^{SAT}$  computed from the SAT analysis is lesser than  $P_n^f$  calculated from the beam flexure theory. Also,  $\phi_v P_n^{SAT} < \phi_f P_n^f$  for both the specimens. However from the experimental results, it was observed that the load at failure for Specimen 1 and 4 was  $P_{Failure}^{Expt} = 474$  kip and 503 kip, respectively. It is apparent from Stage 1 and Stage 2 of the analysis that they do not give a good prediction of the load carrying capacity of the specimens. Therefore, a C-STM analysis is performed to evaluate the performance of the structure.

**STAGE 3: ANALYSIS USING COMPATIBILITY STRUT-AND-TIE METHOD**

The computation of member and material properties of the C-STM model are presented below for Specimen 1 (control specimen) followed by Specimen 4 (with ASR/DEF damage).

**Computation for C-Beam Specimen 1**

A few of the section properties have to be determined beforehand to set up the C-STM geometry. These computations follow.

*Step 1: Calculate section properties.*

**Table A-15: Computation of Section Properties for C-STM.**

	<b>Doubly Reinforced</b>	<b>Column</b>	<b>Singly Reinforced</b>
<b>CROSS-SECTION</b>			
Compression Chord	8-#8 Bars	5-#8 Bars	2-#8 Bars
$h$ (in.)	36	36	36
$d'$ (in.)	2.25	2.25	2.25
$d$ (in.)	33.25	33.25	33.25
$A'_s$ (in <sup>2</sup> )	6.28	3.93	1.57
Steel contributing to tension chord	10-#8 Bars 2 sets of 2-#4	10-#8 Bars 2 sets of 2-#4	10-#8 Bars 2 sets of 2-#8
$A_{s(total)}$ (in <sup>2</sup> )	8.64	11.00	8.64
$\bar{y}$ (in) (centroid of $A_{s(total)}$ )	3.78	4.86	3.78
$A_s$ (in <sup>2</sup> ) $= A_{s(total)} \frac{h - d' - \bar{y}}{d - d'}$	8.35	10.25	8.35
$jd = d - d'$ (in)	31.0	31.0	31.0

Determine the depth of compression zone ( $kd$ ) of the singly and doubly reinforced beams and column using the equation:

$$k = \sqrt{\left(\rho_L + \rho'_L + \left(\frac{P}{f_c'bd}\right)\left(\frac{f_c'}{f_s}\right)\right)^2 n^2 + 2\left(\rho_L + \rho'_L\left(\frac{d'}{d}\right) + \left(\frac{P}{f_c'bd}\right)\left(\frac{f_c'}{f_s}\right)\right)n - \left(\rho_L + \rho'_L + \left(\frac{P}{f_c'bd}\right)\left(\frac{f_c'}{f_s}\right)\right)n}$$

For the beams the axial load  $P$  is zero.

**Table A–16: Determining the Depth of the Compression Zone for Specimen 1.**

$f_c' = 5.4$ <i>ksi</i>	Compression Steel			Tension Steel				Axial Load	Elastic Depth	
	$As'$ <i>(in<sup>2</sup>)</i>	$d'$ <i>(in.)</i>	$\rho'$	$As$ <i>(in<sup>2</sup>)</i>	$d$ <i>(in.)</i>	$b$ <i>(in.)</i>	$\rho$	$P$ <i>(kip)</i>	$k$	$kd$ <i>(in.)</i>
Single Beam	1.57	2.25	0.00197	8.35	33.25	24	0.01046	-	0.307	10.19
Double Beam	6.28	2.25	0.00787	8.35	33.25	24	0.01046	-	0.283	9.42
Column	3.92	2.25	0.00492	10.25	33.25	24	0.01284	430	0.394	13.10

*Step 2: Determine C-STM geometry based on Step 1.*

The tension ties (AK and K1K2 in Figure A–3) and compression chords (BH and L1L2 in Figure A–3) in the beams and the column are placed along the centroids of the tension and compression steel determined in Table A–15. The C-STM geometry is the same in both the singly and double reinforced beams. The overhang portion of the specimen is modeled using the single-point Gauss truss model as presented in Chapter 3. The position of tie CB is determined based on the coefficients for the single point Gauss model. In the beam-column joint region, the ties GF and IH are placed along the position of the U-Bars to better represent the specimen. All the dimensions of the C-STM are shown in Figure A–3.

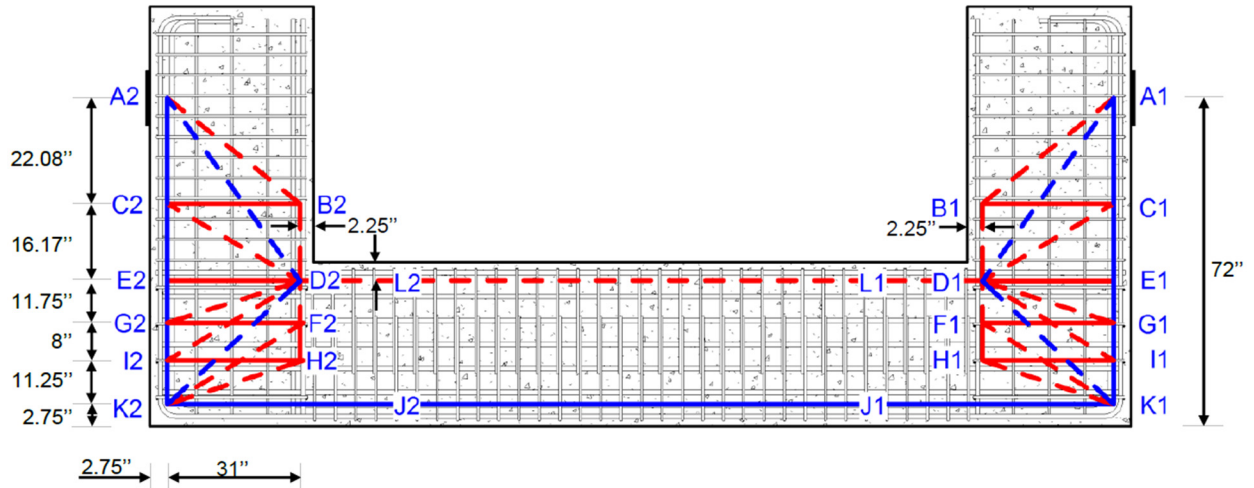


**Figure A-3: C-STM Model for C-Beam Specimen 1.**

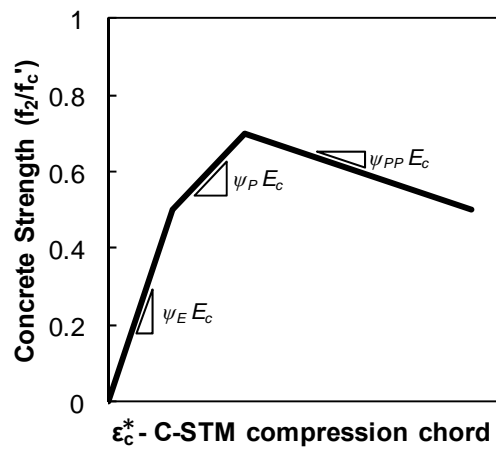
*Step 3: Determine axial rigidities.*

The next step in the C-STM analysis is to determine the axial rigidities of each of the members constituting the C-STM model.

To model the combined response of steel and concrete in the compression chord members, the compatibility correction factor is calculated in Table A-17. Based on these correction scalars, the modified stress-strain relation of the compression chord is determined.

**Table A-17: Computation of Compatibility Correction Scalar for Specimen 1.**

	<b>Singly Reinforced</b>	<b>Doubly Reinforced</b>	<b>Column</b>
$d' (in.)$	2.25	2.25	2.25
$kd (in.)$	10.19	9.42	13.10
$f'_c (ksi)$	5.4	5.4	5.4
$\psi_E = \frac{\sqrt{f'_c (psi)}}{168(1-d'/kd)}$	0.561	0.575	0.528
$\psi_P = \frac{\sqrt{f'_c (psi)}}{480(1-d'/kd)}$	0.196	0.201	0.185
$\psi_{PP} = -\frac{\sqrt{f'_c (psi)}}{1500(1-d'/kd)}$	-0.063	-0.064	-0.059



The arch breadth scalar is calculated to determine the area that needs to be assigned to the inclined arch and struts in the beam and beam-column joints.

**Table A-18: Computing Arch Breadth Scalar.**

$\eta = \frac{V_{Arch}}{V_{Arch} + V_{Truss}} = \frac{\rho_L f_y}{\rho_L f_y + \rho_T f_{yh} j \cot^2 \alpha}$			
	<b>Singly Reinforced</b>	<b>Doubly Reinforced</b>	<b>Column</b>
$d$ (in.)	33.25	33.25	33.25
$b$ (in.)	24	24	24
$s$ (in.)	4.5	4.5	8
$jd$ (in.)	31.0	31.0	31.0
$j$	0.93	0.93	0.93
$f_y = f_{yh}$ (ksi)	65	65	65
$A_s$ (in <sup>2</sup> )	8.35	8.35	10.25
$A_{sh}$ (in <sup>2</sup> )	0.393	0.393	0.393
$\rho_T = A_{sh}/b_w s$	0.00364	0.00364	0.00205
$\rho_L = A_s/bd$	0.0105	0.0105	0.0128
$\alpha$ (degrees)	39.02	39.02	45
$\eta$	0.671	0.671	0.87 (0.75 used)

Based on the properties computed above and the theory presented in Chapter 3, the axial rigidities are computed. The equations used are presented in Table 3-2.



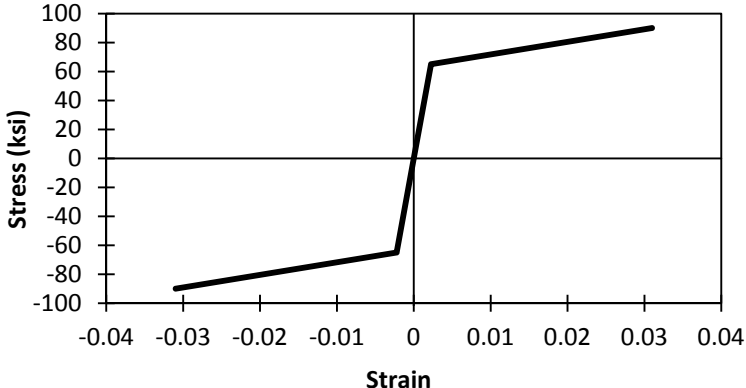
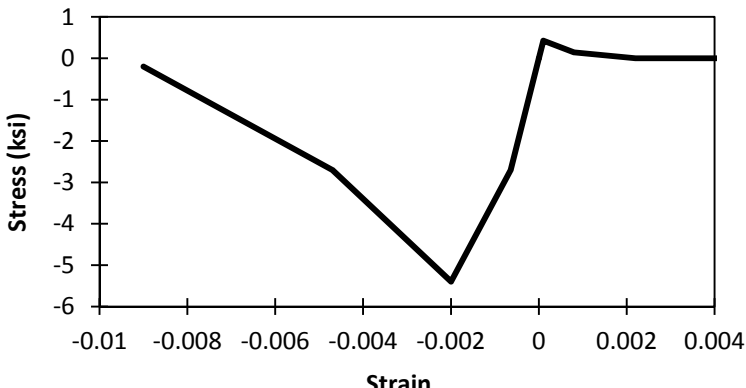
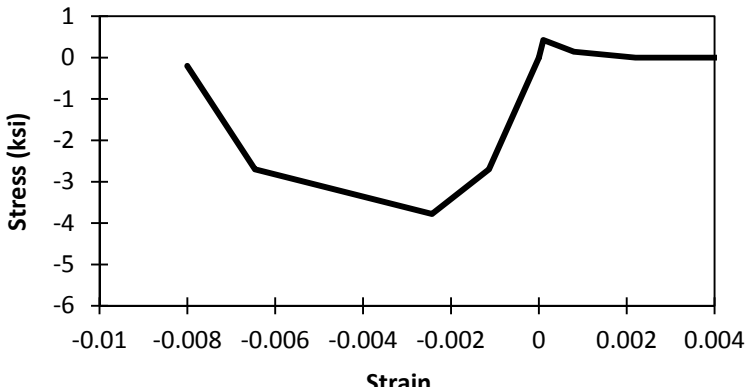
**Table A–19: Axial Rigidities of C-STM Elements: Specimen 1.**

	MEMBER	Steel		Concrete		Comments
		<i>E</i> (ksi)	<i>A</i> (in <sup>2</sup> )	<i>E</i> (ksi)	<i>A</i> (in <sup>2</sup> )	
<b>Beam</b>	<b>A-E (D)</b>	29000	8.35	4190	226.00	Tension Chord
	<b>A-E (S)</b>	29000	8.35	4190	245.00	
	<b>B-D (D)</b>	29000	6.28	2409	226.00	Compression Chord
	<b>B-D (S)</b>	29000	1.57	2351	245.00	
	<b>BC</b>	29000	2.36	4190	162.00	Transverse Steel
	<b>AD</b>	-	-	4190	240.60	Concrete Arch
	<b>AB</b>	-	-	4190	110.52	Concrete Truss
	<b>CD</b>	-	-	4190	118.14	
<b>Beam-Column Joint</b>	<b>E-K (D)</b>	29000	8.35	4190	226.00	Tension Chord
	<b>E-K (S)</b>	29000	8.35	4190	245.00	
	<b>D-H (D)</b>	29000	6.28	2409	226.00	Compression Chord
	<b>D-H (S)</b>	29000	1.57	2351	245.00	
	<b>FG&amp;HI</b>	29000	0.39	4190	54.00	Transverse Steel
	<b>DK</b>	-	-	4190	295.92	Concrete Arch
	<b>DG</b>	-	-	4190	73.64	Concrete Truss
	<b>DI</b>	-	-	4190	78.46	
	<b>FK</b>	-	-	4190	78.15	
	<b>HK</b>	-	-	4190	73.90	
<b>Column</b>	<b>JJ</b>	29000	10.25	4190	314.40	Tension Chord
	<b>LL</b>	29000	3.93	2212	314.40	Compression Chord
Beam: $N_h = 6$ and beam-column joint: $N_h = 2$						
<i>(D) Doubly reinforced beam (S) Singly reinforced beam</i>						

*Step 4: Determine constituent material properties.*

The stress-strain models used for the members in Phase 1 of Specimen 1 are as follows. The only difference for Phase 2 of the specimen is that the concrete tensile strength was reduced to 0.2 ksi to account for the minor concrete cracking that had occurred in Phase 1 of the experiment.

**Table A–20: Stress-Strain Models Used for C-STM Members: Phase 1 of Specimen 1.**

Member	Stress-Strain Model
All steel members.	
All concrete members, except the beam and column compression chord members. AB, CD, GD, ID, FK, HK, AD, CB, GF, IH, J1J2, and AK.	
Beam compression chord. BH	

**Table A-20: Stress-Strain Models Used for C-STM Members: Phase 1 of Specimen 1 (continued).**

<p>Column compression chord. L1L2</p>	
<p>Softened concrete model for the beam-column joint concrete arch. DK (In Phase 2)</p>	

### ***Computation for C-Beam Specimen 4.***

C-Beam Specimen 4 was subjected to moderate amounts of ASR/DEF damage. While the procedure for calculating the member and material properties remains the same as in the case of Specimen 1, certain modifications are required to account for the effects of ASR/DEF in the specimens. The modifications are based on the recommendations made in Chapter 3.

*Step 1: Compute modified material properties to account for ASR/DEF.*

To account for the effects of ASR/DEF on the C-Beam specimens, modified material properties are calculated based on the recommendations presented in Section 3.6.5.

- *Diagonal truss concrete:*

**Table A–21: Modified Concrete Strength for Concrete Truss Members of the C-STM.**

	<b>Specimen 4</b>
ASR/DEF damage level	Moderate
$f'_c$ (ksi)	4.0
$\lambda$	0.70
$f'_{cASR}$ (ksi) = $\lambda f'_c$	2.80

The stress-strain of the following members (Figure A–3) is modified based on the reduced concrete strength of the diagonal truss: AK, AB, CD, GD, ID, FK, HK, CB, GF, and IH.

- *Compute prestress in the beam and column ties:*

Based on the recommendations made in 3.6.5 the prestress in the longitudinal bars and the hoops are calculated.

**Table A–22: Prestress in Longitudinal Bars and Hoops Due to ASR/DEF.**

	<b>Specimen 4</b>
ASR/DEF damage level	Moderate
$f_y = f_{yh}$ (ksi)	65
Prestress in longitudinal bar (ksi)	$f_{ps} = 0.5f_y = 32.5$
Prestress in hoops (ksi)	$f_{ps} = 1.0f_{yh} = 65$

Knowing the prestress in the ties and the tie area, the prestress force to be applied in the C-STM model is computed.

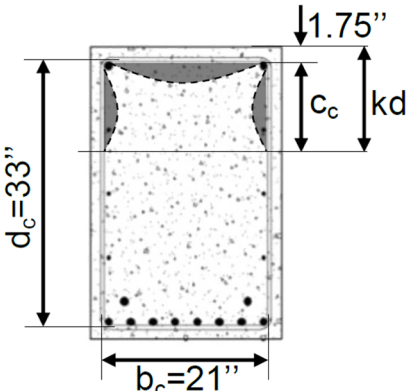
**Table A–23: Prestress Forces Applied to the C-STM Model.**

	<b>Prestress Force (kip)</b>
<b>MEMBER</b>	<b>Specimen 4</b>
<b>A-K</b>	$32.5 \times 8.35 = 271.38$
<b>B-H (D)</b>	$32.5 \times 6.28 = 204.10$
<b>B-H (S)</b>	$32.5 \times 1.57 = 51.03$
<b>BC</b>	$65 \times 2.36 = 153.40$
<b>FG&amp;HI</b>	$65 \times 0.393 = 25.35$
<b>JJ</b>	$32.5 \times 10.25 = 333.13$
<b>LL</b>	$32.5 \times 3.93 = 127.73$

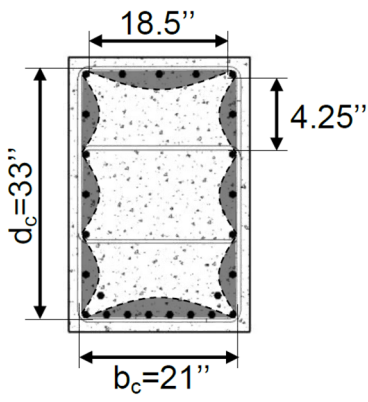
- Compute confinement ratio for the beam and the column:

To account for the confinement caused by the swelling of core concrete, the confinement ratios are computed for the beam and the column.

**Table A–24: Calculating Confinement Ratio of the Beam.**

	
	<b>Specimen 4</b>
$f'_c$ (ksi)	4.0
$kd$ (in.)	11.20
$A_{cc}$ (in <sup>2</sup> ) = $(c_c + d_s / 2) \times b_c$	200.70
$A_e$ (in <sup>2</sup> ) = $(c_c + d_s / 2) \times b_c - \text{area of shaded region}$	122.86
$k_e = A_e / A_{cc}$	0.603
$f_{lx}$ (ksi)	0.176
$f_{ly}$ (ksi)	0.162
Smallest confining stress ratio $f_{ly} / f'_c$	0.041
Largest confining stress ratio $f_{lx} / f'_c$	0.44
$K = f'_{cc} / f'_c$	1.28

**Table A–25: Calculating Confinement Ratio of the Column.**

	
	<b>Specimen 4</b>
$f'_c$ (ksi)	4.0
$kd$ (in.)	11.20
$A_{cc}$ (in <sup>2</sup> ) = $b_c d_c$	693
$A_e$ (in <sup>2</sup> ) = $b_c d_c$ – area of shaded region	560.85
$k_e = A_e / A_{cc}$	0.81
$f_{lx}$ (ksi)	0.278
$f_{ly}$ (ksi)	0.219
Smallest confining stress ratio $f_{ly} / f'_c$	0.055
Largest confining stress ratio $f_{lx} / f'_c$	0.069
$K = f'_{cc} / f'_c$	1.35

*Step 2: Compute section properties.*

The steel areas computed in Table A–15 for Specimen 1 hold good for Specimen 4 as well. However, the depth of compression zone ( $kd$ ) has to be recalculated to account for the prestress forces that are applied on the ties.

**Table A–26: Determining the Depth of the Compression Zone for Specimen 4 With ASR/DEF Damage.**

	Compression Steel			Tension Steel				Axial Load	Elastic Depth	
	$A_s'$ (in <sup>2</sup> )	$d'$ (in)	$\rho'$	$A_s$ (in <sup>2</sup> )	$d$ (in)	$b$ (in)	$\rho$	$P$ (kip)	$k$	$kd$ (in)
Single Beam	1.57	2.25	0.00197	8.35	33.25	24	0.01046	51.0	0.337	11.21
Double Beam	6.28	2.25	0.00787	8.35	33.25	24	0.01046	204.1	0.343	11.40
Column	3.92	2.25	0.00492	10.25	33.25	24	0.01284	763.1	0.458	15.22

*Step 3: Determine C-STM geometry.*

The geometry of the C-STM remains the same as Specimen 1. However, axial loads are applied at the nodes to account for the ASR/DEF effects. The C-STM model for Specimen 4 is shown in Figure A–4.

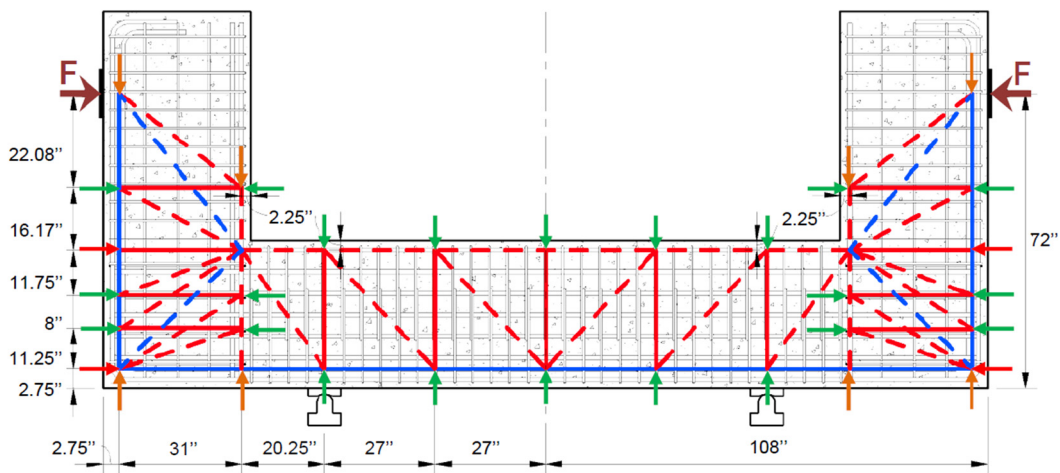


**Figure A–4: C-STM Model for C-Beam Specimen 4.**



Step 4: Determine axial rigidities.

The compatibility correction factor for Specimen 4 is recalculated.

**Table A–27: Computation of Compatibility Correction Scalar for Specimen 4.**

	<b>Singly Reinforced</b>	<b>Doubly Reinforced</b>	<b>Column</b>
$d'$ (in.)	2.25	2.25	2.25
$kd$ (in.)	11.21	11.40	15.22
$f'_c$ (ksi)	4.0	4.0	4.0
$\psi_E = \frac{\sqrt{f'_c(\text{psi})}}{168(1 - d'/kd)}$	0.471	0.469	0.442
$\psi_P = \frac{\sqrt{f'_c(\text{psi})}}{480(1 - d'/kd)}$	0.165	0.164	0.155
$\psi_{PP} = -\frac{\sqrt{f'_c(\text{psi})}}{1500(1 - d'/kd)}$	-0.053	-0.053	-0.049

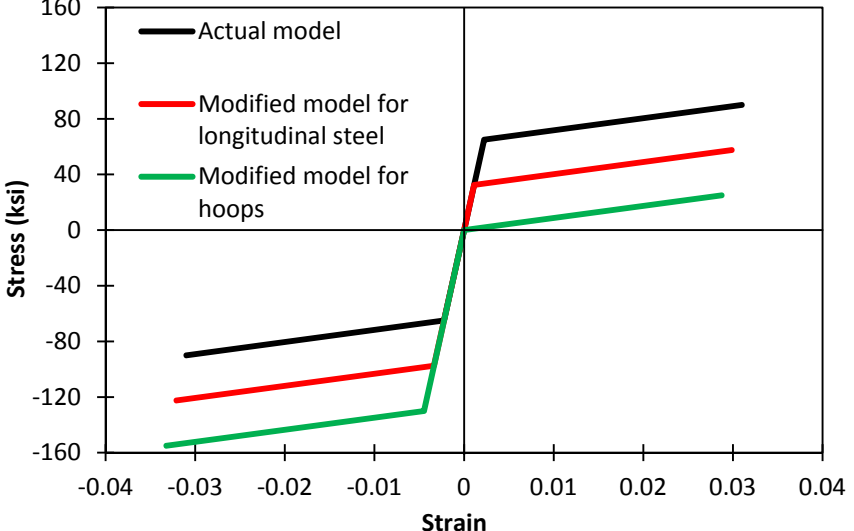
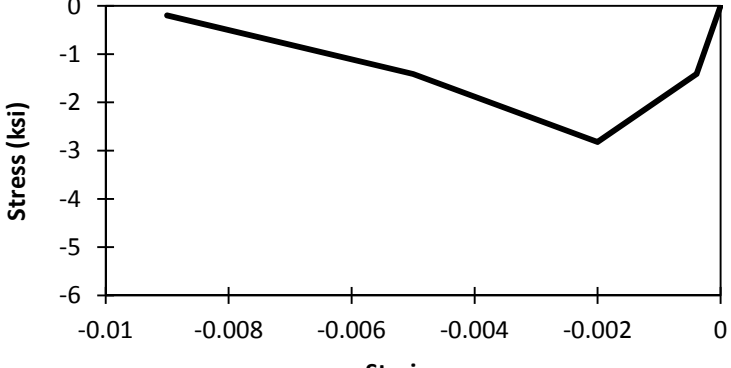
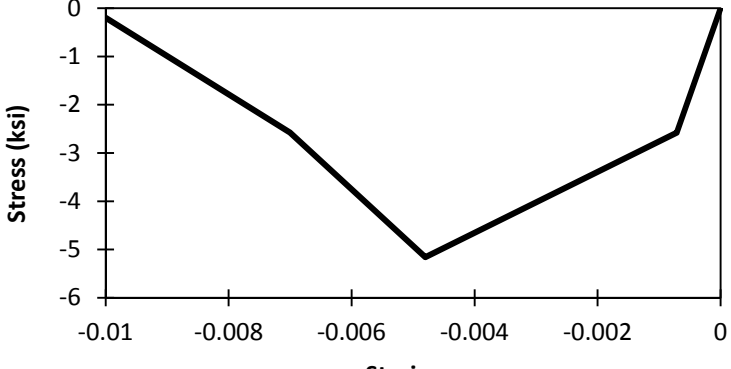
The arch-breadth scalar remains the same as in Table A–18. The axial rigidities are recomputed based on the modified properties calculated above for Specimen 4.

**Table A–28: Axial Rigidities of C-STM Elements: Specimen 4.**

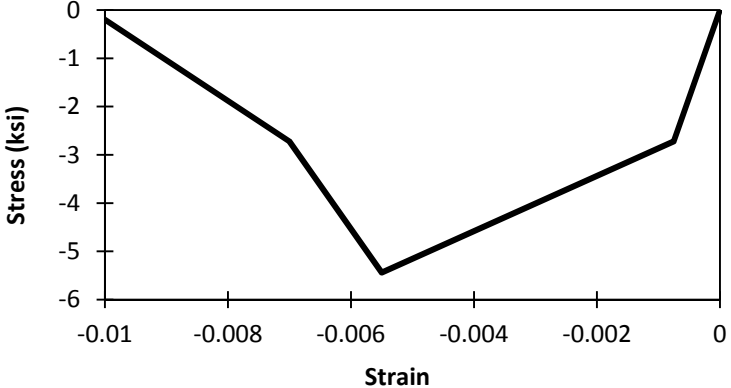
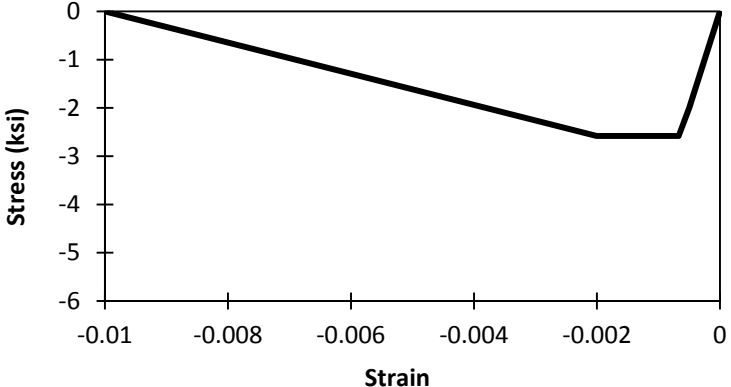
	MEMBER	Steel		Concrete		Comments
		<i>E</i> (ksi)	<i>A</i> (in <sup>2</sup> )	<i>E</i> (ksi)	<i>A</i> (in <sup>2</sup> )	
<b>Beam</b>	<b>A-E (D)</b>	29000	8.35	4190	273.60	Tension Chord
	<b>A-E (S)</b>	29000	8.35	4190	269.04	
	<b>B-D (D)</b>	29000	6.28	1690	273.60	Compression Chord
	<b>B-D (S)</b>	29000	1.57	1698	269.04	
	<b>BC</b>	29000	2.36	4190	162.00	Transverse Steel
	<b>AD</b>	-	-	4190	240.60	Concrete Arch
	<b>AB</b>	-	-	4190	110.52	Concrete Truss
	<b>CD</b>	-	-	4190	118.14	
<b>Beam-Column Joint</b>	<b>E-K (D)</b>	29000	8.35	4190	273.60	Tension Chord
	<b>E-K (S)</b>	29000	8.35	4190	269.04	
	<b>D-H (D)</b>	29000	6.28	1690	273.60	Compression Chord
	<b>D-H (S)</b>	29000	1.57	1698	269.04	
	<b>FG&amp;HI</b>	29000	0.39	4190	54.00	Transverse Steel
	<b>DK</b>	-	-	4190	295.92	Concrete Arch
	<b>DG</b>	-	-	4190	73.64	Concrete Truss
	<b>DI</b>	-	-	4190	78.46	
	<b>FK</b>	-	-	4190	78.15	
	<b>HK</b>	-	-	4190	73.90	
<b>Column</b>	<b>JJ</b>	29000	10.25	4190	365.28	Tension Chord
	<b>LL</b>	29000	3.93	1593	365.28	Compression Chord
Beam: $N_h = 6$ and beam-column joint: $N_h = 2$						
<i>(D) Doubly reinforced beam (S) Singly reinforced beam</i>						

Step 5: Determine constituent material properties.

**Table A–29: Stress-Strain Models for the Elements of the C-STM Model: Specimen 4.**

Member	Stress-Strain Model
All members	 <p>The plot shows three stress-strain curves. The 'Actual model' (black) shows a yield point at approximately 60 ksi in tension and -60 ksi in compression, followed by strain hardening. The 'Modified model for longitudinal steel' (red) shows a yield point at approximately 35 ksi in tension and -35 ksi in compression. The 'Modified model for hoops' (green) shows a yield point at approximately 10 ksi in tension and -10 ksi in compression. All models show a sharp increase in stress at zero strain.</p>
Concrete truss members in the beam. AK, AB, CD, GD, ID, FK, HK, CB, GF, and IH.	 <p>The plot shows a parabolic stress-strain relationship for concrete truss members. The stress is zero at zero strain and reaches a maximum compressive stress of approximately -3.5 ksi at a strain of -0.002. The stress returns to zero at a strain of -0.01.</p>
For remaining concrete members in the beam.	 <p>The plot shows a parabolic stress-strain relationship for remaining concrete members. The stress is zero at zero strain and reaches a maximum compressive stress of approximately -5.5 ksi at a strain of -0.005. The stress returns to zero at a strain of -0.01.</p>

**Table A-29: Stress-Strain Models for the Elements of the C-STM Model: Specimen 4 (continued).**

<p>Column members.</p>	 <p>Stress (ksi)</p> <p>Strain</p>
<p>Softened concrete model for the beam-column joint. DK</p>	 <p>Stress (ksi)</p> <p>Strain</p>